Development of an electrochemical aptasensing platform based on nanomaterials and DNA nanostructures for antibiotics detection in dairy products

by

Jiehao Guan

A dissertation submitted in partial fulfilment of the requirements for the degree of

Doctor of Philosophy

(Biological Systems Engineering)

at the

UNIVERSITY OF WISCONSIN-MADISON

2022

Date of final oral examination: 05/12/2022

The dissertation is approved by the following members of the Final Oral Committee:

Sundaram Gunasekaran, Professor, Biological Systems Engineering

Jae-Hyuk Yu, Professor, Bacteriology

Filiz Yesilkoy, Assistant Professor, Biomedical Engineering

Tu-Anh Huynh, Assistant Professor, Food Science

Abstract

Bovine mastitis is the most common disease in dairy cattle, which causes reduced milk production from immune response to intramammary infections and results in a major economic burden faced by the dairy industry worldwide. Antibiotic has been the veterinary medicine for the prevention and treatment of bovine mastitis as well as the growth promoter to improve food production for decades. However, the abuse of antibiotics leads to resistance to foodborne pathogens in food products and induces serious public health issues. Therefore, routine tests to monitor the levels of antibiotics in farm animals and food products have been in great demand to alleviate food safety concerns.

Electrochemical biosensors are considered simple, powerful, user-friendly, and cost-effective analytical tools providing rapid and accurate responses. Compared to the conventional antibiotic detection methods, the electrochemical sensing platform has much potential for high throughput and on-site analysis, due to its simple operation, fast determination, and miniaturized device. Given the chemical nature and molecular structures of antibiotics and the ultralow tolerance in food, especially β-lactam derivatives, the development of antibiotic detections has been confronted with many challenges such as insufficient sensitivity, unsatisfied selectivity, and inadequate reproducibility. Fortunately, the advancements in nanomaterials and DNA nanotechnologies have brought opportunities to solve the intrinsic deficiency of electrochemical biosensors. Therefore, researchers have made great efforts in sensor surface modification, detection strategy design, and biorecognition probe development.

In this dissertation, we proposed a highly sensitive and selective electrochemical aptasensing platform based on nanomaterial fabrication and DNA nanotechnology and a

universal aptamer screening procedure for small molecule-specific aptamers selection. We started with the optimization and the evaluation of reduced graphene oxide (rGO) and gold nanoparticles (AuNPs) fabrications on the screen-printed electrode (SPE). The electrical performance of SPE was significantly enhanced by the surface morphology modification with several times stronger current response and noticeably reduced surface impedance. As a crucial part of the sensing platform, aptamer was employed for antibiotic identification as a highly selective biorecognition element. However, due to the self-induced perturbations and cross-interactions, the target binding affinity of aptamers was not fully released in most of the reported works. Thus, we developed a self-assemble tetrahedral DNA nanostructure (TDN) to precisely control the orientation of immobilized aptamers and nanospacing from neighbor aptamers on the working surface. The electrical response of TDN-assisted SPE was amplified by almost 100 times and the sensitivity of the sensing platform was remarkably improved because of the superior detecting environment created by TDN. An ultrasensitive label-free electrochemical aptasensor was fabricated to achieve ampicillin (AMP) qualification and quantification in a wide range of concentrations from 10 pM to 1000 nM with a limit of detection (LOD) of 1 pM in less than 30 min in both buffer systems and real milk samples.

To fill the vacancy of high-affinity aptamers to penicillin G (PenG), an immobilization-free aptamer screening procedure based on graphene oxide (GO) adsorption (GO-SELEX) was designed to select functional ssDNA structures for specific PenG identification. The selected aptamer candidates were sequenced, and then the dissociation constants (K_d) were determined as 105.15 ± 1.94 nM, 212.8 ± 4.06 nM, and 501.4 ± 15.3 nM using the electrochemical method based on Langmuir binding isotherm. The mathematic model of electrochemical responses to PenG concentrations was built from 0.2 nM to 1000 nM, yielding a LOD of 0.05 nM.

Additionally, the aptasensor was proved to be practical in a real milk sample test with a great recovery rate from 98% to 109%. The specificity of the aptamer sequence was confirmed by a selectivity test against other antibiotics. The reproducibility and stability of the designed aptasensor were exanimated to show the potential of on-site antibiotic analysis.

Acknowledgments

First and foremost, I would like to take this opportunity to extend my gratitude and appreciation to my research advisor and chair of the dissertation committee, Dr. Sundaram Gunasekaran for his guidance and support during my Ph.D. years. His dedicated involvement and practical advice helped me construct this dissertation and steered me in the right direction. I am very grateful to have him as my academic advisor.

I would also like to show my acknowledgment to the members of my dissertation committee, Dr. Jae-Hyuk Yu from department of Bacteriology, Dr. Filiz Yesilkoy from department of Biomedical Engineering, and Dr. Tu-Anh Huynh from department of Food Science, for their valuable comments and advice. In addition, many thanks to Dr. Yu for the PCR and electrophoresis support as an essential part of this research.

I wish to express my sincere thanks to Dr. Kaiyu He from Zhejiang Academy of Agricultural Sciences. During his visit to University of Wisconsin-Madison, I discussed the early version of my dissertation with him and received precious suggestions and professional advice. His input brought great value to my work.

Getting through my dissertation required more than academic support. I am grateful to have Drs. Yi-Cheng Wang, Lin Lu, and Zong Liu as my dearest friends, who offered great support from the day I arrived in Madison. Their doors were always open whenever I needed it. I would also like to thank Yaoqi Yin and Weizheng Wang, who have been the best friends I could possibly ask for. I am gratefully indebted to their support in both work and life. I am also

thankful to all the staff and members in the department of Biological Systems Engineering for making my Ph.D. years pleasant.

Most importantly, none of this could have been achieved without the unfailing support of my parents and my girlfriend Yuqing Wu. Their unconditional love and consistent encouragement kept me motivated throughout my years of study, especially during the dissertation writing.

Table of Contents

List of Abbreviations

The following is a list of abbreviations and acronyms used in this dissertation along with the page numbers of their first appearance.

Abbreviation	Meaning	Page number
FDA	U.S. Food and Drug Administration	2
TDN	Tetrahedral DNA nanostructures	5
ssDNA	single-stranded DNA	5
SELEX	Systematic Evolution of Ligands by Exponential Enrichment	5
CV	Cyclic voltammetry	5
DPV	Differential pulse voltammetry	5
SWV	Square wave voltammetry	5
EIS	Electrochemical impedance spectroscopy	5
GO	Graphene oxide	7
rGO	Reduced graphene oxide	7
AuNPs	Gold nanoparticles	7
LOD	Limit of detection	16
K_d	Dissociation constant	28
PCR	Polymerase chain reaction	36
AFM	Atomic force microscopy	40
SEM	Scanning electron microscopy	55
XPS	X-ray photoelectron spectroscopy	55
XRD	X-ray diffraction	55

SPE	Screen-printed electrode	55
EDC	1-Ethyl-3-(3-dimethylaminopropyl) carbodiimide	56
NHS	N-hydroxysuccinimide	56
PBS	Phosphate buffered saline	56
TE	Tris-EDTA	56
TEM	Transmission electron microscopy	59
UV/Vis	Ultraviolet-visible spectroscopy	59
FTIR	Fourier-transform infrared spectroscopy	59
R_{ct}	charge-transfer resistance	68
AMP	Ampicillin	73
TCEP	Tris-(2- carboxyethyl) phosphine hydrochloride	76
ΔI	Current difference	83
RSD	Relative Standard Deviation	92
PenG	Penicillin G	97
ΔG	Free energy of formation	99

List of Figures

List of Tables

Chapter 1. Introduction and Research Description

1.1 Background information

1.1.1 Bovine mastitis and antibiotics treatment in the food industry

Bovine mastitis is the most important contagious disease in dairy cattle and a major economic problem faced by the dairy industry worldwide (Halasa et al., 2009). Mastitis costs direct milk losses from the effects of pathogens and indirect milk losses from the immune responses to the intramammary infections, which becomes a financial burden for the dairy industry (Detilleux, Kastelic, & Barkema, 2015). The financial consequences of mastitis include diagnostics, veterinary treatment, reduction in milk yields, quality penalties or even discard of sub-quality milk, premature culling, and extra labor of farmers (Duarte, Freitas, & Bexiga, 2015). The average incident case of clinical bovine mastitis leads to a total cost of $444 during the first 30 days of lactation, where the cost of direct losses for an incident case averages $128 and the cost of indirect losses results in $316 (Rollin, Dhuyvetter, & Overton, 2015). The economic cost of the entire dairy industry is estimated to reach an average of two billion dollars per year, and the long-term indirect losses contribute 71% of the total cost (Bar et al., 2008). The cases occurred as an immune response to bacterial invasion are about 75% to 90%, which are majorly caused by some common bacterial pathogens, such as *Escherichia coli (E. coli)*, *Staphylococcus aureus (S. aureus)*, and *Arcanobacterium Pyogenes (A. pyogenes)* (du Preez, 2000). Therefore, antibiotic therapy has been the main strategy for bovine mastitis treatment for decades.

Antibiotics, also known as antibacterial, are powerful medications that kill bacteria or stop them from reproducing (Wegener, 2003). Antibiotics have been introduced and used extensively

in food industries primarily as veterinary medicine for the prevention and treatment of respiratory, gastrointestinal, and urinary infections shortly after their discovery (Founou, Founou, & Essack, 2016). Later in the antibiotic practices, the feeding of residual antimicrobials at low doses was observed to promote the growth of animals and increase the food products such as egg and milk yield (Edqvist & Pedersen, 2002). In the last four decades, the usage of antibiotics as prophylactics and growth promoters in food animals has revolutionized the entire industry and contributed to the development of the food-producing system (Majdinasab, Mishra, Tang, & Marty, 2020). There are only two classes of antibiotics approved by the U.S. Food and Drug Administration (FDA). The commercialized products include β-lactams (amoxicillin, ampicillin, ceftiofur, cephapirin, cloxacillin, and penicillin) and a lincosamide (lincomycin, clindamycin, pirlimycin) (Administration, 2018). Due to their effectiveness and low cost, β-Lactam derivatives are still widely used as antimicrobial medicine in the dairy industry worldwide (Junza, Montané, Barbosa, Minguillón, & Barrón, 2014).

However, as the discoverer Alexander Fleming predicted, the abuse of antibiotics has been proved correlated to the increasing drug resistance as 'microbes are educated to resist penicillin' (Leibovici et al., 2016). The development of antibiotic resistance and the entrance of resistant pathogens into the food chain creates a serious issue with a reduction in medical treatment efficiency (Gomes & Henriques, 2016). Meanwhile, the overuse of antibiotics in bovine mastitis treatment can potentially lead to raw milk contamination of antibiotic residues which are highly resistant to heat sterilization and then easily transfer into dairy products (Wassenaar, 2005). Research shows traditional milk pasteurization only eliminates the residual β-lactam antibiotics by approximately 10% to 20% and the consumption of contaminated food products with antibiotic residues can cause allergic reactions, disruption of intestinal flora, and other serious human health

problems (Paige, Tollefson, & Miller, 1999; Payne, Craigmill, Riviere, & Webb, 2006). To avoid public health risks, FDA established a tolerance/safe level of drug residues in milk samples, for example, ampicillin at 10 ppb and penicillin G at 5 ppb ("U.S. Food and Drug Administration. Center for Veterinary Medicine. Milk drug residue sampling survey," 2015). Therefore, routine test to qualify and quantify antibiotic residues in milk products has become a major demand for farmers and dairy industries to maintain food quality and safety.

1.1.2 Conventional antibiotics determination

To date, residual antibiotics are screened and tested by conventional antimicrobial assays. These antimicrobial assays test the sample milk by incubating a susceptible organism in the selected milk solutions, which would grow to produce acid for a visible color change or inhibit by the antibiotics and result in no change in color. The approach developed by the United States Department of Agriculture (USDA), Food Safety and Inspection Service (FSIS) is called a seven-plate bioassay system (United States Department of Agriculture, 2010). In addition, *Bacillus stearothermophilus* disc diffusion assay (BsDA) and Delvotest are two of the most commonly used antimicrobial assays to detect β-lactam derivatives in the milk (Bishop, Bodine, O'Dell, & Janzen, 1985). Even though these bioassay protocols are mature and reliable, they are time-consuming, expensive, and lack specificity.

Alternatively, several immunoassays based on the immunoaffinity of antibodies and analytes have been developed to achieve the sensitivity requirement for residual antibiotics determination, such as enzyme-linked immunosorbent assays (ELISAs) (Du et al., 2019), fluorescence-polarization immunoassays (FPIAs) (Pennacchio et al., 2016), and surface plasmon resonance-based (SPR) immunosensors (Rebe Raz, Bremer, Haasnoot, & Norde, 2009). Moreover,

chromatography techniques have been employed and coupled with mass spectroscopy to design specific and ultrasensitive antibiotics detecting methods, including high-performance liquid chromatography (HPLC) (Briscoe, McWhinney, Lipman, Roberts, & Ungerer, 2012), gas chromatography-mass spectrometry (GC-MS) (Yang et al., 2015), liquid chromatography-tandem mass spectrometry (LC-MS/MS) (Berendsen, Wegh, Memelink, Zuidema, & Stolker, 2015), liquid chromatography-electrospray ionization mass spectrometry (LC-ESI/MS) (Li et al., 2008), and capillary electrophoresis (Santos, Henriques, Duarte, & Esteves, 2007). However, chromatography-based methods often require strict sample pretreatments and tedious detection procedures and need highly qualified personnel with sophisticated instruments in the laboratory, which leads to increased operational cost and time. More importantly, the limitation of sensing device miniaturization prevents these methods from adapting to high throughput and on-site analysis (Sharma et al., 2016).

Therefore, the major problem in the area of food quality control is rapid, accurate, stable, low-cost, and portable detection equipment with high specificity and sensitivity for a low tolerant level of antibiotic residues in dairy products.

1.1.3 Aptamer-based electrochemical biosensors

To overcome the limitations of conventional detecting methods, a variety of biosensors has been developed to achieve fast, simple, sensitive, and selective antibiotic determinations. Electrochemical biosensors are the most common and frequently used sensors among various types of biosensors. Electrochemical biosensors are defined as sensing devices consisting of biological recognition elements to identify the target of interest and electrochemical transducers to translate the biorecognition activities into electrical analysis information (Kissinger, 2005). The most

common biological recognition elements are antibodies, enzymes, and oligonucleotides (Eggins, 2013). The ideal recognition element should have a good range of properties: high selectivity, sensitivity to certain targets, wide dynamic range, short response time, and long shelf life. Aptamers, single-stranded DNA (ssDNA) oligonucleotides, offer great specificity, good binding affinity, flexibility, chemical and thermal stability, and cost-efficiency compared to antibodies and enzymes (Song, Wang, Li, Fan, & Zhao, 2008). With a suitable SELEX process (Systematic Evolution of Ligands by Exponential Enrichment), the selected aptamers can specifically recognize and effectively bind to any desired targets with high affinity (Darmostuk, Rimpelova, Gbelcova, & Ruml, 2015) Thus, aptamers have become increasingly important analytical tools in biosensor constructions (Y. S. Kim, Raston, & Gu, 2016). The binding efficiency of aptamers is often diminished by the irregular orientation of fixed aptamers and interference from self-induced perturbation and cross-interaction (Feng et al., 2017). To improve the binding rate, a tetrahedral DNA nanostructure (TDN) has been introduced to control the orientation and surface density of aptamers to increase target accessibility to reach the maximum sensitivity of aptamer-based biosensors (Zeng et al., 2015).

An electrochemical transducer is capable of converting biomolecular recognition events into electrically detectable signals. The electrical signals through physicochemical transducers are detected by various electrochemical characterization techniques such as cyclic voltammetry (CV), differential pulse voltammetry (DPV), square wave voltammetry (SWV), and electrochemical impedance spectroscopy (EIS) (Pohanka & Skládal, 2008). Based on the different types of transducers, electrochemical biosensors can be classified into amperometric, impedimetric, and voltammetric biosensors (L. Lan, Y. Yao, J. Ping, & Y. Ying, 2017). Since the sensitivity of biosensors is highly attributed to the surface morphology of the electron exchange interface, an

increasing number of biosensors use nanomaterials to improve the biosensing performance of electrochemical measurements (Pérez-López & Merkoçi, 2011). Due to the exclusive physical and chemical properties, nanomaterial-modified biosensors show enhanced sensitivity, thermal and chemical stability, and response speed compared to traditional biosensors (Qian, Durairaj, Prins, & Chen, 2021).

1.1.4 Research description

The developments of electrochemical biosensors have attracted tremendous attention to building novel antibiotics sensing platforms to overcome the limitations of the conventional detecting methods. Although electrochemical biosensors exhibit noticeable potential in biosensing applications, the improvements in stability, sensitivity, and selectivity are in great demand to convert the design of experimental approaches to commercial applications. Fortunately, the advancements in nanomaterials and DNA nanotechnologies have brought opportunities to solve the intrinsic deficiency of electrochemical biosensors.

The overall goal of this research is to develop a cost-effective and portable aptasensor to perform simple, rapid, accurate, and stable residual antibiotics monitoring in real food samples and to fulfil the FDA food safety regulations with enough sensitivity and specificity.

The main issues faced by the antibiotics electrochemical aptasensing are listed below:

(1) Ultralow tolerances of antibiotics in FDA food safety regulations require ultrasensitive biosensing capability of electrochemical biosensing platform,

(2) To obtain the sensitivity requirements, the reported aptasensing methods often used tedious signal amplification routes with strict targets or aptamers labeling procedures,

(3) The binding process of aptamer functional structures is interfered with by the self-induced perturbation and cross-interactions with relatively low target accessibility,

(4) A very few effective aptamer sequences of antibiotics have been reported due to the difficulty of aptamer selections for small molecules, which limits the aptasensor development, especially for β-lactams antibiotics.

Nanomaterial modifications with reduced graphene oxide (rGO) and gold nanoparticles (AuNPs) on the aptasensor surface offer surface morphology improvement and electron transmission enhancement on the electron exchange interface, which become the best choice to solve the sensitivity deficiencies of an electrochemical biosensor. Moreover, AuNPs also provide surface availability for biomolecule immobilizations. Aptamers as the biorecognition elements afford great target specificity towards the desired target, which is the ideal biosensing probe candidate for antibiotic detection. The TDN can control the orientation and conformation of the aptasensing probe to achieve an effective target identification and quantification so that the direct label-free aptasensing approach is practical. The difficulty in screening ssDNA sequences for small molecules is expected to be solved with the immobilization-free aptamer selection. The ssDNA functional structures towards the antibiotics can be selected through the assistance of graphene oxide (GO). The developed GO-SELEX along with the designed electrochemical aptasensing platform demonstrates a universal aptasensing model for any desired small molecule targets.

The dissertation works focus on the improvements of electrical behaviors of biosensing surface and biological recognition efficiency of aptamers. The main objectives of this research are listed below:

(1) Design an electrochemical sensing platform with surface modifications of synthesized rGO and AuNPs,

(2) Prepare the self-assembled TDN *via* a temperature-controlled protocol,

(3) Develop a TDN-based aptasensor for ultrasensitive ampicillin detection in real milk samples,

(4) Select ssDNA aptamer sequences with high affinity to penicillin G using GO-SELEX procedure,

(5) Perform sensitive and selective penicillin G quantification in milk samples using the designed TDN-based aptasensor with selected aptamer sequence.

References

Administration, U. S. F. D. (2018). Summary Report on Antimicrobials Sold or Distributed for Use in Food-Producing Animals Retrieved from https://www.fda.gov/media/133411/download

Alarcon-Angeles, G., Álvarez-Romero, G. A., & Merkoçi, A. (2018). Electrochemical Biosensors: Enzyme Kinetics and Role of Nanomaterials. In K. Wandelt (Ed.), *Encyclopedia of Interfacial Chemistry* (pp. 140-155). Oxford: Elsevier.

Bar, D., Tauer, L. W., Bennett, G., Gonzalez, R. N., Hertl, J. A., Schukken, Y. H., . . . Grohn, Y. T. (2008). The cost of generic clinical mastitis in dairy cows as estimated by using dynamic programming. *Journal of Dairy Science, 91*(6), 2205-2214. doi:10.3168/jds.2007-0573

Berendsen, B. J. A., Wegh, R. S., Memelink, J., Zuidema, T., & Stolker, L. A. M. (2015). The analysis of animal faeces as a tool to monitor antibiotic usage. *Talanta, 132*, 258-268. doi:https://doi.org/10.1016/j.talanta.2014.09.022

Bishop, J. R., Bodine, A. B., O'Dell, G. D., & Janzen, J. J. (1985). Quantitative Assay for Antibiotics Used Commonly in Treatment of Bovine Infections1. *Journal of Dairy Science, 68*(11), 3031-3036. doi:https://doi.org/10.3168/jds.S0022-0302(85)81198-X

Briscoe, S. E., McWhinney, B. C., Lipman, J., Roberts, J. A., & Ungerer, J. P. J. (2012). A method for determining the free (unbound) concentration of ten beta-lactam antibiotics in human plasma using high performance liquid chromatography with ultraviolet detection. *Journal of Chromatography B, 907*, 178-184. doi:https://doi.org/10.1016/j.jchromb.2012.09.016

Cho, I.-H., Kim, D. H., & Park, S. (2020). Electrochemical biosensors: perspective on functional nanomaterials for on-site analysis. *Biomaterials Research, 24*(1), 6. doi:10.1186/s40824-019-0181-y

Clark, L. C., Jr., & Lyons, C. (1962). Electrode systems for continuous monitoring in cardiovascular surgery. *Ann N Y Acad Sci, 102*, 29-45. doi:10.1111/j.1749-6632.1962.tb13623.x

Darmostuk, M., Rimpelova, S., Gbelcova, H., & Ruml, T. (2015). Current approaches in SELEX: An update to aptamer selection technology. *Biotechnology advances, 33*(6), 1141-1161.

Detilleux, J., Kastelic, J. P., & Barkema, H. W. (2015). Mediation analysis to estimate direct and indirect milk losses due to clinical mastitis in dairy cattle. *Preventive Veterinary Medicine, 118*(4), 449-456. doi:https://doi.org/10.1016/j.prevetmed.2015.01.009

Du, B., Wen, F., Guo, X., Zheng, N., Zhang, Y., Li, S., . . . Xu, Q. (2019). Evaluation of an ELISA-based visualization microarray chip technique for the detection of veterinary antibiotics in milk. *Food Control, 106*, 106713.

du Preez, J. H. (2000). Bovine mastitis therapy and why it fails. *J S Afr Vet Assoc, 71*(3), 201-208. Retrieved from https://www.ncbi.nlm.nih.gov/pubmed/11205172

Duarte, C. M., Freitas, P. P., & Bexiga, R. (2015). Technological advances in bovine mastitis diagnosis: an overview. *J Vet Diagn Invest, 27*(6), 665-672. doi:10.1177/1040638715603087

Edqvist, L. E., & Pedersen, K. B. r. (2002). *Antimicrobials as growth promoters : resistance to common sense*.

Eggins, B. R. (2013). *Biosensors: an introduction*: Springer-Verlag.

Feng, Q.-M., Zhou, Z., Li, M.-X., Zhao, W., Xu, J.-J., & Chen, H.-Y. (2017). DNA tetrahedral scaffolds-based platform for the construction of electrochemiluminescence biosensor. *Biosensors and Bioelectronics, 90*, 251-257.

Founou, L. L., Founou, R. C., & Essack, S. Y. (2016). Antibiotic Resistance in the Food Chain: A Developing Country-Perspective. *Front Microbiol, 7*, 1881. doi:10.3389/fmicb.2016.01881

Gomes, F., & Henriques, M. (2016). Control of Bovine Mastitis: Old and Recent Therapeutic Approaches. *Curr Microbiol, 72*(4), 377-382. doi:10.1007/s00284-015-0958-8

Gonçalves, L. M., Callera, W. F. A., Sotomayor, M. D. P. T., & Bueno, P. R. (2014). Penicillinase-based amperometric biosensor for penicillin G. *Electrochemistry Communications, 38*, 131-133. doi:https://doi.org/10.1016/j.elecom.2013.11.022

Halasa, T., Nielen, M., De Roos, A. P. W., Van Hoorne, R., de Jong, G., Lam, T. J. G. M., . . . Hogeveen, H. (2009). Production loss due to new subclinical mastitis in Dutch dairy cows estimated with a test-day model (vol 92, pg 599, 2009). *Journal of Dairy Science, 92*(3), 1315-1315. doi:10.3168/jds.2009-92-3-1315

Hayat, A., Catanante, G., & Marty, J. L. (2014). Current Trends in Nanomaterial-Based Amperometric Biosensors. *Sensors, 14*(12), 23439-23461. Retrieved from https://www.mdpi.com/1424-8220/14/12/23439

Hong, F., Chen, X., Cao, Y., Dong, Y., Wu, D., Hu, F., & Gan, N. (2018). Enzyme- and label-free electrochemical aptasensor for kanamycin detection based on double stir bar-assisted toehold-mediated strand displacement reaction for dual-signal amplification. *Biosensors and Bioelectronics, 112*, 202-208. doi:https://doi.org/10.1016/j.bios.2018.04.017

Junza, A., Montané, A., Barbosa, J., Minguillón, C., & Barrón, D. (2014). High resolution mass spectrometry in the identification of transformation products and metabolites from β-lactam antibiotics in thermally treated milk. *Journal of Chromatography A, 1368*, 89-99. doi:https://doi.org/10.1016/j.chroma.2014.09.056

Kim, D.-M., Rahman, M. A., Do, M. H., Ban, C., & Shim, Y.-B. (2010). An amperometric chloramphenicol immunosensor based on cadmium sulfide nanoparticles modified-dendrimer bonded conducting polymer. *Biosensors and Bioelectronics, 25*(7), 1781-1788. doi:https://doi.org/10.1016/j.bios.2009.12.024

Kim, Y. S., Raston, N. H. A., & Gu, M. B. (2016). Aptamer-based nanobiosensors. *Biosensors and Bioelectronics, 76*, 2-19.

Kissinger, P. T. (2005). Biosensors—a perspective. *Biosensors and Bioelectronics, 20*(12), 2512-2516. doi:https://doi.org/10.1016/j.bios.2004.10.004

Lan, L., Yao, Y., Ping, J., & Ying, Y. (2017). Recent advances in nanomaterial-based biosensors for antibiotics detection. *Biosensors and Bioelectronics, 91*, 504-514. doi:https://doi.org/10.1016/j.bios.2017.01.007

Lan, L., Yao, Y., Ping, J., & Ying, Y. (2017). Recent advances in nanomaterial-based biosensors for antibiotics detection. *Biosensors & Bioelectronics, 91*, 504-514. doi:10.1016/j.bios.2017.01.007

Leibovici, L., Paul, M., Garner, P., Sinclair, D. J., Afshari, A., Pace, N. L., . . . Tovey, D. (2016). Addressing resistance to antibiotics in systematic reviews of antibiotic interventions. *J Antimicrob Chemother, 71*(9), 2367-2369. doi:10.1093/jac/dkw135

Li, D., Yang, M., Hu, J., Zhang, Y., Chang, H., & Jin, F. (2008). Determination of penicillin G and its degradation products in a penicillin production wastewater treatment plant and the receiving river. *Water Res, 42*(1-2), 307-317. doi:10.1016/j.watres.2007.07.016

Liu, X., Zheng, S., Hu, Y., Li, Z., Luo, F., & He, Z. (2016). Electrochemical Immunosensor Based on the Chitosan-Magnetic Nanoparticles for Detection of Tetracycline. *Food Analytical Methods, 9*(10), 2972-2978. doi:10.1007/s12161-016-0480-z

Liu, Y., Yan, K., Okoth, O. K., & Zhang, J. (2015). A label-free photoelectrochemical aptasensor based on nitrogen-doped graphene quantum dots for chloramphenicol determination. *Biosensors and Bioelectronics, 74*, 1016-1021. doi:https://doi.org/10.1016/j.bios.2015.07.067

Magar, H. S., Hassan, R. Y. A., & Mulchandani, A. (2021). Electrochemical Impedance Spectroscopy (EIS): Principles, Construction, and Biosensing Applications. *Sensors (Basel, Switzerland), 21*(19), 6578. doi:10.3390/s21196578

Majdinasab, M., Mishra, R. K., Tang, X., & Marty, J. L. (2020). Detection of antibiotics in food: New achievements in the development of biosensors. *TrAC Trends in Analytical Chemistry, 127*, 115883. doi:https://doi.org/10.1016/j.trac.2020.115883

Paige, J. C., Tollefson, L., & Miller, M. A. (1999). Health implications of residues of veterinary drugs and chemicals in animal tissues. *Vet Clin North Am Food Anim Pract, 15*(1), 31-43, viii. Retrieved from https://www.ncbi.nlm.nih.gov/pubmed/10088210

Payne, M. A., Craigmill, A., Riviere, J. E., & Webb, A. I. (2006). Extralabel use of penicillin in food animals. *J Am Vet Med Assoc, 229*(9), 1401-1403. doi:10.2460/javma.229.9.1401

Pennacchio, A., Varriale, A., Scala, A., Marzullo, V. M., Staiano, M., & D'Auria, S. (2016). A novel fluorescence polarization assay for determination of penicillin G in milk. *Food Chemistry, 190*, 381-385.

Pérez-López, B., & Merkoçi, A. (2011). Nanomaterials based biosensors for food analysis applications. *Trends in Food Science & Technology, 22*(11), 625-639. doi:https://doi.org/10.1016/j.tifs.2011.04.001

Pietrzyk, D. J., & Frank, C. W. (1979). Chapter Twenty-Eight - Introduction to Electrochemistry. In D. J. Pietrzyk & C. W. Frank (Eds.), *Analytical Chemistry* (pp. 581-597): Academic Press.

Poghossian, A., Jablonski, M., Koch, C., Bronder, T. S., Rolka, D., Wege, C., & Schöning, M. J. (2018). Field-effect biosensor using virus particles as scaffolds for enzyme immobilization. *Biosensors and Bioelectronics, 110*, 168-174. doi:https://doi.org/10.1016/j.bios.2018.03.036

Pohanka, M., & Skládal, P. (2008). Electrochemical biosensors--principles and applications. *Journal of applied biomedicine, 6*(2).

Qian, L., Durairaj, S., Prins, S., & Chen, A. (2021). Nanomaterial-based electrochemical sensors and biosensors for the detection of pharmaceutical compounds. *Biosensors and Bioelectronics, 175*, 112836.

Qin, X., Yin, Y., Yu, H., Guo, W., & Pei, M. (2016). A novel signal amplification strategy of an electrochemical aptasensor for kanamycin, based on thionine functionalized graphene and hierarchical nanoporous PtCu. *Biosensors and Bioelectronics, 77*, 752-758. doi:https://doi.org/10.1016/j.bios.2015.10.050

Rebe Raz, S., Bremer, M. G., Haasnoot, W., & Norde, W. (2009). Label-free and multiplex detection of antibiotic residues in milk using imaging surface plasmon resonance-based immunosensor. *Analytical Chemistry, 81*(18), 7743-7749.

Rezaei, B., & Irannejad, N. (2019). Chapter 2 - Electrochemical detection techniques in biosensor applications. In A. A. Ensafi (Ed.), *Electrochemical Biosensors* (pp. 11-43): Elsevier.

Rollin, E., Dhuyvetter, K. C., & Overton, M. W. (2015). The cost of clinical mastitis in the first 30 days of lactation: An economic modeling tool. *Preventive Veterinary Medicine, 122*(3), 257-264. doi:https://doi.org/10.1016/j.prevetmed.2015.11.006

Ronkainen, N. J., Halsall, H. B., & Heineman, W. R. (2010). Electrochemical biosensors. *Chemical society reviews, 39*(5), 1747-1763.

Rosati, G., Ravarotto, M., Scaramuzza, M., De Toni, A., & Paccagnella, A. (2019). Silver nanoparticles inkjet-printed flexible biosensor for rapid label-free antibiotic detection in milk. *Sensors and Actuators B: Chemical, 280*, 280-289. doi:https://doi.org/10.1016/j.snb.2018.09.084

Santos, S. M., Henriques, M., Duarte, A. C., & Esteves, V. I. (2007). Development and application of a capillary electrophoresis based method for the simultaneous screening of six antibiotics in spiked milk samples. *Talanta, 71*(2), 731-737. doi:10.1016/j.talanta.2006.05.049

Sharma, A., Catanante, G., Hayat, A., Istamboulie, G., Ben Rejeb, I., Bhand, S., & Marty, J. L. (2016). Development of structure switching aptamer assay for detection of aflatoxin M1 in milk sample. *Talanta, 158*, 35-41. doi:10.1016/j.talanta.2016.05.043

Song, S., Wang, L., Li, J., Fan, C., & Zhao, J. (2008). Aptamer-based biosensors. *TrAC Trends in Analytical Chemistry, 27*(2), 108-117. doi:https://doi.org/10.1016/j.trac.2007.12.004

Sui, C., Zhou, Y., Wang, M., Yin, H., Wang, P., & Ai, S. (2018). Aptamer-based photoelectrochemical biosensor for antibiotic detection using ferrocene modified DNA as both aptamer and electron donor. *Sensors and Actuators B: Chemical, 266*, 514-521. doi:https://doi.org/10.1016/j.snb.2018.03.171

U.S. Food and Drug Administration. Center for Veterinary Medicine. Milk drug residue sampling survey. (2015).

United States Department of Agriculture, F. S. a. I. S., Office of Public Health Science. (2010). Bioassay for the Detection, Identification and Quantitation of Antimicrobial Residues in Meat and Poultry Tissue. Retrieved from https://www.fsis.usda.gov/wps/wcm/connect/2fe04085-1d55-46ea-bcab-2dcdc5adeed5/MLG_34_03.pdf?MOD=AJPERES

Wassenaar, T. M. (2005). Use of antimicrobial agents in veterinary medicine and implications for human health. *Crit Rev Microbiol, 31*(3), 155-169. doi:10.1080/10408410591005110

Wegener, H. C. (2003). Antibiotics in animal feed and their role in resistance development. *Curr Opin Microbiol, 6*(5), 439-445. doi:10.1016/j.mib.2003.09.009

Wei, Q., Zhao, Y., Du, B., Wu, D., Li, H., & Yang, M. (2012). Ultrasensitive detection of kanamycin in animal derived foods by label-free electrochemical immunosensor. *Food Chemistry, 134*(3), 1601-1606. doi:https://doi.org/10.1016/j.foodchem.2012.02.126

Yan, K., Liu, Y., Yang, Y., & Zhang, J. (2015). A Cathodic "Signal-off" Photoelectrochemical Aptasensor for Ultrasensitive and Selective Detection of Oxytetracycline. *Analytical Chemistry, 87*(24), 12215-12220. doi:10.1021/acs.analchem.5b03139

Yang, S., Zhu, X., Wang, J., Jin, X., Liu, Y., Qian, F., . . . Chen, J. (2015). Combustion of hazardous biological waste derived from the fermentation of antibiotics using TG–FTIR and Py–GC/MS techniques. *Bioresource Technology, 193*, 156-163. doi:https://doi.org/10.1016/j.biortech.2015.06.083

Yin, J., Guo, W., Qin, X., Zhao, J., Pei, M., & Ding, F. (2017). A sensitive electrochemical aptasensor for highly specific detection of streptomycin based on the porous carbon

nanorods and multifunctional graphene nanocomposites for signal amplification. *Sensors and Actuators B: Chemical, 241*, 151-159. doi:https://doi.org/10.1016/j.snb.2016.10.062

Zamfir, L.-G., Puiu, M., & Bala, C. (2020). Advances in electrochemical impedance spectroscopy detection of endocrine disruptors. *Sensors, 20*(22), 6443.

Zeng, D., Zhang, H., Zhu, D., Li, J., San, L., Wang, Z., . . . Zuo, X. (2015). A novel ultrasensitive electrochemical DNA sensor based on double tetrahedral nanostructures. *Biosensors and Bioelectronics, 71*, 434-438.

Zhao, J., Guo, W., Pei, M., & Ding, F. (2016). GR–Fe 3 O 4 NPs and PEDOT–AuNPs composite based electrochemical aptasensor for the sensitive detection of penicillin. *Analytical Methods, 8*(22), 4391-4397.

Zhou, L., Li, D.-J., Gai, L., Wang, J.-P., & Li, Y.-B. (2012). Electrochemical aptasensor for the detection of tetracycline with multi-walled carbon nanotubes amplification. *Sensors and Actuators B: Chemical, 162*(1), 201-208. doi:https://doi.org/10.1016/j.snb.2011.12.067

Zhou, Y., Li, F., Wu, H., Chen, Y., Yin, H., Ai, S., & Wang, J. (2019). Electrochemical aptasensing strategy for kanamycin detection based on target-triggered single-strand DNA adsorption on MoS2 nanosheets and enzymatic signal amplification. *Sensors and Actuators B: Chemical, 296*, 126664. doi:https://doi.org/10.1016/j.snb.2019.126664

Zhu, Y., Chandra, P., Song, K.-M., Ban, C., & Shim, Y.-B. (2012). Label-free detection of kanamycin based on the aptamer-functionalized conducting polymer/gold nanocomposite. *Biosensors and Bioelectronics, 36*(1), 29-34. doi:https://doi.org/10.1016/j.bios.2012.03.034

Chapter 2. Background Information and Literature Review

2.1 Introduction

This chapter provides a comprehensive literature review of basic concepts of electrochemical biosensors for antibiotic detection, nanomaterial and DNA nanotechnology, oligonucleotide sensing probes (aptamers), and Systematic Evolution of Ligands by Exponential enrichment (SELEX). In this review, the merits and limitations of electrochemical biosensors will be evaluated, the improvement strategies using aptamer functionalization and nanomaterials-nanotechnology modifications will be addressed, and the demand for effective aptamer sequences will be discussed.

2.2 Electrochemical biosensors

A biosensor is defined as a device where a biological recognition element is built-in for sensing purposes (Kissinger, 2005). The most common biological recognition elements are antibodies, enzymes, and oligonucleotides, which can be sensitive and selective for given targets and usually be physically attached or confined on or within the biosensor (Eggins, 2013). Electrochemical techniques have been combined with biosensors to create a fast, accurate, reliable, and cost-effective method for a qualitative and quantitative determination of a wide range of target analytes (Cho, Kim, & Park, 2020). The appearance of target analytes is converted to electrical signals through physicochemical transducers and detected by various electrochemical characterization techniques such as cyclic voltammetry (CV), differential pulse voltammetry (DPV), square wave voltammetry (SWV), and electrochemical impedance spectroscopy (EIS) (Pohanka & Skládal, 2008). Since the original electrochemical biosensor was invented to continually monitor blood glucose during cardiovascular surgery (Clark & Lyons, 1962), a

massive number of electrochemical biosensors have been generated and commercialized for diverse applications (Ronkainen, Halsall, & Heineman, 2010). Based on the types of signal transduction, the electrochemical biosensors can be classified as amperometric, voltammetric, impedimetric, and photoelectrochemical biosensors (Lingyi Lan, Yao Yao, Jianfeng Ping, & Yibin Ying, 2017). Herein, we review recent advances in biosensing applications for antibiotics based on the classification of these types of electrochemical biosensors (**Table 2.1**)

The working scheme of amperometric biosensors is to measure the electrical current response versus time (*i* - *t*) at a constant electric potential, which is generated by an enzymatic redox reaction of electroactive substances on the electrode surface (Alarcon-Angeles, Álvarez-Romero, & Merkoçi, 2018). The magnitude of current change is considered to be correlated to the concentration of analytes (Hayat, Catanante, & Marty, 2014). A chloramphenicol immunosensor was reported based on the competitive immune interaction between the free and labeled chloramphenicol for the antibody binding site on the sandwich structure built by surface nanocomposite modifications and modified-cadmium quantum dots (D.-M. Kim, Rahman, Do, Ban, & Shim, 2010). The electrical signal was generated by the hydrazine catalyzed H_2O_2 reduction reaction, while the labeled chloramphenicol was captured on the electrode surface. A label-free immunosensor was designed with the signal amplification by the nanocomposites of graphene sheet-Nafion, thionine, and Pt nanoparticles (Wei et al., 2012). The immune binding of the antibody to kanamycin inhibited the electron transferring resulting in a current deduction. Gonçalves et al. proposed a penicillase based immunosensor for penicilin G detection (Gonçalves, Callera, Sotomayor, & Bueno, 2014). The penicillase was connected to the electrode surface *via* a cysteine self-assembled monolayer, and a current signal was generated as a response to catalytic hydrolysis of penicillin G.

The voltammetric biosensors, however, identify the analytes by measuring the current signals of electroactive substances at the specific voltammetric peak, while the working electrode is interrogated by varying potentials (Rezaei & Irannejad, 2019). The most commonly used voltammetric techniques are CV, DPV, and SWV, while CV is often used to characterize the target analytes and DPV and SWV are mostly reported as quantitative determination methods (Pietrzyk & Frank, 1979). In these methods, $Fe(CN)_6^{3-}/Fe(CN)_6^{4-}$ redox pair is a common substance for the electric current generation, as a tetracycline aptamer-based biosensor was proposed to monitor electrochemical signals from this electroactive redox pair with multi-walled carbon nanotubes (MWCNTs) modification (L. Zhou, Li, Gai, Wang, & Li, 2012). In the other reported work, the electrical signal from the same redox pair was amplified by a novel deliciated nanocomposite formed by porous carbon nanorods (PCNR) and multifunctional graphene composite (GR–Fe_3O_4–AuNPs) to produce a stronger response current for streptomycin detection (Yin et al., 2017). An ultrasensitive kanamycin detection was achieved by a deliciated electrode fabrication approach based on thionine functionalized graphene (GR-TH) and hierarchical nanoporous (HNP) PtCu alloy (Qin, Yin, Yu, Guo, & Pei, 2016). Methylene blue (MB) is a competitive rival as the redox indicator. Hong et al. presented a dual-signal amplification based on the hybridization chain reaction and used MB as redox probes to produce the current change for ultrasensitive kanamycin quantification (Hong et al., 2018). In addition, MB is capable of coupling with other amplifiers to reach a low limit of detection (LOD), for example, MB was intercalated into the double-helix DNA and further enhanced the kanamycin signal by forming an aptamer-based Y-shape dsDNA (Y. Zhou et al., 2019).

Impedimetric biosensors work based on transducing the biological binding information to interfacial impedimetric properties, i.e. double-layer capacitance, charge transfer resistance,

solution resistance, and substance diffusion of an electrochemical system (Magar, Hassan, & Mulchandani, 2021). EIS is used as a label-free sensing tool to extract this impedimetric information from antibiotic detections. The impedimetric biosensors often require surface modifications by conducting polymers or nanocomposites to achieve high sensitive quantifications, for example, self-assembling poly-[2, 5-di-(2-thienyl)-1H-pyrrole-1-(p-benzoic acid)] (poly-DPB) on AuNPs (Zhu, Chandra, Song, Ban, & Shim, 2012), chitosan-carboxyl-Fe_3O_4 nanoparticles (CS-MNPs) (X. Liu et al., 2016), magnetic graphene nanocomposite (GR–Fe_3O_4NPs) and a poly(3,4-ethylenedioxythiophene) - gold nanoparticles composite (PEDOT–AuNPs) (Zhao, Guo, Pei, & Ding, 2016), nanotubular *tobacco mosaic virus* (TMV) (Poghossian et al., 2018), and silver nanoparticles (Rosati, Ravarotto, Scaramuzza, De Toni, & Paccagnella, 2019). EIS-based impedimetric biosensors have been proven to be an effective label-free tool with a high signal-to-noise ratio for real sample detections (Zamfir, Puiu, & Bala, 2020).

Photoelectrochemical biosensors combine the conventional biological recognition elements with photoactive materials to construct a novel photocurrent signal generation route. Several photoelectrochemical biosensors were proposed employing aptamers as recognition probes to specifically bind to the target antibiotics, and transducing photon irradiation to electrical signals *via* photoactive nanocomposites under visible light illumination, for instance, p-type semiconductor BiOI doped graphene (Yan, Liu, Yang, & Zhang, 2015), nitrogen-doped graphene quantum dots (N-G QDs) (Y. Liu, Yan, Okoth, & Zhang, 2015), and graphite-like carbon nitride (g-C_3N_4) (Sui et al., 2018).

In order to develop more sensitive, miniaturized, and reliable electrochemical biosensors, nanomaterial modifications have become a major trend in platform design. A variety of novel nanomaterials or integration of various nanomaterials have been utilized in biosensing applications,

which offers better physical and chemical properties and unique biological functions of biosensing surface. In addition, the development of biorecognition elements is the other challenge for electrochemical biosensors. The expectation of biosensing probes to be highly sensitive and selective as well as flexible and stable in various detecting environments limits the electrochemical biosensor from building an effective route analysis.

Table 2.1. A list of electrochemical biosensors for antibiotic detections

Sensor type	Target	Nanomaterial modifications	Linear range	LOD	Reference
Amperometric	Chloramphenicol	CdS QDs, AuNPs, poly-TTCA, dendrimers	50 to 950 pg/mL	45 pg/mL	(Kim, Rahman, Do, Ban, & Shim, 2010)
	Kanamycin	GS-Nafion, PtNPs,	0.01 to 12.0 ng/mL	5.74 pg/mL	(Wei et al., 2012)
	Penicillin G	cysteine SAM	10–50 nM	4.5 nM	(Gonçalves, Callera, Sotomayor, & Bueno, 2014)
Voltametric	Tetracycline	MWCNTs	10 to 50000 nM	5 nM	(L. Zhou, Li, Gai, Wang, & Li, 2012)
	Kanamycin	GR-TH, HNP-PtCu	0.005 to 50 ng/mL	0.42 pg/mL	(Qin, Yin, Yu, Guo, & Pei, 2016)
	Streptomycin	PCNR, GR- Fe_3O_4-AuNPs,	0.05 to 200 ng/mL	0.028 ng/mL	(Yin et al., 2017)
	Kanamycin	N.A.	0.05 to 50000 pM	16 fM	(Hong et al., 2018)

	Kanamycin	MoS_2 nanosheet	0.1 to 100 nM	29 pM	(Y. Zhou et al., 2019)
	Chloramphenicol Ciprofloxacin	AuNPs/carbon nitride/graphene nanocomposite	0.7 to 120 μM 0.2 to 120 μM	27 nM 420 nM	(Yuan, Zhang, Wang, Gao, & Wang, 2018)
Impedimetric	Kanamycin	AuNPs, Poly-DPB	0.05 to 9.0 μM	9.4 nM	(Zhu, Chandra, Song, Ban, & Shim, 2012)
	Tetracycline	CS-MNPs	0.08 to 1 ng/mL	0.0321 ng/mL	(X. Liu et al., 2016)
	Penicillin	GR-Fe_3O_4NPs, PEDOT-AuNPs	0.1 to 200 ng/mL	0.057 ng/mL	(Zhao, Guo, Pei, & Ding, 2016)
	Penicillin	TMV nanotube	0.1 to 10 mM	50 μM	(Poghossian et al., 2018)
	Ampicillin	AgNPs	100 to 10000 μg/mL	10 μg/mL	(Rosati, Ravarotto, Scaramuzza, De Toni, & Paccagnella, 2019)
Photo-electrochemical	Oxytetracycline	BiOI doped graphene	4.0 to 150 nM	0.9 nM	(Yan, Liu, Yang, & Zhang, 2015)
	Chloramphenicol	N-G QDs,	10 to 250 nM	3.1 nM	(Y. Liu, Yan, Okoth, & Zhang, 2015)
	Chloramphenicol	g-C_3N_4	0.01 to 100 nM	0.22 pM	(Sui et al., 2018)

2.3 Nanomaterials in biosensing applications

Nanoscale materials have attracted major attention due to their unique properties from the size and shape effects offering a great potential to develop and improve the performance of electrical and electronic devices (Joseph Wang, 2005). Nanoscale materials have a surprisingly long history of being prepared and used as synthetic pigments by humans back at an ancient age more than four thousand years ago (Heiligtag & Niederberger, 2013). The first reported chemical synthesis of nanoparticles for scientific purpose was colloidal AuNPs by Michael Faraday in 1857 (Jeevanandam, Barhoum, Chan, Dufresne, & Danquah, 2018). In addition, he firstly revealed a fascinating fact that the nanosized Au colloid has completely different physical properties compared to its bulk material. Since then, the new nanomaterials synthesis and characterizations have always been an intriguing development for nanotechnology applications (S. H. Lee, Sung, & Park, 2012). Upon the discovery of various nanomaterials, the unique physical and chemical properties such as tailorable sizes and shapes, surface plasmon resonance, electrical and thermal conductivity, optical characteristics, and catalytic activity, have been exploited for biosensing applications (Lan, Yao, Ping, & Ying, 2017). Nanomaterial-based biosensors exhibit significant advantages over the conventional bio-recognizing process, including diverse transformed signals in the form of electrical, thermal, or optical outputs, high sensitivity and specificity, flexibility to surface modifications, and wide ranges of sensing targets (Qian, Durairaj, Prins, & Chen, 2021). The nanomaterial-based electrochemical biosensor has an intuitive analysis scheme (**Figure 2.1**), where the appearance of substrates is transduced to a detectable electrochemical signal by the biological binding molecules, such as enzyme, antibody, or aptamer (Cho, Kim, & Park, 2020). Generally, the output signal needs amplification to generate a sensitive and accurate analytical

result. Thus, researchers utilize the nanomaterial to construct the electrode, modify the detecting interface, or design the sensing probe (Maduraiveeran, Sasidharan, & Ganesan, 2018).

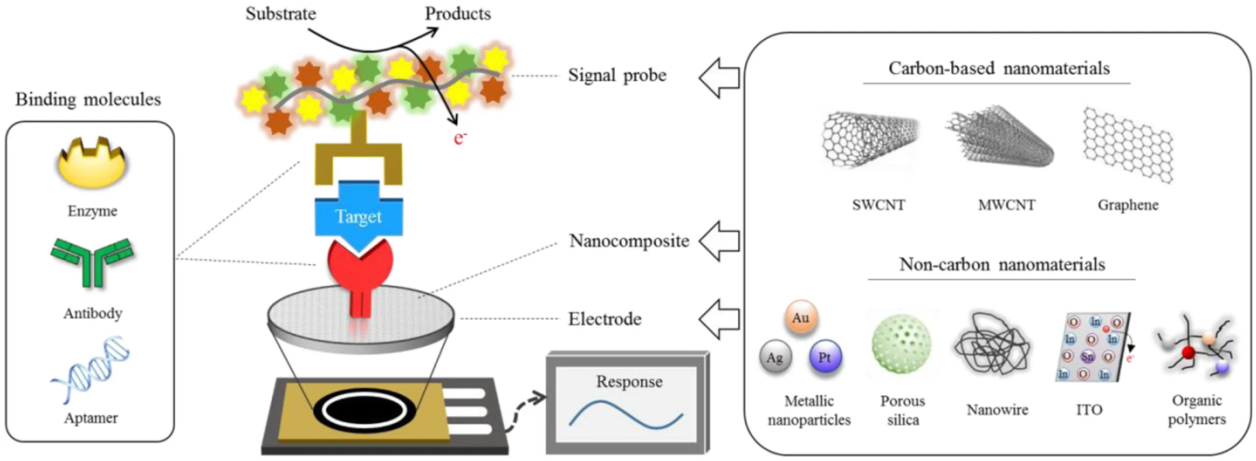

Figure 2.1. Analytical principle of electrochemical biosensor based on nanomaterials (Cho et al., 2020)

Carbon-based nanomaterials have been the most commonly used nanomaterial for the biosensing planform designs, due to their low cost and unique physicochemical properties, i.e. high surface to volume ratio, electrical conductivity, small background signal, large potential window, nice biocompatibility, and mechanical strength (Kour et al., 2020). Scientists have developed a variety of carbon nanomaterials, including carbon nanotubes (CNTs), graphene, graphene oxide (GO), reduced graphene oxide (rGO), and graphene-based quantum dots.

CNTs can be further divided into signal-wall carbon nanotubes (SWCNT), which is considered a molecular wire with every atom on the surface, and multi-wall carbon nanotubes, which is a cylindrical nanostructure of multiple nanotubes nested inside one another (Joseph Wang, 2005). Because of the large surface area and capability of surface customization, CNTs were used to covalently or non-covalently linked to the biosensing molecules and then attached to the working surface to enhance the electrochemical performance by controlling the density and

orientation of biomolecules and electron transferring efficiency of electrode surface (Y.-C. Wang, Cokeliler, & Gunasekaran, 2015; J. Yang, Zhang, & Gunasekaran, 2010; L. Zhou, Li, Gai, Wang, & Li, 2012).

Graphene is a typical two-dimensional carbon nanostructure, which can be produced by a 'top-down' method *via* chemical or electrochemical exfoliation of bulky graphite (Sadak, Prathap, & Gunasekaran, 2019) or a 'bottom-up' method via chemical vapor deposition of CH_4 (Deokar et al., 2015). Because of the large surface area, excellent electron transmission capacity, and good catalytic behavior of biomolecules, it quickly becomes a popular building block for electrochemical biosensors (Shao et al., 2010). Zhao et al. employed the graphene sheet as a building base to combine Prussian blue-chitosan and nanoporous gold, and utilized this nanocomposite to modify an immunosensor for kanamycin detection (B. Y. Zhao et al., 2011). Qin et al. constructed the kanamycin aptasensor using thionine functionalized graphene doped with hierarchical nanoporous (HNP) PtCu alloy (Qin, Yin, Yu, Guo, & Pei, 2016). Yuan et al. improved the performance of a chloramphenicol and ciprofloxacin biosensor by a graphene/carbon nitride/AuNPs nanocomposite (Yuan, Zhang, Wang, Gao, & Wang, 2018).

GO is a cost-effective alternative to graphene, which can be simply and rapidly synthesized by the chemical oxidation of graphite with a very low production cost (J. Chen, Yao, Li, & Shi, 2013). The structural defects of GO with oxidative functional groups can be further removed by an electrochemical reduction (Guan, He, & Gunasekaran, 2022). Due to the structural comparability of rGO to graphene, rGO shares similar physical and chemical properties, which makes it a good electrode modification option (J. Yang & Gunasekaran, 2013). Various electrochemical biosensors were reported based on rGO modification, showing fascinating electron transferring capacity and great compatibility with other nanoparticles, i.e. AuNPs (L. Lu,

Seenivasan, Wang, Yu, & Gunasekaran, 2016), silver nanoparticles (Y. Guo et al., 2019), cuprous nanoparticles (Z. Yang et al., 2019), and nickel nanoparticles (J. Yang, Yu, Rudi Strickler, Chang, & Gunasekaran, 2013).

AuNPs have been the most widely used noble metal nanoparticles for the biosensing platform construction due to their excellent electrical conductivity, great biocompatibility, chemical stability, and high catalytic activity (Giljohann et al., 2020). Additionally, AuNPs can be simply synthesized by various chemical reduction methods in several shapes to suit the diverse requirements of different applications, and are easily fabricated on different surfaces (L. Lu & Gunasekaran, 2019). In some scenarios, AuNPs are modified on the electrode surface, intercalated in the nanocomposite, or attached to sensing probe terminals to assist in transferring electrons from substrates to the electrode surface (Kim, Rahman, Do, Ban, & Shim, 2010; L. Lu et al., 2016; Yin et al., 2017; Zhu, Chandra, Song, Ban, & Shim, 2012). For another detection scheme, AuNPs act as a crosslinker using their biocompatibility to fix the biosensing probes on the electrode surface (Guan et al., 2022; J. Zhao, Guo, Pei, & Ding, 2016).

2.4 Tetrahedral DNA nanostructures

DNA nanostructure has become a promising building block over the last decade due to its nanoscale size, excellent programmability, high surface accessibility and biocompatibility, and self-assembly principle (Xie et al., 2017). Because of its tailorable size and shape, a variety of DNA nanostructure was reported and applied to various scenarios, including chemical biology, analytical chemistry, disease diagnostics, and therapeutics (Bujold, Lacroix, & Sleiman, 2018). The tetrahedral DNA nanostructure (TDN), a rigid three-dimensional nanoscale structure with six edges and four vertices, was first reported by Turberfield's group (Goodman, Berry, & Turberfield,

2004; Goodman et al., 2005). The TDN can be synthesized by a simple temperature-controlled self-assembly approach, consisting of four single-stranded DNA (ssDNA) sequences that are partially complementary to one another (Gao et al., 2021). The size of TDN, depending on the size of ssDNA that constitute one of four faces of the tetrahedron, is highly programmable by adjusting the sequence length, which is usually under ten nanometers on each side (Pei, Zuo, Zhu, Huang, & Fan, 2014). Thus, TDN has become very popular in biological applications (**Figure 2.2**).

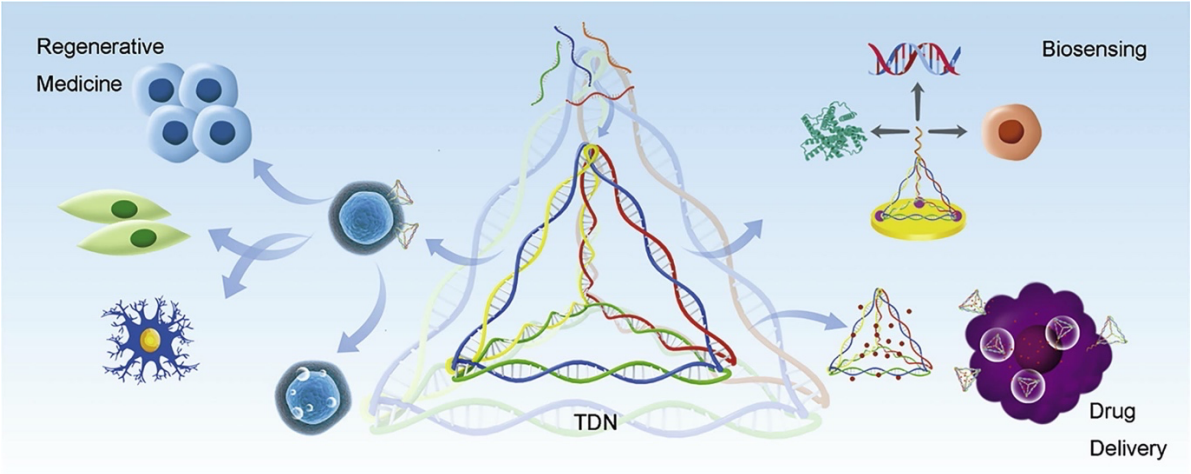

Figure 2.2. Biological applications of self-assembled TDN (S. Li, Tian, Zhang, Cai, & Lin, 2019)

The high programmability and decorated accessibility of all four vertices and six edges make TDN an ideal biomolecule carrier for cellular research and drug delivery in disease diagnostics and therapeutics (Walsh, Yin, Erben, Wood, & Turberfield, 2011). The nanoscale size of TDN and the ability to independently penetrate cellular membrane through endocytic internalization offers single-cell level delivery in medical applications (Liang et al., 2014). The biological and thermal stability and structure rigidity help TDN maintain the structural integrity and functionality during the *in vivo* analysis by resisting the nuclease degradation (Zhang et al., 2020). Moreover, TDN has little cytotoxicity to the living cells and organisms compared to nanomaterials (J. Li, Fan, Pei, Shi, & Huang, 2013). To this day, many researchers reported therapeutic applications of TDN to

precisely control the delivery route to the living cells and the types of carrying biomolecules, i.e., anti-cancer molecules, siRNA, antibodies, peptides, and photosensitizer. (Xie et al., 2017).

Because of its surface accessibility and biocompatibility, TDN can also be integrated into the delicate biosensing platform with other nanomaterials, biorecognition molecules, and functional oligonucleotide structures, such as aptamers (Wen et al., 2011), antibodies (X. Chen et al., 2014), microRNAs (Lin et al., 2014), G-Quadruplex (J. Lu et al., 2019), and proteins (Lin et al., 2016). TDN can be easily anchored on the solid surface through the functionalized vertices, for example, thiol group modified vertices help fix TDN on the gold surface *via* covalent Au-S bonds (Abi et al., 2014). The anchored TDN can precisely control the orientation of attached biorecognition elements to increase the target accessibility by minifying the steric hindrance effect and offer maximum degrees of freedom to create an in-solution-like binding environment (Feng et al., 2017). Additionally, the surface occupation of TDN noticeably reduces the self-induced perturbation and the intermolecular interaction between the sensor surface and the adjacent biosensing probes by providing appropriate offset distance and controlling surface density (Zeng et al., 2015). Moreover, TDN modification passivates the working surface of biosensor and prevents the nonspecific adsorption of interferences and impurities to limit the false positive signals (Fan et al., 2021).

Given the fast development of this novel nanotechnology in various fields, TDN is expected to become a key element in biosensing applications with the further exploration of its potential with other nanomaterials.

2.5 Aptamers in antibiotics detection

Aptamers are single-stranded DNA or RNA oligonucleotides that are usually generated by an *in vitro* process (Tuerk & Gold, 1990), which can recognize and bind to a wide range of targets including proteins, peptides, amino acids, drugs, metal ions and microorganisms with high affinity and specificity (Torres-Chavolla & Alocilja, 2009). As a biological recognition probe, aptamer offers great specificity, flexibility, chemical and thermal stability, and affordability compared to its conventional rivals, antibodies and enzymes (S. Song, Wang, Li, Fan, & Zhao, 2008). Therefore, aptamers have become the prominent bioanalytical element for the ultrasensitive biosensing platform design over decades (Luan, Wang, Li, Guo, & Lu, 2020; Xiang, Lv, Shi, Xie, & Gao, 2020).

The biorecognition process of the aptamer is achieved by the distinct three-dimensional conformational change while binding to the target of interest and forming an aptamer-target complex *via* various interactions, i.e., hydrogen binding, π–π stacking of aromatic structures, and Van der Waals forces. Due to its special binding mechanism as well as unparalleled physical and chemical properties, aptamer-based biosensors possess unprecedented merits over antibody-based biosensors and enzyme-based biosensors.

(1) Aptamers undergo unique three-dimensional (3D) conformational change while recognizing target analytes. The shifting shape of biosensing probes offers great flexibility for biosensor platform design.

(2) Compared to the larger size of antibody (150 kDa), the smaller size of aptamers (10 to 30 kDa) makes aptamer modifications practical for some special scenarios.

(3) The chemical and thermal stability of aptamers allows aptamer-based biosensors to maintain their original biological functions under extreme detecting environments.

(4) Unlike denaturation of protein, denaturation of aptamers is a reversible process as aptamers can reconstruct the functional structures under ambient conditions, which offers a unique on-off switch for biosensing.

(5) Aptamers are selected *via* an *in vitro* procedure (SELEX) with chemically synthesized substrates and reagents, which is more environment friendly compared to antibody production by the immune system.

(6) Theoretically, SELEX selection is capable of screening desired aptamers for any given target of interest, ranging from small molecules to whole cells.

(7) Once the specific aptamer sequences are determined, aptamers can be artificially synthesized with high reproducibility.

Since aptamers possess irreplaceable advantages, researchers have fabricated aptamers onto various types of antibiotics biosensing platforms, such as electrochemical biosensors, surface plasmon resonance biosensors, optical biosensors, fluorometric biosensors, etc. (**Table 2.2**) (Mehlhorn, Rahimi, & Joseph, 2018).

Kanamycin is an aminoglycoside bactericidal antibiotic and is used to treat a wide variety of infections as a veterinary drug or a second-line antibiotic (Robati et al., 2016). Kanamycin is a mixture of Kanamycin A, B, C, where Kanamycin A is usually the majority if not specified. The kanamycin aptasensors have developed rapidly in terms of quality and quantity among all the other antibiotics due to the excellent binding affinity of reported kanamycin aptamers. The first kanamycin aptamer was selected from a SELEX method using an affinity chromatograph coupled with kanamycin immobilized Sepharose beads (K.-M. Song et al., 2011). The excellent affinity to kanamycin with a low dissociation constant (K_d = 78.8 nM) makes these aptamer sequences the most popular aptasensing probes for various biosensor designs in another research. The original

study utilized this aptamer to build an AuNPs-based colorimetric biosensor to deliver a visible color change from salt-induced AuNPs aggregation. A similar system was improved by using the intrinsic peroxidase-like activity of AuNPs to generate color change (T. K. Sharma et al., 2014). This optical detecting mechanism was later optimized (Xu et al., 2015) and developed into a novel paper chip-based biosensing assay (Ha, Jung, Kim, Kim, & Yoon, 2017). The paper chip was able to perform a fast, simple, and sensitive kanamycin detection available to the naked eyes and used for the food sample test. A similar system was applied to a lateral flow strip biosensor with DNA-modified silver nanoparticles as signal amplifiers (J. Liu, Zeng, Tian, & Zhou, 2018).

This aptamer sequence was tagged by a fluorescence dye to invent a fluorescence biosensing system (H. Li, Sun, Liu, & Liu, 2014). However, labeling aptamer generally leads to a reduced aptamer activity and decreased binding affinity. Thus, various nanomaterial was used to amplify the fluorometric signals to reach the requested sensitivity, including upconversion nanoparticles (H. Li et al., 2014), AuNPs (Ramezani, Danesh, Lavaee, Abnous, & Taghdisi, 2016), silica nanoparticles (Khabbaz et al., 2015), magnetic nanoparticles modified with labelled complementary ssDNA (C. Liu et al., 2015), carbon nanotubes (Liao, Wei, & Luo, 2017), and GO (Tang et al., 2018).

A variety of electrochemical biosensors were proposed based on the same aptamer sequence. A label-free impedimetric biosensor was designed to detect the surface impedance change of aptamer-coated AuNPs (Zhu et al., 2012). The direct fabrication and simple signal generation scheme make the label-free biosensor a good candidate for a portable sensor for repeatable on-site analysis (A. Sharma et al., 2017; N. Zhou, Luo, Zhang, You, & Tian, 2015). The label-free system often needs a signal amplifier to replace the amplification of labelled module, for example, a novel nanocomposite film of MWCNTs, 1-hexyl-3-methylimidazolium hexafluorophosphate, and

nanoporous PtTi (NP-PtTi) alloy was constructed to reach the low detection limit (W. Guo, Sun, Qin, Pei, & Wang, 2015).

To achieve a picomolar or femtomolar level detection, a multiple recycling amplification was designed to repeatably capture and release the target antibiotics to initialize the enzymatic activity of exonuclease digestion to generate enough current signal for ultrasensitive analysis of kanamycin (H. Wang et al., 2016). Another dual recycling amplification strategy was reported based on enzymatic activity with metal ions (Cd^{2+} or Pb^{2+}) labelled signal modules (M. Chen et al., 2016) and MB or FC tagged signal modules for multiple target antibiotics detections (Huang et al., 2018). A MoS_2 nanosheet modified biosensor was designed based on the signal amplification of Y-shaped DNA nanostructures (Y. Zhou et al., 2019). The aptamer-based Y-shaped DNA nanostructure released the aptamer while binding to kanamycin, leading to an immobilization of the left half-hybrid nanostructure on the electrode surface with enzyme catalyzed signal amplification.

β-lactam antibiotics are the most famous antibiotic class and are even considered the most important antibiotics in terms of quantities and values, including ampicillin and penicillin. The first reported ampicillin sensor was based on a colorimetric method based on the AuNPs aggregation mechanism (K.-M. Song, Jeong, Jeon, Cho, & Ban, 2012). The sensor was initialized by wrapping AuNPs with FAM-labeled aptamers as surfactants and activated when AuNPs released the aptamers once ampicillin presented and naturally aggregated to produce a color change. The reported aptamer was selected by a magnetic bead-based SELEX (Daprà, Lauridsen, Nielsen, & Rozlosnik, 2013). A microfluidic impedimetric biosensor was constructed using conductive polymer to covalently link to the aptamer probes to perform an electrochemical measurement (Daprà et al., 2013). This biosensor was later evaluated and optimized in terms of

surface geometry (Rosati, Daprà, Cherré, & Rozlosnik, 2014). A similar SELEX method was used to screen a new ampicillin-specific sequence, which was later used to build a fluorescent sensor (Luo et al., 2017). To increase the limits of detection, a target-induced and T7 exonuclease-aided recycling amplification strategy was developed to design a voltammetric detecting system (X. Wang, Dong, Gai, Duan, & Li, 2016). Briefly, the electrical signal was originally suppressed by a hairpin probe. Once the electrode was exposed to ampicillin, the aptamer sequence on the hairpin was recognized and bound to the target and left the primer sequence with elongation to form a duplex region until the binding of ampicillin was displaced. Then, the duplex was digested by exonuclease to release the attached methylene blue to electrode surface. The dual-recycle of ampicillin and exonuclease digestion kept releasing methylene blue and amplify the electrical signal (X. Wang et al., 2016). Another signal amplification method utilized ssDNA binding protein functionalized AuNPs as electrical resistance modules to prohibit electron transmission for the modified biosensor (Jun Wang, Ma, Yin, Zhou, & Ai, 2017). When target ampicillin was present, the aptamers bind to the ampicillin and release the module, and the biosensor received an increased current response.

Zhao et al. reported the first penicillin aptasensor based on impedimetric detection (J. Zhao et al., 2016). The sensor was modified by a magnetic graphene nanocomposite (GR–Fe3O4NPs) and a poly(3,4-ethylenedioxythiophene) gold nanoparticle composite (PEDOT–AuNPs). A novel rGO-SELEX was proposed for an immobilization-free selection of penicillin aptamers with the assistance of the quenched FAM-labeled ssDNA library (A. Y. Lee et al., 2017). The selected aptamer was used to build a fluorescence aptasensor for a fast and sensitive penicillin determination. Another penicillin aptamer sequence was reported using the capture-SELEX and used to design an impedimetric biosensor (Paniel et al., 2017). This aptamer sequence showed

binding affinity not only to penicillin but to other β-lactam antibiotics with less affinity, such as amoxicillin and ampicillin.

In summary, the development of antibiotic aptasensors has been an intriguing process over the decades. During this process, the quality of aptamer probes is the major reason limiting the design of sensitive aptasensors to meet the food safety requirement of residue antibiotics, especially for β-lactam antibiotics. The selection of high-affinity aptamers can help release the full potential of aptamer biosensing.

Table 2.2. A list of aptamer-based biosensors for antibiotic detections

Antibiotics	Sensor type	Aptamer sequence (5' to 3')	Dissociation rate (Kd)	LOD	Reference
Kanamycin	Colorimetric	TGGGGGTTGAGGCTAAGCCGA	78.8 nM	25 nM	(Song et al., 2011)
	Colorimetric	TGGGGGTTGAGGCTAAGCCGA	-	1.49 nM	(T. K. Sharma et al., 2014)
	Colorimetric	TGGGGGTTGAGGCTAAGCCGA	-	2.6 ng/mL	(Xu et al., 2015)
	Colorimetric	TGGGGGTTGAGGCTAAGCCGA	-	3.35 nM	(Ha, Jung, Kim, Kim, & Yoon, 2017)
	Colorimetric	TGGGGGTTGAGGCTAAGCCGA	-	0.0778 nM	(J. Liu, Zeng, Tian, & Zhou, 2018)
	Fluorescence	AGATGGGGGTTGAGGCTAAGCCGA	-	9 pM	(Li, Sun, Liu, & Liu, 2014)
	Fluorescence	AGATGGGGGTTGAGGCTAAGCCGA	-	437 pM	(Ramezani, Danesh, Lavaee, Abnous, & Taghdisi, 2016)
	Fluorescence	AGATGGGGGTTGAGGCTAAGCCGA	-	612 pM	(Khabbaz et al., 2015)

	Fluorescence	TGGGGGTTGAGGCTAAGCCGA	-	0.92 ng/mL	(C. Liu et al., 2015)
	Fluorescence	TGGGGGTTGAGGCTAAGCCGA	-	0.4 nM	(Liao, Wei, & Luo, 2017)
	Fluorescence	TGGGGGTTGAGGCTAAGCCGA	-	26 nM	(Tang et al., 2018)
	Impedimetric	TGGGGGTTGAGGCTAAGCCGA	-	9.4 nM	(Zhu, Chandra, Song, Ban, & Shim, 2012)
	Impedimetric	TGGGGGTTGAGGCTAAGCCGA	-	10 nM	(N. Zhou, Luo, Zhang, You, & Tian, 2015)
	Impedimetric	TGGGGGTTGAGGCTAAGCCGA	-	0.11 ng/mL	(A. Sharma et al., 2017)
	Voltametric	AGATGGGGGTTGAGGCTAAGCCGA	-	3.7 pg/mL	(Guo, Sun, Qin, Pei, & Wang, 2015)
	Voltametric	TCTGGGGGTTGAGGCTAAGCCGAC	-	0.15 pM	(Chen et al., 2016)
	Voltametric	TGGGGGTTGAGGCT - AAGCCGACTCAGAGATCCATAT - AAGCCGA	-	1.3 fM	(H. Wang et al., 2016)
	Voltametric	TGGGGGTTGAGGCTAAGCCGA	-	35 fM	(Huang et al., 2018)
	Voltametric	TGGGGGTTGAGGCTAAGCCGA	-	29 pM	(Y. Zhou et al., 2019)
Ampicillin	Colorimetric	AMP7: CACGGCATGGTGGGCGTCGTG AMP18: TTAGTTGGGGTTCAGTTGG	9.4 nM 9.8 nM	14.3 nM	(Song, Jeong, Jeon, Cho, & Ban, 2012)

	Impedimetric	GCGGGCGGTTGTATAGCGG	13.4 nM	0.1 nM	(Daprà, Lauridsen, Nielsen, & Rozlosnik, 2013)
	Impedimetric	GCGGGCGGTTGTATAGCGG	-	0.1 nM	(Rosati, Daprà, Cherré, & Rozlosnik, 2014)
	Fluorescence	GCGGGCGGTTGTATAGCGGTTTTTTT	-	0.2 nM	(Luo et al., 2017)
	Voltametric	GCGGGCGGTTGTATAGCGG	-	4.0 pM	(X. Wang, Dong, Gai, Duan, & Li, 2016)
	Voltametric	TGGGGGTTGAGGCTAAGCCGAC	-	3.8 pM	(J. Wang, Ma, Yin, Zhou, & Ai, 2017)
	Voltametric	TTAGTTGGGGTTCAGTTGG	-	1000 nM	(Yu & Lai, 2018)
Penicillin	Impedimetric	CTGAATTGGATCTCTCTTCTTGAGCG ATCTCCACA	-	0.057 ng/mL	(Zhao, Guo, Pei, & Ding, 2016)
	Fluorescence	GGGTCTGAGGAGTGCGCGGTGCCAG TGAGT	84.4 nM	9.2 nM	(Lee et al., 2017)
	Impedimetric	GGGAGGACGAAGCGGAACGAGATGT AGATGAGGCTCGATCCGAATGCGTG ACGTCTATCGGAATACTCGTTTTTAC GCCTCATAAGACACGCCCGACA	-	0.49 nM	(Paniel et al., 2017)

2.6 SELEX

The RNA or DNA sequence (aptamer) is capable of folding into a stable three-dimensional structure, which may offer a ligand binding to a specific molecule (Singer, Shtatland, Brown, & Gold, 1997). Since the discovery of these incredible functional tools, aptamer has attracted tremendous attention in both research areas and industrial fields over decades (Tombelli, Minunni, & Mascini, 2007). However, it is particularly difficult to estimate the number of necessary complex structures providing the same affinity to a given target of interest without a further fundamental understanding of RNA or DNA structure and its related function (Gold et al., 1997).

In 1990, an '*in-vitro selection' and 'in-vitro evolution'* technique was developed to screen ligand-binding sequences with specific functionality from a large DNA library of random chemically synthesized DNA molecules (typically with 10^{13}-10^{16} sequences) (Tuerk & Gold, 1990). This day, this specific method is commonly known as SELEX in the scientific community. In the early days, SELEX was designed by using repeated cycles of the screening steps of affinity chromatography followed by the amplification steps of polymerase chain reaction (PCR) (Ellington & Szostak, 1992). It is believed that only an extremely small fraction of the DNA library with high complexity, roughly one in 10^{10} random sequences, will fold into such a structure with a given ligand-binding ability to a designed target molecule (Ellington & Szostak, 1990). Therefore, only a very small number of functional structures is expected to be bounded to the target molecules and be amplified by the PCR from each cycle. Through the iterative process of selecting the specific DNA molecules from the random pool and duplicating the selected sequences, the number of functional structures is exponentially amplified until these structures dominate the resulted DNA pool (Regina Stoltenburg, Reinemann, & Strehlitz, 2007).

At the early stage of SELEX development, researchers quickly discovered the superiority of this selection procedure allowing the fast isolation of functional DNA molecules from a randomized library without any knowledge of their secondary structures and the way they recognize the ligands. However, the limitations of the early SELEX were realized alongside the promising future of this unique technique (Klug & Famulok, 1994).

(1) A bias in the selection process is caused by the nature of affinity chromatography that the DNA molecules with a higher dissociation rate (K_d) are preferably enriched by the affinity selection rather than those with potent ligand-binding functions. Thus, aptamer sequences with lower K_d values are more difficult to be discovered.

(2) The partitioning step that recovers only a limited number of functional structures often requires an efficient separation technique, especially for small molecules with light molecular weight.

(3) The amplification step of SELEX often uses PCR to duplicate the functional structures that survive the previous screening step. However, the PCR contains build-in selection as some structures are simply more active during the PCR than those functional ones, which is almost impossible for the operators to control. As an undesired result, the sequences kinetically favored by PCR will be overrepresented in the final pool than their competitors which are functionally more effective.

Over the last three decades, researchers have been developing a variety of SELEX procedures with various modifications to overcome these limitations. Despite dozens of different improvements, a typical SELEX procedure nowadays remains the similar repeated cycles of screening steps (**Figure 2.3**), including library design, a target binding step, a partitioning step with separation from unbound sequences and elution of bound sequences, an amplification step by

PCR, and a purification step to prepare the pool for the next round (Shamah, Healy, & Cload, 2008).

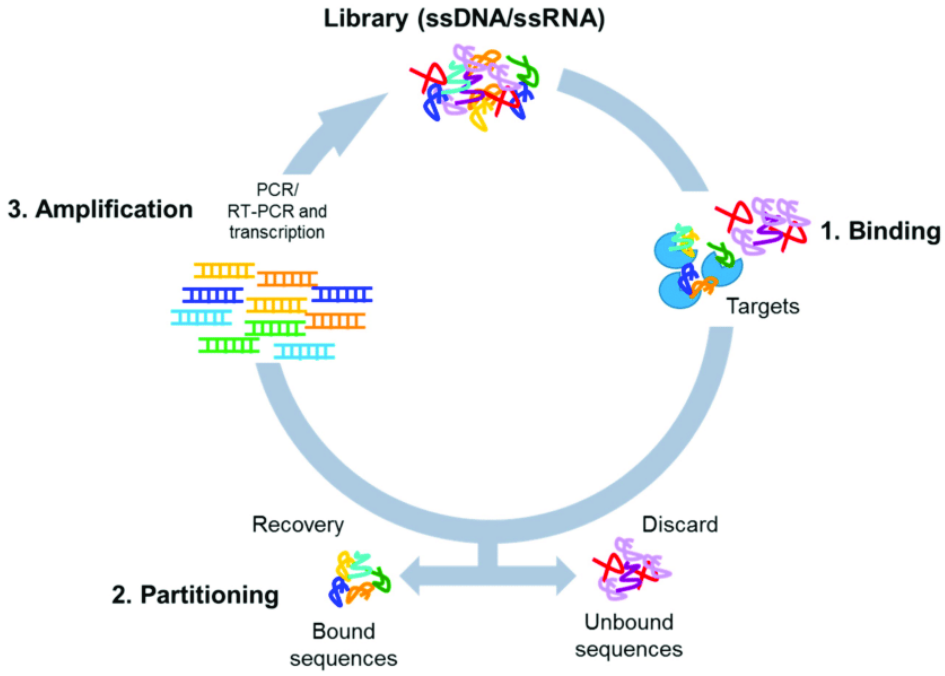

Figure 2.3. Scheme of a typical SELEX process (Catuogno & Esposito, 2017).

To improve the SELEX efficiency, various methods with different modifications were reported to change the oligonucleotide library, improve the target binding strategy, adapt the sequence separation approach, or revise the PCR procedure (Ozer, Pagano, & Lis, 2014). Regardless of which step was focused on by these methods, the ultimate goal is to either increase the binding affinity of functional aptamers or simplify the SELEX protocol. **Table 2.3** shows some typical modified SELEX methods reported over decades.

Electrophoresis-based SELEX was reported to create an in-solution environment for the aptamer-target binding to reach a steady-state equilibrium during the screening step (Mendonsa & Bowser, 2004). Gel-electrophoresis is well known as a separation tool of DNA or protein according to the molecular size, which makes the Capillary Electrophoresis (CE-SELEX) naturally

a great implement for partitioning the functional sequences for proteins (Mosing, Mendonsa, & Bowser, 2005). However, the size of the DNA library (~10^{12} sequences) is restricted by the volume of CE-SELEX, which may affect the affinity of final products. Besides, this method is not suitable for small molecules due to the light mobility change of the aptamer-target complex, which results in difficulty to separate the desired structures.

Cell-SELEX was invented to fulfill therapeutic needs for disease cells (especially cancer cells) diagnosis (Guo, Paul, Schichor, Ziemer, & Wendel, 2008). Based on the complex monitoring environment of cell detections, the selected aptamers are required to identify the specific targets without being interfered with by other substances such as protein, viruses, and other cell types (Ohuchi, 2012). Therefore, a negative SELEX cycle is designed using the nontarget substances as screening objects to eliminate the structures that have an affinity to any other interferences (Sefah, Shangguan, Xiong, O'donoghue, & Tan, 2010). This SELEX method is limited to the targets on the cell surface, and the selected aptamers are not capable of recognizing dead cells from live ones.

The magnetic bead has become an excellent tool to offer both solid support for target immobilization and a fast and convenient separation to overcome the target limitations of SELEX applications (Oh et al., 2009). Briefly, the magnetic bead can be covalently bonded to the target molecule and form a bead-target-aptamer complex, and then easily separated by a magnetic field, which makes small molecules with light molecular weight available for SELEX (R Stoltenburg, Reinemann, & Strehlitz, 2005). Moreover, because of its unique physical and chemical properties, magnetic bead provides great compatibility with other SELEX applications (Huang, Lin, Shiesh, & Lee, 2010; Paul, Avci-Adali, Ziemer, & Wendel, 2009; Regina Stoltenburg, Nikolaus, & Strehlitz, 2012).

To reduce the cost of aptamer screening in terms of time and labor, a microfluidic platform was employed to generate high-affinity aptamers by an automatic process in a short period of selection (Hybarger, Bynum, Williams, Valdes, & Chambers, 2006). The miniaturized nanofabricated devices are capable of performing parallel aptamer screening for multiple targets with only 3-6 rounds of SELEX process (Ahmad et al., 2011). This method requires the assistance of micromagnetic beads immobilization or encapsulation (Lou et al., 2009).

A novel SELEX method using atomic force microscopy (AFM) to perform a single-round selection was reported (Peng, Stephens, Bonin, Cubicciotti, & Guthold, 2007). The AFM cantilever was used as the probe to create controllable and sensitive contact between aptamers and targets of interest (Miyachi, Shimizu, Ogino, & Kondo, 2010). Since AFM is a highly sensitive microscopic technique with high resolutions, ideally, the aptamer and target contact can be precisely controlled and visualized (Takenaka et al., 2017).

Aptamer selection of small molecules has always been a major challenge due to the difficulty of separating aptamer-target complex from unbound sequences with light molecular weight and a lack of immobilization sites. Magnetic beads provide an alternative solution using target immobilization on the beads to perform a simple partition. However, the immobilization on a solid matrix may have unpredictable effects on the target accessibility for some small molecules, for example, increasing the steric hindrance on targets and blocking the potential binding sites for aptamers. Capture-SELEX offers a non-immobilization option using an aptamer sequence with a docking sequence, which is captured by the complementary sequence on a solid matrix, to release the aptamers once incubating with the target molecules (Takenaka et al., 2017). Thus, the aptamer-target binding takes place in the solution phase with a steady equilibrium to maximize the probability of achieving the best affinity of aptamer (Lyu, Khan, & Wang, 2021).

Another immobilization-free SELEX method by using GO as a solid support matrix was introduced (Boussebayle, Groher, & Suess, 2019). The oligonucleotide library is incubated with target molecules in a solution to reach the binding equilibrium with maximum degrees of freedom. The unspecific adsorption between the unbounded oligonucleotide sequences and the surface of GO is achieved via hydrophobic and π–π stacking interactions, while the adsorption of well-folded sequences on GO is much lower (Jia et al., 2012). Because of the adsorption property, an immobilization-free strategy is available to select aptamers for small molecules by using centrifugation to recover the desired structures with the unbound sequences.

To summarize, SELEX is a powerful aptamer screening tool to select aptamers for any given molecules with appropriate modifications. However, the aptamer partitioning for small molecule targets is generally more difficult than substrates with large molecule weight, due to little difference in mass change of target binding and a lack of immobilization sites of small targets. Thus, a delicate SELEX procedure is required to select effective aptamers for desired targets, for example, β-lactam antibiotics, to pave the pathway to the development of an ultrasensitive biosensing platform for commercial applications.

Table 2.3. A list of novel modified SELEX methods

Methods	Description	Reference
Capillary Electrophoresis SELEX	Capillary electrophoresis is employed to build the binding environment and perform the separation of functional structures	(Mendonsa & Bowser, 2004; Mosing, Mendonsa, & Bowser, 2005; Yang & Bowser, 2013; Zhu, Yang, Ghulam, Li, & Qu, 2019)
Cell-SELEX	The selected aptamers can identify the specific cell from other interferences via a negative SELEX cycle.	(M. Chen et al., 2016; Guo, Paul, Schichor, Ziemer, & Wendel, 2008; Ohuchi, 2012; Sefah, Shangguan, Xiong, O'donoghue, & Tan, 2010)
Magnetic beads SELEX	The target molecule is covalently linked to a magnetic bead and immobilized with aptamer to make a fast and convenient separation by applying a magnetic field	(Huang, Lin, Shiesh, & Lee, 2010; Oh et al., 2009; Paul, Avci-Adali, Ziemer, & Wendel, 2009; Regina Stoltenburg, Nikolaus, & Strehlitz, 2012; R Stoltenburg, Reinemann, & Strehlitz, 2005)
Microfluidic SELEX	A microfluidic device is utilized to accomplish an automatic platform for rapid aptamer selection	(Ahmad et al., 2011; Hybarger, Bynum, Williams, Valdes, & Chambers, 2006; Lou et al., 2009)
AFM SELEX	Atomic force microscopy uses its dynamic tip to contact with oligonucleotide pool to form the target-aptamer complex	(Miyachi, Shimizu, Ogino, & Kondo, 2010; Peng, Stephens, Bonin, Cubicciotti, & Guthold, 2007; Takenaka et al., 2017)

Capture SELEX	Capture-SELEX can screen the aptamer pool without performing target immobilization	(Boussebayle, Groher, & Suess, 2019; Boussebayle, Torka, et al., 2019; Lyu, Khan, & Wang, 2021; Takenaka et al., 2017; Tian, Duan, Wu, & Wang, 2019)
GO-SELEX	Graphene oxide is utilized as the solid matrix to perform immobilization-free adsorption for unbounded oligonucleotide sequences. The aptamer-target complex is separated by centrifugation.	(X. Chen et al., 2014; Nguyen, Kwon, Kim, & Gu, 2014; Shi et al., 2021; WooáKim & BockáGu, 2012; Xing, Zhang, & Yang, 2019)

References

Abi, A., Lin, M., Pei, H., Fan, C., Ferapontova, E. E., & Zuo, X. (2014). Electrochemical switching with 3D DNA tetrahedral nanostructures self-assembled at gold electrodes. *ACS applied materials & interfaces, 6*(11), 8928-8931.

Ahmad, K. M., Oh, S. S., Kim, S., McClellen, F. M., Xiao, Y., & Soh, H. T. (2011). Probing the limits of aptamer affinity with a microfluidic SELEX platform. *PloS one, 6*(11), e27051.

Alarcon-Angeles, G., Álvarez-Romero, G. A., & Merkoçi, A. (2018). Electrochemical Biosensors: Enzyme Kinetics and Role of Nanomaterials. In K. Wandelt (Ed.), *Encyclopedia of Interfacial Chemistry* (pp. 140-155). Oxford: Elsevier.

Boussebayle, A., Groher, F., & Suess, B. (2019). RNA-based capture-SELEX for the selection of small molecule-binding aptamers. *Methods, 161*, 10-15.

Boussebayle, A., Torka, D., Ollivaud, S., Braun, J., Bofill-Bosch, C., Dombrowski, M., . . . Suess, B. (2019). Next-level riboswitch development—implementation of Capture-SELEX facilitates identification of a new synthetic riboswitch. *Nucleic acids research, 47*(9), 4883-4895.

Bujold, K. E., Lacroix, A., & Sleiman, H. F. (2018). DNA Nanostructures at the Interface with Biology. *Chem, 4*(3), 495-521. doi:https://doi.org/10.1016/j.chempr.2018.02.005

Catuogno, S., & Esposito, C. L. (2017). Aptamer cell-based selection: Overview and advances. *Biomedicines, 5*(3), 49.

Chen, J., Yao, B., Li, C., & Shi, G. (2013). An improved Hummers method for eco-friendly synthesis of graphene oxide. *Carbon, 64*, 225-229.

Chen, M., Gan, N., Zhou, Y., Li, T., Xu, Q., Cao, Y., & Chen, Y. (2016). An electrochemical aptasensor for multiplex antibiotics detection based on metal ions doped nanoscale MOFs as signal tracers and RecJf exonuclease-assisted targets recycling amplification. *Talanta, 161*, 867-874. doi:https://doi.org/10.1016/j.talanta.2016.09.051

Chen, M., Yu, Y., Jiang, F., Zhou, J., Li, Y., Liang, C., . . . Zhang, G. (2016). Development of cell-SELEX technology and its application in cancer diagnosis and therapy. *International journal of molecular sciences, 17*(12), 2079.

Chen, X., Huang, Y., Duan, N., Wu, S., Xia, Y., Ma, X., . . . Wang, Z. (2014). Screening and identification of DNA aptamers against T-2 toxin assisted by graphene oxide. *Journal of agricultural and food chemistry, 62*(42), 10368-10374.

Chen, X., Zhou, G., Song, P., Wang, J., Gao, J., Lu, J., . . . Zuo, X. (2014). Ultrasensitive electrochemical detection of prostate-specific antigen by using antibodies anchored on a DNA nanostructural scaffold. *Analytical Chemistry, 86*(15), 7337-7342.

Cho, I.-H., Kim, D. H., & Park, S. (2020). Electrochemical biosensors: perspective on functional nanomaterials for on-site analysis. *Biomaterials Research, 24*(1), 6. doi:10.1186/s40824-019-0181-y

Clark, L. C., Jr., & Lyons, C. (1962). Electrode systems for continuous monitoring in cardiovascular surgery. *Ann N Y Acad Sci, 102*, 29-45. doi:10.1111/j.1749-6632.1962.tb13623.x

Daprà, J., Lauridsen, L. H., Nielsen, A. T., & Rozlosnik, N. (2013). Comparative study on aptamers as recognition elements for antibiotics in a label-free all-polymer biosensor. *Biosensors and Bioelectronics, 43*, 315-320. doi:https://doi.org/10.1016/j.bios.2012.12.058

Deokar, G., Avila, J., Razado-Colambo, I., Codron, J.-L., Boyaval, C., Galopin, E., . . . Vignaud, D. (2015). Towards high quality CVD graphene growth and transfer. *Carbon, 89*, 82-92.

Eggins, B. R. (2013). *Biosensors: an introduction*: Springer-Verlag.

Ellington, A. D., & Szostak, J. W. (1990). In vitro selection of RNA molecules that bind specific ligands. *nature, 346*(6287), 818-822.

Ellington, A. D., & Szostak, J. W. (1992). Selection in vitro of single-stranded DNA molecules that fold into specific ligand-binding structures. *nature, 355*(6363), 850-852.

Fan, Z., Yao, B., Ding, Y., Zhao, J., Xie, M., & Zhang, K. (2021). Entropy-driven amplified electrochemiluminescence biosensor for RdRp gene of SARS-CoV-2 detection with self-assembled DNA tetrahedron scaffolds. *Biosens Bioelectron, 178*, 113015. doi:10.1016/j.bios.2021.113015

Feng, Q.-M., Zhou, Z., Li, M.-X., Zhao, W., Xu, J.-J., & Chen, H.-Y. (2017). DNA tetrahedral scaffolds-based platform for the construction of electrochemiluminescence biosensor. *Biosensors and Bioelectronics, 90*, 251-257.

Gao, L., Liu, L., Tian, Y., Yang, Q., Wu, P., Fan, C., . . . Li, F. (2021). Probing the Formation Kinetics and Thermodynamics with Rationally Designed Analytical Tools Enables One-Pot Synthesis and Purification of a Tetrahedral DNA Nanostructure. *Analytical Chemistry, 93*(18), 7045-7053. doi:10.1021/acs.analchem.1c00363

Giljohann, D. A., Seferos, D. S., Daniel, W. L., Massich, M. D., Patel, P. C., & Mirkin, C. A. (2020). Gold nanoparticles for biology and medicine. *Spherical Nucleic Acids*, 55-90.

Gold, L., Brown, D., He, Y.-y., Shtatland, T., Singer, B. S., & Wu, Y. (1997). From oligonucleotide shapes to genomic SELEX: novel biological regulatory loops. *Proceedings of the National Academy of Sciences, 94*(1), 59-64.

Gonçalves, L. M., Callera, W. F. A., Sotomayor, M. D. P. T., & Bueno, P. R. (2014). Penicillinase-based amperometric biosensor for penicillin G. *Electrochemistry Communications, 38*, 131-133. doi:https://doi.org/10.1016/j.elecom.2013.11.022

Goodman, R. P., Berry, R. M., & Turberfield, A. J. (2004). The single-step synthesis of a DNA tetrahedron. *Chem Commun (Camb)*(12), 1372-1373. doi:10.1039/b402293a

Goodman, R. P., Schaap, I. A., Tardin, C. F., Erben, C. M., Berry, R. M., Schmidt, C. F., & Turberfield, A. J. (2005). Rapid chiral assembly of rigid DNA building blocks for molecular nanofabrication. *Science, 310*(5754), 1661-1665. doi:10.1126/science.1120367

Guan, J., He, K., & Gunasekaran, S. (2022). Self-assembled tetrahedral DNA nanostructures-based ultrasensitive label-free detection of ampicillin. *Talanta, 243*, 123292. doi:https://doi.org/10.1016/j.talanta.2022.123292

Guo, K.-T., Paul, A., Schichor, C., Ziemer, G., & Wendel, H. P. (2008). CELL-SELEX: Novel perspectives of aptamer-based therapeutics. *International journal of molecular sciences, 9*(4), 668-678.

Guo, W., Sun, N., Qin, X., Pei, M., & Wang, L. (2015). A novel electrochemical aptasensor for ultrasensitive detection of kanamycin based on MWCNTs–HMIMPF6 and nanoporous PtTi alloy. *Biosensors and Bioelectronics, 74*, 691-697. doi:https://doi.org/10.1016/j.bios.2015.06.081

Guo, Y., Yang, X., Ruan, K., Kong, J., Dong, M., Zhang, J., . . . Guo, Z. (2019). Reduced graphene oxide heterostructured silver nanoparticles significantly enhanced thermal conductivities in hot-pressed electrospun polyimide nanocomposites. *ACS applied materials & interfaces, 11*(28), 25465-25473.

Ha, N.-R., Jung, I.-P., Kim, S.-H., Kim, A. R., & Yoon, M.-Y. (2017). Paper chip-based colorimetric sensing assay for ultra-sensitive detection of residual kanamycin. *Process Biochemistry, 62*, 161-168. doi:https://doi.org/10.1016/j.procbio.2017.07.008

Hayat, A., Catanante, G., & Marty, J. L. (2014). Current Trends in Nanomaterial-Based Amperometric Biosensors. *Sensors, 14*(12), 23439-23461. Retrieved from https://www.mdpi.com/1424-8220/14/12/23439

Heiligtag, F. J., & Niederberger, M. (2013). The fascinating world of nanoparticle research. *Materials Today, 16*(7), 262-271. doi:https://doi.org/10.1016/j.mattod.2013.07.004

Hong, F., Chen, X., Cao, Y., Dong, Y., Wu, D., Hu, F., & Gan, N. (2018). Enzyme- and label-free electrochemical aptasensor for kanamycin detection based on double stir bar-assisted toehold-mediated strand displacement reaction for dual-signal amplification. *Biosensors and Bioelectronics, 112*, 202-208. doi:https://doi.org/10.1016/j.bios.2018.04.017

Huang, C.-J., Lin, H.-I., Shiesh, S.-C., & Lee, G.-B. (2010). Integrated microfluidic system for rapid screening of CRP aptamers utilizing systematic evolution of ligands by exponential enrichment (SELEX). *Biosensors and Bioelectronics, 25*(7), 1761-1766.

Huang, S., Gan, N., Li, T., Zhou, Y., Cao, Y., & Dong, Y. (2018). Electrochemical aptasensor for multi-antibiotics detection based on endonuclease and exonuclease assisted dual recycling amplification strategy. *Talanta, 179*, 28-36. doi:https://doi.org/10.1016/j.talanta.2017.10.016

Hybarger, G., Bynum, J., Williams, R. F., Valdes, J. J., & Chambers, J. P. (2006). A microfluidic SELEX prototype. *Analytical and bioanalytical chemistry, 384*(1), 191-198.

Jeevanandam, J., Barhoum, A., Chan, Y. S., Dufresne, A., & Danquah, M. K. (2018). Review on nanoparticles and nanostructured materials: history, sources, toxicity and regulations. *Beilstein journal of nanotechnology, 9*(1), 1050-1074.

Jia, Y., Yin, X.-B., Zhang, J., Zhou, S., Song, M., & Xing, K.-L. (2012). Graphene oxide modified light addressable potentiometric sensor and its application for ssDNA monitoring. *Analyst, 137*(24), 5866-5873.

Khabbaz, L. S., Hassanzadeh-Khayyat, M., Zaree, P., Ramezani, M., Abnous, K., & Taghdisi, S. M. (2015). Detection of kanamycin by using an aptamer-based biosensor using silica nanoparticles. *Analytical Methods, 7*(20), 8611-8616.

Kim, D.-M., Rahman, M. A., Do, M. H., Ban, C., & Shim, Y.-B. (2010). An amperometric chloramphenicol immunosensor based on cadmium sulfide nanoparticles modified-dendrimer bonded conducting polymer. *Biosensors and Bioelectronics, 25*(7), 1781-1788. doi:https://doi.org/10.1016/j.bios.2009.12.024

Kissinger, P. T. (2005). Biosensors—a perspective. *Biosensors and Bioelectronics, 20*(12), 2512-2516. doi:https://doi.org/10.1016/j.bios.2004.10.004

Klug, S. J., & Famulok, M. (1994). All you wanted to know about SELEX. *Molecular biology reports, 20*(2), 97-107.

Kour, R., Arya, S., Young, S.-J., Gupta, V., Bandhoria, P., & Khosla, A. (2020). Recent advances in carbon nanomaterials as electrochemical biosensors. *Journal of The Electrochemical Society, 167*(3), 037555.

Lan, L., Yao, Y., Ping, J., & Ying, Y. (2017). Recent advances in nanomaterial-based biosensors for antibiotics detection. *Biosensors and Bioelectronics, 91*, 504-514. doi:https://doi.org/10.1016/j.bios.2017.01.007

Lee, A. Y., Ha, N.-R., Jung, I.-P., Kim, S.-H., Kim, A. R., & Yoon, M.-Y. (2017). Development of a ssDNA aptamer for detection of residual benzylpenicillin. *Analytical biochemistry, 531*, 1-7. doi:https://doi.org/10.1016/j.ab.2017.05.013

Lee, S. H., Sung, J. H., & Park, T. H. (2012). Nanomaterial-based biosensor as an emerging tool for biomedical applications. *Annals of biomedical engineering, 40*(6), 1384-1397.

Li, H., Sun, D.-e., Liu, Y., & Liu, Z. (2014). An ultrasensitive homogeneous aptasensor for kanamycin based on upconversion fluorescence resonance energy transfer. *Biosensors and Bioelectronics, 55*, 149-156. doi:https://doi.org/10.1016/j.bios.2013.11.079

Li, J., Fan, C., Pei, H., Shi, J., & Huang, Q. (2013). Smart drug delivery nanocarriers with self-assembled DNA nanostructures. *Advanced Materials, 25*(32), 4386-4396.

Li, S., Tian, T., Zhang, T., Cai, X., & Lin, Y. (2019). Advances in biological applications of self-assembled DNA tetrahedral nanostructures. *Materials Today, 24*, 57-68. doi:https://doi.org/10.1016/j.mattod.2018.08.002

Liang, L., Li, J., Li, Q., Huang, Q., Shi, J., Yan, H., & Fan, C. (2014). Single-particle tracking and modulation of cell entry pathways of a tetrahedral DNA nanostructure in live cells. *Angewandte Chemie International Edition, 53*(30), 7745-7750.

Liao, Q. G., Wei, B. H., & Luo, L. G. (2017). Aptamer based fluorometric determination of kanamycin using double-stranded DNA and carbon nanotubes. *Microchimica Acta, 184*(2), 627-632. doi:10.1007/s00604-016-2050-x

Lin, M., Wen, Y., Li, L., Pei, H., Liu, G., Song, H., . . . Huang, Q. (2014). Target-responsive, DNA nanostructure-based E-DNA sensor for microRNA analysis. *Analytical Chemistry, 86*(5), 2285-2288.

Liu, C., Lu, C., Tang, Z., Chen, X., Wang, G., & Sun, F. (2015). Aptamer-functionalized magnetic nanoparticles for simultaneous fluorometric determination of oxytetracycline and kanamycin. *Microchimica Acta, 182*(15), 2567-2575. doi:10.1007/s00604-015-1628-z

Liu, J., Zeng, J., Tian, Y., & Zhou, N. (2018). An aptamer and functionalized nanoparticle-based strip biosensor for on-site detection of kanamycin in food samples. *Analyst, 143*(1), 182-189.

Liu, X., Zheng, S., Hu, Y., Li, Z., Luo, F., & He, Z. (2016). Electrochemical Immunosensor Based on the Chitosan-Magnetic Nanoparticles for Detection of Tetracycline. *Food Analytical Methods, 9*(10), 2972-2978. doi:10.1007/s12161-016-0480-z

Liu, Y., Yan, K., Okoth, O. K., & Zhang, J. (2015). A label-free photoelectrochemical aptasensor based on nitrogen-doped graphene quantum dots for chloramphenicol determination. *Biosensors and Bioelectronics, 74*, 1016-1021. doi:https://doi.org/10.1016/j.bios.2015.07.067

Lou, X., Qian, J., Xiao, Y., Viel, L., Gerdon, A. E., Lagally, E. T., . . . Soh, H. T. (2009). Micromagnetic selection of aptamers in microfluidic channels. *Proceedings of the National Academy of Sciences, 106*(9), 2989-2994.

Lu, J., Wang, J., Hu, X., Gyimah, E., Yakubu, S., Wang, K., . . . Zhang, Z. (2019). Electrochemical Biosensor Based on Tetrahedral DNA Nanostructures and G-Quadruplex–Hemin Conformation for the Ultrasensitive Detection of MicroRNA-21 in Serum. *Analytical Chemistry, 91*(11), 7353-7359. doi:10.1021/acs.analchem.9b01133

Lu, L., & Gunasekaran, S. (2019). Dual-channel ITO-microfluidic electrochemical immunosensor for simultaneous detection of two mycotoxins. *Talanta, 194*, 709-716. doi:https://doi.org/10.1016/j.talanta.2018.10.091

Lu, L., Seenivasan, R., Wang, Y.-C., Yu, J.-H., & Gunasekaran, S. (2016). An Electrochemical Immunosensor for Rapid and Sensitive Detection of Mycotoxins Fumonisin B1 and Deoxynivalenol. *Electrochimica Acta, 213*, 89-97. doi:https://doi.org/10.1016/j.electacta.2016.07.096

Luan, Y., Wang, N., Li, C., Guo, X., & Lu, A. (2020). Advances in the Application of Aptamer Biosensors to the Detection of Aminoglycoside Antibiotics. *Antibiotics, 9*(11), 787. Retrieved from https://www.mdpi.com/2079-6382/9/11/787

Luo, Z., Wang, Y., Lu, X., Chen, J., Wei, F., Huang, Z., . . . Duan, Y. (2017). Fluorescent aptasensor for antibiotic detection using magnetic bead composites coated with gold nanoparticles and a nicking enzyme. *Analytica chimica acta, 984*, 177-184. doi:https://doi.org/10.1016/j.aca.2017.06.037

Lyu, C., Khan, I. M., & Wang, Z. (2021). Capture-SELEX for aptamer selection: A short review. *Talanta, 229*, 122274.

Maduraiveeran, G., Sasidharan, M., & Ganesan, V. (2018). Electrochemical sensor and biosensor platforms based on advanced nanomaterials for biological and biomedical applications. *Biosensors and Bioelectronics, 103*, 113-129.

Magar, H. S., Hassan, R. Y. A., & Mulchandani, A. (2021). Electrochemical Impedance Spectroscopy (EIS): Principles, Construction, and Biosensing Applications. *Sensors (Basel, Switzerland), 21*(19), 6578. doi:10.3390/s21196578

Mehlhorn, A., Rahimi, P., & Joseph, Y. (2018). Aptamer-Based Biosensors for Antibiotic Detection: A Review. *Biosensors, 8*(2). doi:10.3390/bios8020054

Mendonsa, S. D., & Bowser, M. T. (2004). In vitro evolution of functional DNA using capillary electrophoresis. *Journal of the American Chemical Society, 126*(1), 20-21.

Miyachi, Y., Shimizu, N., Ogino, C., & Kondo, A. (2010). Selection of DNA aptamers using atomic force microscopy. *Nucleic acids research, 38*(4), e21-e21.

Mosing, R. K., Mendonsa, S. D., & Bowser, M. T. (2005). Capillary electrophoresis-SELEX selection of aptamers with affinity for HIV-1 reverse transcriptase. *Analytical Chemistry, 77*(19), 6107-6112.

Nguyen, V. T., Kwon, Y. S., Kim, J. H., & Gu, M. B. (2014). Multiple GO-SELEX for efficient screening of flexible aptamers. *Chem Commun (Camb), 50*(72), 10513-10516. doi:10.1039/c4cc03953j

Oh, S. S., Qian, J., Lou, X., Zhang, Y., Xiao, Y., & Soh, H. T. (2009). Generation of highly specific aptamers via micromagnetic selection. *Anal Chem, 81*(13), 5490-5495. doi:10.1021/ac900759k

Ohuchi, S. (2012). Cell-SELEX technology. *BioResearch open access, 1*(6), 265-272.

Ozer, A., Pagano, J. M., & Lis, J. T. (2014). New technologies provide quantum changes in the scale, speed, and success of SELEX methods and aptamer characterization. *Molecular Therapy-Nucleic Acids, 3*, e183.

Paniel, N., Istamboulié, G., Triki, A., Lozano, C., Barthelmebs, L., & Noguer, T. (2017). Selection of DNA aptamers against penicillin G using Capture-SELEX for the development of an impedimetric sensor. *Talanta, 162*, 232-240. doi:https://doi.org/10.1016/j.talanta.2016.09.058

Paul, A., Avci-Adali, M., Ziemer, G., & Wendel, H. P. (2009). Streptavidin-coated magnetic beads for DNA strand separation implicate a multitude of problems during cell-SELEX. *Oligonucleotides, 19*(3), 243-254.

Pei, H., Zuo, X., Zhu, D., Huang, Q., & Fan, C. (2014). Functional DNA nanostructures for theranostic applications. *Accounts of Chemical Research, 47*(2), 550-559.

Peng, L., Stephens, B. J., Bonin, K., Cubicciotti, R., & Guthold, M. (2007). A combined atomic force/fluorescence microscopy technique to select aptamers in a single cycle from a small pool of random oligonucleotides. *Microsc Res Tech, 70*(4), 372-381. doi:10.1002/jemt.20421

Pietrzyk, D. J., & Frank, C. W. (1979). Chapter Twenty-Eight - Introduction to Electrochemistry. In D. J. Pietrzyk & C. W. Frank (Eds.), *Analytical Chemistry* (pp. 581-597): Academic Press.

Poghossian, A., Jablonski, M., Koch, C., Bronder, T. S., Rolka, D., Wege, C., & Schöning, M. J. (2018). Field-effect biosensor using virus particles as scaffolds for enzyme immobilization. *Biosensors and Bioelectronics, 110*, 168-174. doi:https://doi.org/10.1016/j.bios.2018.03.036

Pohanka, M., & Skládal, P. (2008). Electrochemical biosensors--principles and applications. *Journal of applied biomedicine, 6*(2).

Qian, L., Durairaj, S., Prins, S., & Chen, A. (2021). Nanomaterial-based electrochemical sensors and biosensors for the detection of pharmaceutical compounds. *Biosensors and Bioelectronics, 175*, 112836.

Qin, X., Yin, Y., Yu, H., Guo, W., & Pei, M. (2016). A novel signal amplification strategy of an electrochemical aptasensor for kanamycin, based on thionine functionalized graphene and hierarchical nanoporous PtCu. *Biosensors and Bioelectronics, 77*, 752-758. doi:https://doi.org/10.1016/j.bios.2015.10.050

Ramezani, M., Danesh, N. M., Lavaee, P., Abnous, K., & Taghdisi, S. M. (2016). A selective and sensitive fluorescent aptasensor for detection of kanamycin based on catalytic recycling activity of exonuclease III and gold nanoparticles. *Sensors and Actuators B: Chemical, 222*, 1-7. doi:https://doi.org/10.1016/j.snb.2015.08.024

Rezaei, B., & Irannejad, N. (2019). Chapter 2 - Electrochemical detection techniques in biosensor applications. In A. A. Ensafi (Ed.), *Electrochemical Biosensors* (pp. 11-43): Elsevier.

Robati, R. Y., Arab, A., Ramezani, M., Langroodi, F. A., Abnous, K., & Taghdisi, S. M. (2016). Aptasensors for quantitative detection of kanamycin. *Biosensors and Bioelectronics, 82*, 162-172.

Ronkainen, N. J., Halsall, H. B., & Heineman, W. R. (2010). Electrochemical biosensors. *Chemical society reviews, 39*(5), 1747-1763.

Rosati, G., Daprà, J., Cherré, S., & Rozlosnik, N. (2014). Performance Improvement by Layout Designs of Conductive Polymer Microelectrode Based Impedimetric Biosensors. *Electroanalysis, 26*(6), 1400-1408. doi:https://doi.org/10.1002/elan.201400062

Rosati, G., Ravarotto, M., Scaramuzza, M., De Toni, A., & Paccagnella, A. (2019). Silver nanoparticles inkjet-printed flexible biosensor for rapid label-free antibiotic detection in milk. *Sensors and Actuators B: Chemical, 280*, 280-289. doi:https://doi.org/10.1016/j.snb.2018.09.084

Sadak, O., Prathap, M. U. A., & Gunasekaran, S. (2019). Facile fabrication of highly ordered polyaniline–exfoliated graphite composite for enhanced charge storage. *Carbon, 144*, 756-763. doi:https://doi.org/10.1016/j.carbon.2018.12.062

Sefah, K., Shangguan, D., Xiong, X., O'donoghue, M. B., & Tan, W. (2010). Development of DNA aptamers using Cell-SELEX. *Nature Protocols, 5*(6), 1169-1185.

Shamah, S. M., Healy, J. M., & Cload, S. T. (2008). Complex Target SELEX. *Accounts of Chemical Research, 41*(1), 130-138. doi:10.1021/ar700142z

Shao, Y., Wang, J., Wu, H., Liu, J., Aksay, I. A., & Lin, Y. (2010). Graphene Based Electrochemical Sensors and Biosensors: A Review. *Electroanalysis, 22*(10), 1027-1036. doi:https://doi.org/10.1002/elan.200900571

Sharma, A., Istamboulie, G., Hayat, A., Catanante, G., Bhand, S., & Marty, J. L. (2017). Disposable and portable aptamer functionalized impedimetric sensor for detection of kanamycin residue in milk sample. *Sensors and Actuators B: Chemical, 245*, 507-515. doi:https://doi.org/10.1016/j.snb.2017.02.002

Sharma, T. K., Ramanathan, R., Weerathunge, P., Mohammadtaheri, M., Daima, H. K., Shukla, R., & Bansal, V. (2014). Aptamer-mediated 'turn-off/turn-on'nanozyme activity of gold nanoparticles for kanamycin detection. *Chemical Communications, 50*(100), 15856-15859.

Shi, H., Kou, Q., Wu, P., Sun, Q., Wu, J., & Le, T. (2021). Selection and Application of DNA Aptamers Against Sulfaquinoxaline Assisted by Graphene Oxide–Based SELEX. *Food Analytical Methods, 14*(2), 250-259.

Singer, B. S., Shtatland, T., Brown, D., & Gold, L. (1997). Libraries for genomic SELEX. *Nucleic acids research, 25*(4), 781-786.

Song, K.-M., Cho, M., Jo, H., Min, K., Jeon, S. H., Kim, T., . . . Ban, C. (2011). Gold nanoparticle-based colorimetric detection of kanamycin using a DNA aptamer. *Analytical biochemistry, 415*(2), 175-181. doi:https://doi.org/10.1016/j.ab.2011.04.007

Song, K.-M., Jeong, E., Jeon, W., Cho, M., & Ban, C. (2012). Aptasensor for ampicillin using gold nanoparticle based dual fluorescence–colorimetric methods. *Analytical and bioanalytical chemistry, 402*(6), 2153-2161. doi:10.1007/s00216-011-5662-3

Song, S., Wang, L., Li, J., Fan, C., & Zhao, J. (2008). Aptamer-based biosensors. *TrAC Trends in Analytical Chemistry, 27*(2), 108-117. doi:https://doi.org/10.1016/j.trac.2007.12.004

Stoltenburg, R., Nikolaus, N., & Strehlitz, B. (2012). Capture-SELEX: selection of DNA aptamers for aminoglycoside antibiotics. *Journal of analytical methods in chemistry, 2012*.

Stoltenburg, R., Reinemann, C., & Strehlitz, B. (2005). FluMag-SELEX as an advantageous method for DNA aptamer selection. *Analytical and bioanalytical chemistry, 383*(1), 83-91.

Stoltenburg, R., Reinemann, C., & Strehlitz, B. (2007). SELEX—a (r) evolutionary method to generate high-affinity nucleic acid ligands. *Biomolecular engineering, 24*(4), 381-403.

Sui, C., Zhou, Y., Wang, M., Yin, H., Wang, P., & Ai, S. (2018). Aptamer-based photoelectrochemical biosensor for antibiotic detection using ferrocene modified DNA as both aptamer and electron donor. *Sensors and Actuators B: Chemical, 266*, 514-521. doi:https://doi.org/10.1016/j.snb.2018.03.171

Takenaka, M., Okumura, Y., Amino, T., Miyachi, Y., Ogino, C., & Kondo, A. (2017). DNA-duplex linker for AFM-SELEX of DNA aptamer against human serum albumin. *Bioorganic & medicinal chemistry letters, 27*(4), 954-957.

Tang, Y., Gu, C., Wang, C., Song, B., Zhou, X., Lou, X., & He, M. (2018). Evanescent wave aptasensor for continuous and online aminoglycoside antibiotics detection based on target binding facilitated fluorescence quenching. *Biosensors and Bioelectronics, 102*, 646-651. doi:https://doi.org/10.1016/j.bios.2017.12.006

Tian, H., Duan, N., Wu, S., & Wang, Z. (2019). Selection and application of ssDNA aptamers against spermine based on Capture-SELEX. *Analytica chimica acta, 1081*, 168-175.

Tombelli, S., Minunni, M., & Mascini, M. (2007). Aptamers-based assays for diagnostics, environmental and food analysis. *Biomolecular engineering, 24*(2), 191-200.

Torres-Chavolla, E., & Alocilja, E. C. (2009). Aptasensors for detection of microbial and viral pathogens. *Biosensors & Bioelectronics, 24*(11), 3175-3182. doi:10.1016/j.bios.2008.11.010

Tuerk, C., & Gold, L. (1990). Systematic Evolution of Ligands by Exponential Enrichment - Rna Ligands to Bacteriophage-T4 DNA-Polymerase. *Science, 249*(4968), 505-510. doi:DOI 10.1126/science.2200121

Tuerk, C., & Gold, L. (1990). Systematic evolution of ligands by exponential enrichment: RNA ligands to bacteriophage T4 DNA polymerase. *Science, 249*(4968), 505-510.

Walsh, A. S., Yin, H., Erben, C. M., Wood, M. J. A., & Turberfield, A. J. (2011). DNA Cage Delivery to Mammalian Cells. *ACS Nano, 5*(7), 5427-5432. doi:10.1021/nn2005574

Wang, H., Wang, Y., Liu, S., Yu, J., Guo, Y., Xu, Y., & Huang, J. (2016). Signal-on electrochemical detection of antibiotics at zeptomole level based on target-aptamer binding triggered multiple recycling amplification. *Biosensors and Bioelectronics, 80*, 471-476. doi:https://doi.org/10.1016/j.bios.2016.02.014

Wang, J. (2005). Nanomaterial-based electrochemical biosensors. *Analyst, 130*(4), 421-426.

Wang, J., Ma, K., Yin, H., Zhou, Y., & Ai, S. (2017). Aptamer based voltammetric determination of ampicillin using a single-stranded DNA binding protein and DNA functionalized gold nanoparticles. *Microchimica Acta, 185*(1), 68. doi:10.1007/s00604-017-2566-8

Wang, X., Dong, S., Gai, P., Duan, R., & Li, F. (2016). Highly sensitive homogeneous electrochemical aptasensor for antibiotic residues detection based on dual recycling amplification strategy. *Biosensors and Bioelectronics, 82*, 49-54. doi:https://doi.org/10.1016/j.bios.2016.03.055

Wang, Y.-C., Cokeliler, D., & Gunasekaran, S. (2015). Reduced Graphene Oxide/Carbon Nanotube/Gold Nanoparticles Nanocomposite Functionalized Screen-Printed Electrode for Sensitive Electrochemical Detection of Endocrine Disruptor Bisphenol A. *Electroanalysis, 27*(11), 2527-2536. doi:https://doi.org/10.1002/elan.201500120

Wei, Q., Zhao, Y., Du, B., Wu, D., Li, H., & Yang, M. (2012). Ultrasensitive detection of kanamycin in animal derived foods by label-free electrochemical immunosensor. *Food Chemistry, 134*(3), 1601-1606. doi:https://doi.org/10.1016/j.foodchem.2012.02.126

Wen, Y., Pei, H., Wan, Y., Su, Y., Huang, Q., Song, S., & Fan, C. (2011). DNA nanostructure-decorated surfaces for enhanced aptamer-target binding and electrochemical cocaine sensors. *Analytical Chemistry, 83*(19), 7418-7423.

WooáKim, D., & BockáGu, M. (2012). Immobilization-free screening of aptamers assisted by graphene oxide. *Chemical Communications, 48*(15), 2071-2073.

Xiang, W., Lv, Q., Shi, H., Xie, B., & Gao, L. (2020). Aptamer-based biosensor for detecting carcinoembryonic antigen. *Talanta, 214*, 120716. doi:https://doi.org/10.1016/j.talanta.2020.120716

Xie, N., Liu, S., Yang, X., He, X., Huang, J., & Wang, K. (2017). DNA tetrahedron nanostructures for biological applications: biosensors and drug delivery. *Analyst, 142*(18), 3322-3332.

Xing, L., Zhang, Y., & Yang, J. (2019). Graphene oxide-assisted non-immobilized SELEX of chiral drug ephedrine aptamers and the analytical binding mechanism. *Biochemical and biophysical research communications, 514*(1), 134-139.

Xu, Y., Han, T., Li, X., Sun, L., Zhang, Y., & Zhang, Y. (2015). Colorimetric detection of kanamycin based on analyte-protected silver nanoparticles and aptamer-selective sensing mechanism. *Analytica chimica acta, 891*, 298-303. doi:https://doi.org/10.1016/j.aca.2015.08.013

Yan, K., Liu, Y., Yang, Y., & Zhang, J. (2015). A Cathodic "Signal-off" Photoelectrochemical Aptasensor for Ultrasensitive and Selective Detection of Oxytetracycline. *Analytical Chemistry, 87*(24), 12215-12220. doi:10.1021/acs.analchem.5b03139

Yang, J., & Bowser, M. T. (2013). Capillary electrophoresis–SELEX selection of catalytic DNA aptamers for a small-molecule porphyrin target. *Analytical Chemistry, 85*(3), 1525-1530.

Yang, J., & Gunasekaran, S. (2013). Electrochemically reduced graphene oxide sheets for use in high performance supercapacitors. *Carbon, 51*, 36-44. doi:https://doi.org/10.1016/j.carbon.2012.08.003

Yang, J., Yu, J.-H., Rudi Strickler, J., Chang, W.-J., & Gunasekaran, S. (2013). Nickel nanoparticle–chitosan-reduced graphene oxide-modified screen-printed electrodes for enzyme-free glucose sensing in portable microfluidic devices. *Biosensors and Bioelectronics, 47*, 530-538. doi:https://doi.org/10.1016/j.bios.2013.03.051

Yang, J., Zhang, W.-D., & Gunasekaran, S. (2010). An amperometric non-enzymatic glucose sensor by electrodepositing copper nanocubes onto vertically well-aligned multi-walled carbon nanotube arrays. *Biosensors and Bioelectronics, 26*(1), 279-284. doi:https://doi.org/10.1016/j.bios.2010.06.014

Yang, Z., Hao, X., Chen, S., Ma, Z., Wang, W., Wang, C., . . . Murugadoss, V. (2019). Long-term antibacterial stable reduced graphene oxide nanocomposites loaded with cuprous oxide nanoparticles. *Journal of colloid and interface science, 533*, 13-23.

Yin, J., Guo, W., Qin, X., Zhao, J., Pei, M., & Ding, F. (2017). A sensitive electrochemical aptasensor for highly specific detection of streptomycin based on the porous carbon nanorods and multifunctional graphene nanocomposites for signal amplification. *Sensors and Actuators B: Chemical, 241*, 151-159. doi:https://doi.org/10.1016/j.snb.2016.10.062

Yu, Z.-g., & Lai, R. Y. (2018). A reagentless and reusable electrochemical aptamer-based sensor for rapid detection of ampicillin in complex samples. *Talanta, 176*, 619-624. doi:https://doi.org/10.1016/j.talanta.2017.08.057

Yuan, Y., Zhang, F., Wang, H., Gao, L., & Wang, Z. (2018). A sensor based on Au nanoparticles/carbon nitride/graphene composites for the detection of chloramphenicol and ciprofloxacin. *ECS Journal of Solid State Science and Technology, 7*(12), M201.

Zamfir, L.-G., Puiu, M., & Bala, C. (2020). Advances in electrochemical impedance spectroscopy detection of endocrine disruptors. *Sensors, 20*(22), 6443.

Zeng, D., Zhang, H., Zhu, D., Li, J., San, L., Wang, Z., . . . Zuo, X. (2015). A novel ultrasensitive electrochemical DNA sensor based on double tetrahedral nanostructures. *Biosensors and Bioelectronics, 71*, 434-438.

Zhang, T., Tian, T., Zhou, R., Li, S., Ma, W., Zhang, Y., . . . Xie, X. (2020). Design, fabrication and applications of tetrahedral DNA nanostructure-based multifunctional complexes in drug delivery and biomedical treatment. *Nature Protocols, 15*(8), 2728-2757.

Zhao, B. Y., Wei, Q., Xu, C., Li, H., Wu, D., Cai, Y., . . . Du, B. (2011). Label-free electrochemical immunosensor for sensitive detection of kanamycin. *Sensors and Actuators B: Chemical, 155*(2), 618-625. doi:https://doi.org/10.1016/j.snb.2011.01.019

Zhao, J., Guo, W., Pei, M., & Ding, F. (2016). GR–Fe 3 O 4 NPs and PEDOT–AuNPs composite based electrochemical aptasensor for the sensitive detection of penicillin. *Analytical Methods, 8*(22), 4391-4397.

Zhou, L., Li, D.-J., Gai, L., Wang, J.-P., & Li, Y.-B. (2012). Electrochemical aptasensor for the detection of tetracycline with multi-walled carbon nanotubes amplification. *Sensors and Actuators B: Chemical, 162*(1), 201-208.

Zhou, N., Luo, J., Zhang, J., You, Y., & Tian, Y. (2015). A label-free electrochemical aptasensor for the detection of kanamycin in milk. *Analytical Methods, 7*(5), 1991-1996.

Zhou, Y., Li, F., Wu, H., Chen, Y., Yin, H., Ai, S., & Wang, J. (2019). Electrochemical aptasensing strategy for kanamycin detection based on target-triggered single-strand DNA adsorption on MoS2 nanosheets and enzymatic signal amplification. *Sensors and Actuators B: Chemical, 296*, 126664. doi:https://doi.org/10.1016/j.snb.2019.126664

Zhu, C., Yang, G., Ghulam, M., Li, L., & Qu, F. (2019). Evolution of multi-functional capillary electrophoresis for high-efficiency selection of aptamers. *Biotechnology advances, 37*(8), 107432.

Zhu, Y., Chandra, P., Song, K.-M., Ban, C., & Shim, Y.-B. (2012). Label-free detection of kanamycin based on the aptamer-functionalized conducting polymer/gold nanocomposite. *Biosensors and Bioelectronics, 36*(1), 29-34. doi:https://doi.org/10.1016/j.bios.2012.03.034

Chapter 3. Nanomaterials-based Electrochemical Biosensing Platform[1]

Abstract

Electrochemical biosensors have attracted enormous attention in environmental biosensing and medical diagnosis due to their rapid, accurate, reliable, and cost-effective target identification and quantification. Because of the strict requirements of sensitivity and specificity for the trace analytes, the electrochemical sensing surface often needs further modifications to be qualified for practical applications. Fortunately, the advancement of nanomaterials brings the opportunity to solve the intrinsic deficiency of electrochemical biosensors. The unique physicochemical properties of nanomaterials, such as reduced graphene oxide (rGO) and gold nanoparticles (AuNPs), offer excellent electron transfer rate for enhanced sensitivity and great biocompatibility to incorporate with novel biorecognition elements for specific target identification. In this chapter, the rGO and AuNPs modifications on the electrode surface were introduced and optimized to improve the electrical performance of the biosensing platform, and the oligonucleotide hybridization sensor was designed to examine the detecting ability of this electrochemical biosensor. The nanomaterial modified oligo-sensor was proved to sensitively detect target DNA from 60 to 1500 ng/mL in 15 min with a LOD at 2 ng/mL.

---

[1]The synthesis of AuNPs was published: Guan, J., Wang, Y. C., & Gunasekaran, S. (2015). Using l-arginine-functionalized gold nanorods for visible detection of mercury (II) ions. Journal of Food Science, 80(4), N828-N833.

The preparation of GO was published: Wang, W., Sadak, O., Guan, J., & Gunasekaran, S. (2020). Facile synthesis of graphene paper/polypyrrole nanocomposite as electrode for flexible solid-state supercapacitor. Journal of Energy Storage, 30, 101533.

3.1 Introduction

The electrochemical technique has become the most popular biosensing principle over the last decades, owing to the great performance of electrochemical biosensors with simple, rapid, label-free, sensitive, and selective qualification and quantification methods coupled with several types of biological recognition elements, i.e. antibodies, enzymes, and oligonucleotides (Cesewski & Johnson, 2020). The electrochemical biosensing system often consists of a working electrode surface, electron transmission interface, and biorecognition element (Cho, Kim, & Park, 2020). To execute an ultrasensitive detection, especially for small molecules like antibiotics, it requires a specific and sensitive biosensing probe as well as an efficient substrate exchange interface with good conductivity and biocompatibility to provide an effective solid matrix for probe immobilizations (Eggins, 2013). Therefore, various nanomaterials have been discovered and applied to construct an electrical sensitive interface for highly efficient target identification (Maduraiveeran, Sasidharan, & Ganesan, 2018).

Carbon-based nanomaterials have been the most prominent materials for biosensing surface modification, due to their unique physicochemical properties, such as mechanical strength, high surface to volume ratio, small background signal, large potential window, and diverse shapes and forms (Y. Song et al., 2016). Among all carbon-based nanomaterials, rGO offers unique advantages of uniform surface modification, where a two-dimensional film structure can be easily coated on the electrode surface to enhance the electrical conductivity of the entire working surface (Robinson, Perkins, Snow, Wei, & Sheehan, 2008). Unlike graphene with low hydrophobicity, rGO film modification has higher thermal and chemical stability and better biological compatibility with other nanomaterials and biomolecules (Tarcan et al., 2020). Moreover, rGO is generally a cost-effective nanomaterial with a simple synthesis procedure. GO can be easily

synthesized by chemical oxidation (J. Chen, Yao, Li, & Shi, 2013) or electrochemical exfoliation of graphite (Sadak, Prathap, & Gunasekaran, 2019) with a very low production cost. The structural defects of GO with oxidative functional groups can be further removed by an electrochemical reduction (Guan, He, & Gunasekaran, 2022).

The biocompatibility of AuNPs makes a good surface modification option to fix the biomolecules on the desired surface (Elahi, Kamali, & Baghersad, 2018). In addition, the intrinsic features of AuNPs, such as alterable size and shape, optical properties, electrical conductivity, and surface plasmon resonance, lead to enormous applications in various research fields, i.e., biosensing, bioimaging, drug delivery, diagnostics, and therapeutics (Singh et al., 2018).

In this chapter, a biosensing surface with rGO and AuNPs modification was prepared and evaluated. The electrical properties were optimized based on the quantities of GO and AuNPs coating, surface morphology change, and electrical response in the electrochemical sensing system. The sensor surface was verified and characterized via scanning electron microscopy (SEM), X-ray photoelectron spectroscopy (XPS), X-ray diffraction (XRD), Raman confocal microscopy, and electrochemical methods. The nanomaterial coated SPE (screen-printed electrode) was immobilized with oligonucleotide probes to perform *E. coli* genomic DNA detection to validate the biosensing capability of the designed platform.

3.2 Experimental Section

3.2.1 Materials and Reagents

SPE (TE100) was supplied by CH Instruments, Inc. (Bee Cave, TX, USA). Graphite electrodes were purchased from Graphitestore (North- brook, IL). Hydrogen tetrachloroaurate (III) trihydrate ($HAuCl_4 \cdot 3H_2O$) and Nitric acid (63%) were ordered from ACROS Organics (Morris

Plains, NJ, USA). Cysteine, 1-Ethyl-3-(3-dimethylaminopropyl) carbodiimide (EDC) and N-hydroxysuccinimide (NHS) were utilized for DNA immobilization. ssDNA oligonucleotide was purchased from IDT Corporation. Phosphate buffered saline (PBS) 10X, sulfuric acid (96%), hydrochloric acid (37%), hydrogen peroxide (50%), potassium ferrocyanide trihydrate ($K_4[Fe(CN)_6]\cdot 3H_2O$), potassium ferricyanide ($K_3[Fe(CN)_6]$), potassium chloride, sodium phosphate monobasic (NaH_2PO_4), and sodium phosphate dibasic (Na_2HPO_4) were purchased from Thermo Fisher Scientific (Rockford, IL, USA).

Ordered chemicals were used as originally received without further purification for all experiments. All solutions were prepared using deionized water with resistivity ≥18.2 MΩ·cm (Ultrapure water system, Millipore, Billerica, MA, USA).

3.2.2 Solution preparations

PBS buffer was prepared as 1X solution at pH of 7.4 unless mentioned otherwise. Tris-EDTA (TE) buffer was prepared in the concentration of 10 mM Tris and 1 mM EDTA at pH of 7.4. The electrolyte of the electrochemical system was prepared in 0.5 mM K_4 $[Fe(CN)_6]$ and 0.5 mM $K_3[Fe(CN)_6$ with 0.1 M KCl as supporting electrolyte at pH of 7.4. The ssDNA oligonucleotides were dispersed in 10 mM TE buffer at various concentrations for DNA hybridization sensing.

3.2.3 Graphene oxide preparations

In this research, GO solution was prepared by a previously reported method (Sadak, Sundramoorthy, & Gunasekaran, 2018; Sadak, Wang, Guan, Sundramoorthy, & Gunasekaran, 2019; W. Wang, Sadak, Guan, & Gunasekaran, 2020). Briefly, graphite electrodes were used as both anode and cathode to build a two-electrode system in the 100 mM PBS solution. The graphite

sheet was electrochemically exfoliated at the cathode after applying 10 V across the electrodes (Tektronix PS280). The obtained graphite flakes were vacuum filtrated through cellulose filter paper (pore size = 0.22 μm) and then washed several times with deionized water to remove buffer salts. The upper layer of the graphite suspension was collected after one-hour ultrasonication and 30 min centrifugation and then reduced by a 9:1 mixture of concentrated H_3PO_4/H_2SO_4 (360:40 mL) solution. The mixture was heated at 50 ℃ under constant stirring for 12 h. After cooled to room temperature, the suspension was poured slowly onto the ice with 3 mL of 30% H_2O_2 and washed with 200 mL HCl. One week dialysis was performed for suspension purification to remove the remaining acids and metal species. Finally, GO was re-dispersed into deionized water and ultrasonicated to obtain a homogeneous suspension (4 mg/mL) for further use.

3.2.4 Gold nanoparticles synthesis

AuNPs were synthesized via the Turkevich's method (Turkevich, Stevenson, & Hillier, 1951). In brief, 2 mL of 10 mM $HAuCl_4$ precursor was diluted in 98 mL DI water and then heated with constant stirring. The chemical reduction of $AuCl_4^-$ ions to Au^0 particles was initialized by adding 4 mL of 5% tri-sodium citrate solution to the boiling solution. The solution was kept boiling for 3 min while the color gradually turned wine-red. The solution was continually heated for another 10 min until the chemical reducing process was completed. The final product was cooled down at room temperature and stored in refrigerator for further use.

3.2.5 Electrode fabrication

The SPE fabrication scheme was illustrated in **Figure 3.1**. The SPE was rinsed by the DI water to remove any existing impurities before use. Electrochemically rGO-modified SPE was prepared by the drop-coated method using the dispersed 4 mg/mL GO solution at room

temperature, followed by the electrochemical reduction procedure using cyclic voltammetry (CV) technique. The surface reduction was achieved by applying 100 cycles of potential sweep between 0 to -1.4 V with a scan rate of 100 mV/s in nitrogen-purged PBS at pH 7.4. In this process, GO layer was successfully coated on the working surface of SPE and was effectively reduced to rGO to form a sensitive electron-transfer interface. The modified SPE was rinsed with DI water and dried at room temperature. The rGO-coated electrode (rGO-SPE) was then drop-coated with 20 µL as-prepared AuNPs solution under ambient conditions.

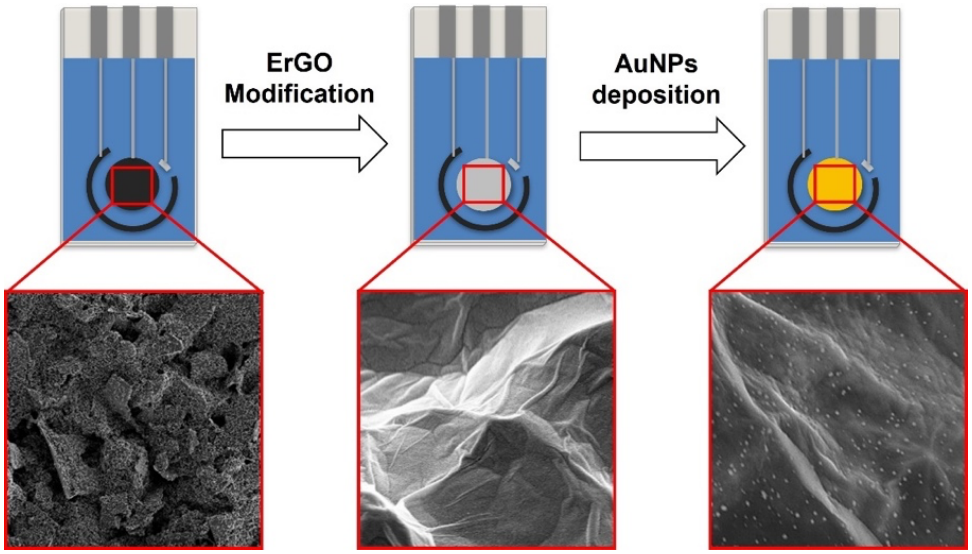

Figure 3.1. Scheme of nanomaterial modification on the working channel of SPE

The nanomaterial coated SPE was immersed in 5 mL of 0.1 M cysteine solution for 4 hours at room temperature to covalently form Au-S bond, and then transferred into 5 mL of 50 mM EDC and 200 mM NHS solution for 2 hours to fix the carbodiimide crosslinker on the working surface. After activating carboxyl groups into efficient amine-reactive intermediates, the SPE surface was further immobilized with 5 uL of 1 mM amine-modified oligonucleotide probes overnight to form a covalent amide bond. The fabricated SPE was cleaned with DI water and immersed in 1X PBS (pH 7.4) at 4 ℃ for long-term storage.

3.2.6 Nanomaterial and electrode characterization

Ultraviolet-visible spectroscopy (UV/Vis Lambda-25, PerkinElmer), Fourier-transform infrared spectroscopy (FTIR, Spectrum-100, PerkinElmer), Transmission electron microscopy (TEM, Tecnai 12), SEM (Zeiss/LEO 1530, Zeiss), XPS (K-Alpha, ThermoFisher), Raman confocal microscopy (LabRAM Aramis Raman, Horiba Jobin Yvon), and XRD (Bruker D8 Discovery) were employed to characterize the prepared nanomaterials and validate the changes of surface morphology on the functionalized SPE. Cyclic voltammetry (CV), differential pulse voltammetry (DPV), and electrochemical Impedance Spectroscopy (EIS) with redox couple $[Fe(CN)_6]^{3-}$/ $[Fe(CN)_6]^{4-}$ as supporting electrolyte was used to explore the electrical behaviors of SPE after each surface modification. The CHI-660D electrochemical workstation (CHI Instruments, Inc. USA) was utilized to perform all electrochemical measurements.

3.3 Results and discussions

3.3.1 Graphene oxide Characterization

The morphology properties of the synthesized GO were examined by the TEM micrograph (**Figure 3.2**). The TEM image of GO (**Figure 3.2A**) shows a semitransparent view with a relatively high resolution, which suggests the oxidative groups of GO are partially removed by the acid reduction process and the nanomaterial is relatively stable under the high energy beam. The thin flake structure demonstrates the efficiency of electrochemical exfoliation and the elimination of intercalated oxidative groups (Dreyer, Park, Bielawski, & Ruoff, 2010).

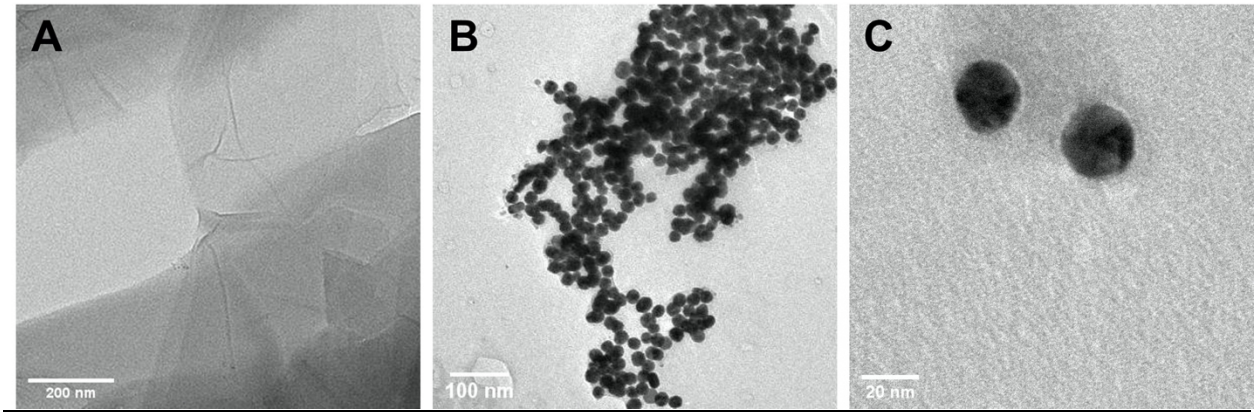

Figure 3.2. TEM images of synthesized (A) GO and (B) AuNPs at 100 nm and (C) 20 nm

UV/Vis spectroscopy, Raman microscopy, and XRD were used to characterize the synthesized GO (**Figure 3.3**). Two characteristic absorbance peaks are observed in UV/Vis spectrum. The first peak at 232 nm represents the $\pi \Rightarrow \pi*$ transitions of aromatic groups, while the second one at 298 nm expresses the $n \Rightarrow \pi*$ transitions of C=O groups (Çiplak, Yildiz, & Çalimli, 2015). The hidden shoulder of the second peak suggests a reduced intensity of intercalated oxidative groups.

Figure 3.3B shows the D, G, and 2D bands of GO and rGO on the Raman spectra comparing to those on the carbon printed SPE. The D band at 1330 cm^{-1} is the result of out-of-plane vibrations, while G band 1585 cm^{-1} is allocated to in-plane vibrations of sp2 carbon bonds. The ratio of D/G band is often used to analyze the structural defects presented on carbon nanomaterial (Johra, Lee, & Jung, 2014). In **Figure 3.3B**, the D/G ratio of rGO is significantly boosted due to the formation of new graphitic domains where the sp2 bonds are disrupted and the sp3 bonds are created, which proves the elimination of oxidative groups by the electrochemical reduction. The Raman spectra demonstrate a successful rGO coating and an effective electrochemical reduction.

The FTIR spectra is an excellent technique to validate the appearance of various functional groups in the carbon nanostructures. **Figure 3.3C** illustrate obvious O-H band at 3408 cm^{-1}, C=O band at 1725 cm^{-1}, C=C band at 1630 cm^{-1}, C-OH band at 1368 cm^{-1}, and C-O band at 1080 cm^{-1} for GO, which has good agreement with reported research (Strankowski, Włodarczyk, Piszczyk, & Strankowska, 2016). After the reduction process, C=O band and C-OH band for rGO disappear, while O-H band and C-O band still exist with much less intensity. The result reveals that the electrochemical reduction effective eliminated the oxidative groups in GO structure, which suggests a better 2D structure of rGO.

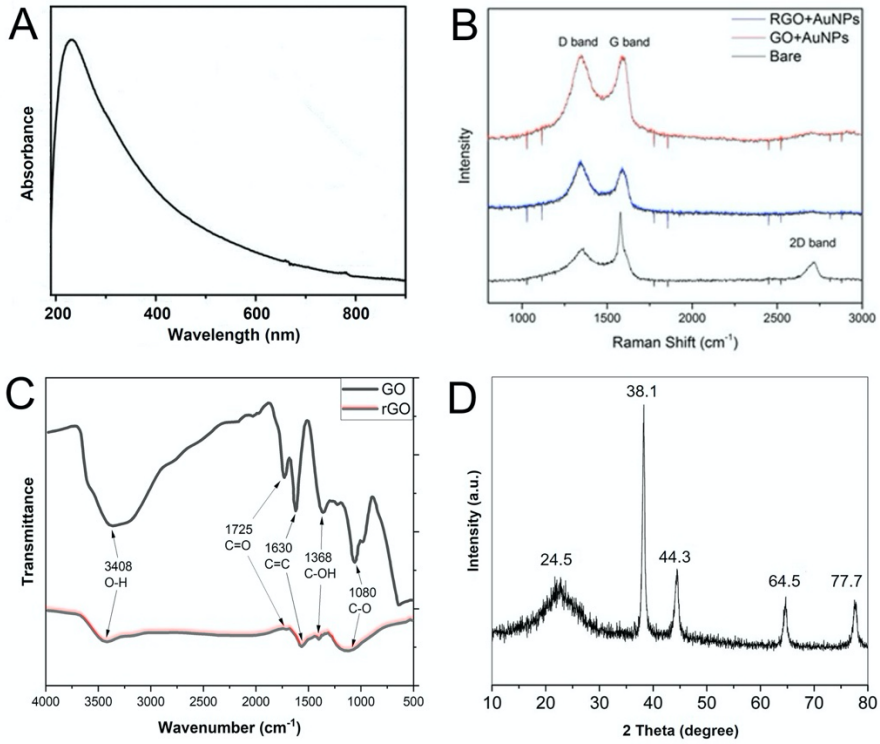

Figure 3.3. (A) UV/Vis spectrum of as-prepared GO. (B) Raman spectra of GO and rGO with AuNPs on the SPE surface compared to the bare SPE. (C) FTIR spectra of GO and rGO comparison. (D) XRD spectra of rGO-AuNPs nanocomposite

The XRD spectrum is a fast analytical tool primarily used to determine the atomic and molecular structures of crystalline materials. From **Figure 3.3D**, XRD spectrum displays five distinguishable 2θ peaks, which suggests an rGO-AuNPs nanocomposite is presented. The 2θ peak at 24.10° is attributed to the π-conjugated structure of rGO rather than the regular 10° peak on GO (Hidayah et al., 2017). In addition, four typical Au nanoparticle peaks at 38.1°, 44.3°, 64.5°, and 77.7°, corresponding to standard Bragg reflections (111), (200), (220), and (311) of face center cubic (fcc) lattice (Krishnamurthy, Esterle, Sharma, & Sahi, 2014), are observed on the XRD spectrum. This spectrum confirms the rGO/AuNPs modification on SPE surface is successful.

3.3.2 AuNPs Characterization

The as-prepared AuNPs solution was characterized by UV/Vis spectroscopy (**Figure 3.4**) and showed a significant absorbance peak at 520 nm, which matches the typical surface plasmon resonance peak of AuNPs from the previous reports (Saha, Agasti, Kim, Li, & Rotello, 2012). The size and concentration of synthesized AuNPs were determined using the measured UV/Vis spectrum by the corrected Mie method (Haiss, Thanh, Aveyard, & Fernig, 2007). The particle diameter of the AuNPs was calculated from

$$d = \exp\left(B_1 \frac{A_{spr}}{A_{450}} - B_2\right) \quad (1)$$

Here, A_{spr} is the absorbance at the surface plasma resonance peak and A_{450} is the absorbance at 450 nm. B_1 and B_2 are experimentally determined in the article as 3.00 and 2.20, respectively. The average particle diameter was then calculated using **eq. 1** as 22 nm. The size estimation was confirmed by TEM micrograph (**Figure 3.2C**). **Figure 2B** shows that the synthesized AuNPs have a uniform size and shape, which improves the reproducibility of AuNPs-modified biosensor.

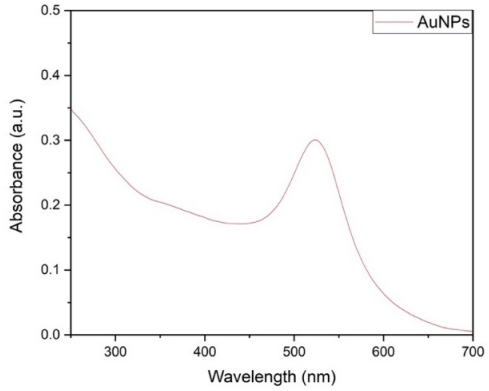

Figure 3.4. UV/Vis spectrum of AuNPs with 520 nm absorbance peak

With the calculated diameter, we determined the concentration of AuNPs using the Gauss function (**eq.2**) presented in the Mie method based on the corresponding fit parameters to be 0.5 nM. With the known concentration of AuNPs solution, an optimization of AuNPs modification based on the quantity is available in later research.

$$N = \frac{A_{450} \times 10^{14}}{d^2[-0.295+1.36\ exp(-(\frac{d-96.8}{78.2})^2)]} \quad (2)$$

3.3.3 Optimization of nanomaterial modification

To achieve the best electrical performance of the SPE, we optimized the nanomaterial coating regarding to the quantities of GO and AuNPs. GO with different concentrations was drop-coated on the working surface, which was further electrochemically reduced to rGO. The rGO-SPE was tested using DPV, and the peak currents were obtained to build a comparison graph (**Figure 3.5**). As the concentration of rGO raised, the current magnitude was initially increased indicating that the sensor conductivity was improved with the generated rGO layer. However, SPE displayed a reduced response current trend with the continuously increased amount of rGO coated on the surface where multiple layers of rGO film was formed with random stacking angles between

each interface, which inhibited the electron exchange from detecting environment and resulted in a current deduction. In addition, an unstable GO structure created by the intensive coating was adsorbed on the electrode surface only through Van der Waals' force, which was easy to detach from the electrode after each washing step. The unstable structure limited the detecting stability and sensor reusability. Thus, 4 mg/mL of rGO was selected for all the sensor preparations in later research to obtain the best electrical performance and stability.

The purpose of AuNPs modification is to provide the aptamer-TDN immobilization site as well as to improve the surface sensitivity, but only sensitivity enhancement is discussed in this chapter. The aptamer-TDN immobilization effect is evaluated in the next chapter. The SPE was first coated with rGO at optimized conditions before the AuNPs optimization. The concentration range of 0.1 to 2.0 nM was chosen to examine the electrical current enhancement. At a concentration around 1 nM, the response current reached the maximum value, suggesting the surface was fully occupied by AuNPs. Thus, 1 nM AuNPs solution was used for electrode modification later.

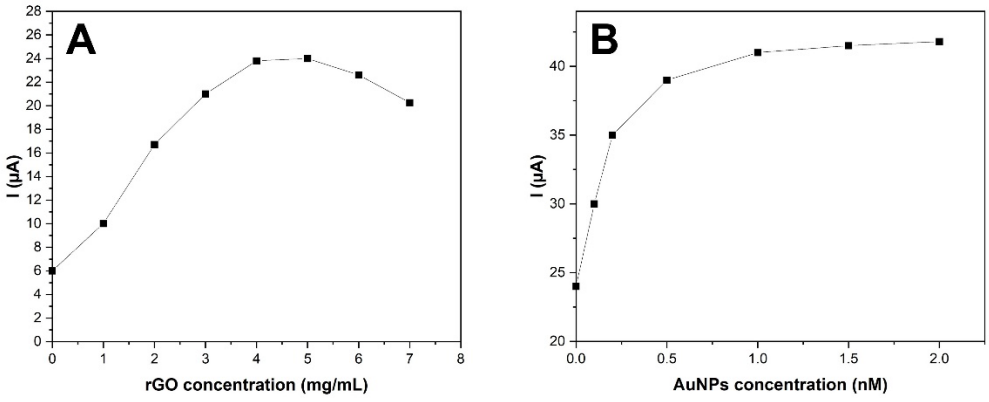

Figure 3.5. Optimization of nanomaterial modifications (A) rGO coating at 1, 2, 3, 4, 5, 6, 7 mg/mL, (B) AuNPs coating at 0.1, 0.2, 0.5, 1, 1.5, 2 nM

3.3.4 SEM validation of surface modification

The SEM micrographs were used to validate the surface morphology of the SPE with each modification step (**Figure 3.6)**. The bare electrode surface reveals a rough surface with irregular and uniform structures **(Figure 3.6A)**. Electron transmission was hindered by this irregular surface, and the redox reaction on the surface was impeded, which explains the unsatisfied electrical response of the bare SPE. On the other hand, the rGO-SPE surface is covered with a thin, crumpled, paper-like film (**Figure 3.6B**), indicating a successful modification of rGO layer. The unique consistent smooth film structures between adjacent layers were associated with an increased π-π stacking and Van der Waals interaction due to the effective electrochemical exfoliation and the efficient elimination of intercalated oxidative groups by the electrochemical reduction process. Furthermore, because the oxidative functional groups were eliminated by electrochemical reduction, the surface zeta potential of GO was reduced from negative to almost zero, which provided a better electron exchange environment for redox reaction and improved the electrical performance of SPE.

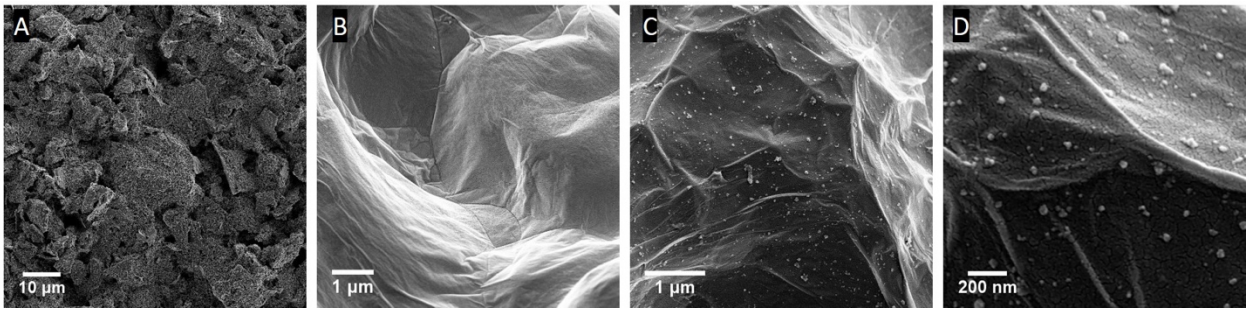

Figure 3.6. SEM images of (A) bare SPE, (B) rGO/SPE, (C) AuNPs/rGO/SPE, and (D) AuNPs/rGO/SPE at nanoscale

Upon the AuNPs deposition, the surface of AuNPs/rGO/SPE is shown in **Figures 3.6C, D.** The as-prepared 22-nm diameter AuNPs was evenly coated on the SPE without aggregation, which

affords ideal immobilization sites for biosensing probes in later research. Besides, the even distribution of AuNPs offers a better electron transfer interface to enhance the electrical response. These SEM images demonstrate the successfully fabrication of the SPE surface (AuNPs/rGO/SPE) and explain the good electrical conductivity and the immune-binding ability obtained by the modified sensor due to the flat and smooth electrode surface with enhanced electron transmission rate and evenly distributed immobilization sites.

3.3.5 XPS characterization of nanomaterial coating

XPS is a surface-sensitive spectroscopy that can identify the specific elements on the material surface as well as the chemical bonding states. We used XPS to provide evidence for the SPE fabrication. XPS spectra in **Figure 3.7** show that the modified SPE contains both C_{1s} and Au_{4f} characteristic peaks, which suggests the rGO-AuNPs nanocomposite is assembled on the surface. **Figure 3.7A** exhibits three C_{1s} characteristic peaks of GO, including a C_{sp2} band at 284.7 eV, a C-OH band at 286.6 eV, and a C=O band at 288.3 eV. It is clear in **Figure 3.7B** that the intensities of both C-OH and C=O bands of rGO are significantly deducted after applying 0 to -1.4 V potential to reduce the GO on the electrode surface. Thus, the elimination of oxidative functional groups by the electrochemical reduction process is clearly evidenced by the XPS spectra. Based on the result, we infer that carbon tends to form a planar C_{sp2}-C_{sp2} structure after the electrochemical reduction, which offers a better π-π stacking condition between adjacent rGO layers, and then constructs a more stable layer-layer rGO structure. In addition, the element Au is identified in **Figure 7C**, which confirmed the previous result of AuNPs formation on the SPE surface.

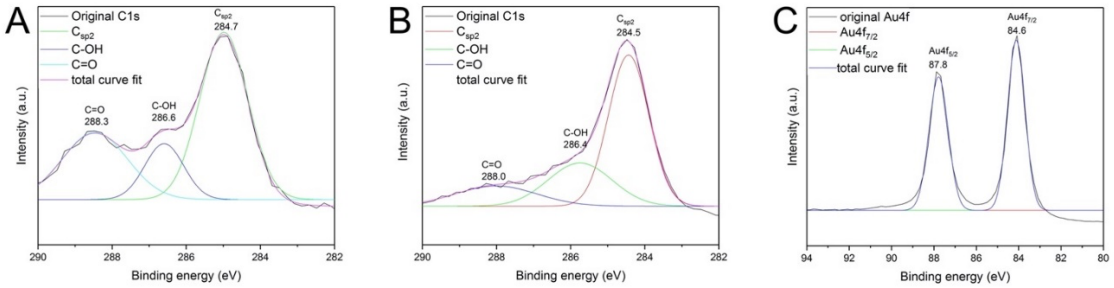

Figure 3.7. XPS C_{1s} spectra of SPE surface modified with (A) GO and (B) rGO, and Au_{4f} spectra of SPE surface modified with (C) AuNPs

3.3.6 Electrical behavior of modified SPE

CV, DPV, and EIS were employed to evaluate the electrical behaviors with each nanomaterial coating step on the SPE surface (**Figure 3.8)**. The bare SPE (curve a) presented a low electrical signal and a large gap between oxidation and reduction peaks in CV (**Figure 3.8A**), indicating a relatively low redox reaction rate and poor electron transferring ability. With GO deposition, the current signal peak substantially increased from 18 µA to 26 µA (curve b), representing a better electrical property of carbon nanomaterial compared to the original screen-printed carbon. Moreover, a narrower gap between the oxidation peak and reduction peak proved the enhanced conductivity of the surface structure. After the electrochemical reduction step of GO, the removal of oxidative functional groups on rGO amplified the response current signal (curve c), which agrees with the assumption of forming a more sensitive electron-transfer interface by the reduction of GO. The electrical signal was further amplified (curve d) by the AuNPs coating due to the assistance of transferring electrons from specific biological compounds to the electrode surface based on their unique chemical and physical properties (Hamza, Ignaszak, & Kiani, 2017). The DPV graph (**Figure 3.8B**) shows the same signal increasing trend as CV graphs, indicating

the formation of the rGO-AuNPs 3D structure improves the surface conductivity and electrical performance of SPE.

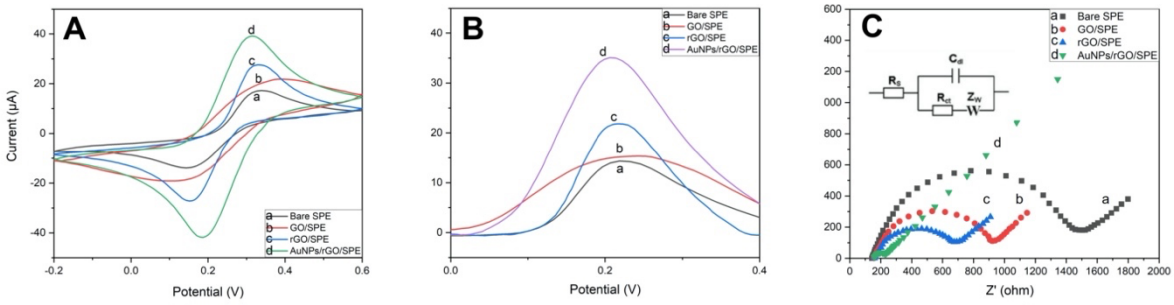

Figure 3.8. (A) CV graph, (B) DPV graph and (C) EIS graph of (a) bare SPE, (b) GO/SPE, (c) rGO/SPE, (d) AuNPs/rGO/SPE in 1 mM $[Fe(CN)_6]^{3-/4-}$

Furthermore, the EIS graph displays an obvious deduction in the diameter of the semicircle upon each nanomaterial coating step on the SPE surface, suggesting a reducing charge-transfer resistance (R_{ct}) after each modification (**Figure 3.8C**). The bare SPE (curve a) displays the largest semicircle diameter that is equal to the largest R_{ct} value, demonstrating the resistivity of electrons transmission due to its irregular surface. A significantly smaller semicircle diameter lower R_{ct} value is exhibited upon the rGO and AuNPs coating (curve d), which is strong proof that a better electrical behavior was achieved by nanomaterial modifications.

3.3.7 DNA hybridization biosensing

DPV technique was employed to monitor the electrical signal change for target DNA hybridization. A wide range of *E. coli* DNA concentrations was incubated with the fabricated SPE to test the biosensing sensitivity and accuracy. The DPV result (**Figure 3.9A**) confirmed that the hybridization between *E. coli* DNA sequence and its complementary ssDNA oligo probe

interrupted the electron transmission on the SPE surface and led to a current signal deduction. The changes in current were considerably correlated to the spiked target DNA amounts. The potential linear relationship between the target DNA amounts and DPV peak current decrement was measured to build a mathematical model. The fitted linear model (**Figure 3.9B**) displays excellent linearity with R^2=0.985 in the range of 60 to 1500 ng/mL. Therefore, the designed biosensor can qualify and quantify the target genomic DNA in the range of 60 to 1500 ng/mL and detect at least 2 ng/mL of target DNA in less than 15 min. The LOD of the system was defined as three times standard deviation of the control sample with 3:1 signal-to-noise ratio.

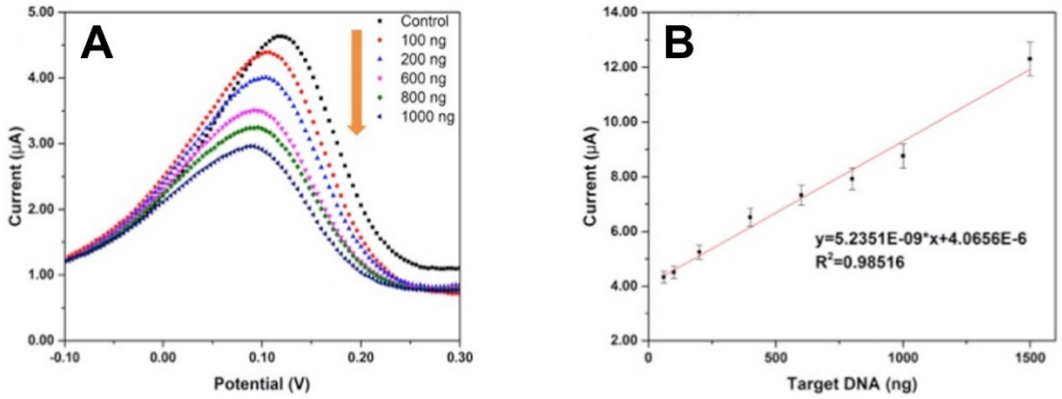

Figure 3.9. (A) DPV current response of the fabricated SPE when exposed to different amounts of target DNA after 15 min incubation, and (B) Calibration curve of electrical signal decrement with target DNA amounts ranged from 60 ng to 1500 ng.

3.4 Conclusions

The nanomaterials were synthesized by simple, fast, and cost-effective methods, and the morphology of as-prepared reduced GO and AuNPs was characterized by TEM microscopy with the desired nanostructures. Electrochemically reduced GO was further validated by UV/Vis, FTIR,

XRD, and Raman spectrum to confirm the successful removal of oxidative functional groups and the formation of flexible and electrical sensitive film nanostructure. The nanomaterial coating procedures were optimized based on the current signal response. The electrochemical properties of nanomaterial coated SPE were interrogated by CV, DPV, and EIS, and a remarkable electrical enhancement was observed with the rGO/AuNPs nanocomposites modification, resulting in several times stronger current response and significantly reduced surface impedance. The surface morphology changes of SPE from each coating step were measured by SEM microscopy, and the surface composition was evaluated by the XPS spectrum, which explains the advancement of electrical behavior based on the electrode surface improvement. The fabricated SPE was tested by *E. coli* genomic DNA in a wide range of concentrations. The DPV results demonstrate that the nanomaterial coated SPE can perform a sensitive and accurate biosensing activity to detect target DNA in the range of 60 to 1500 ng/mL and achieve a low LOD at 2 ng/mL in 15 min, which suggests the designed biosensing platform has potential in practical applications of ultrasensitive antibiotic detections.

Reference

Cesewski, E., & Johnson, B. N. (2020). Electrochemical biosensors for pathogen detection. *Biosensors and Bioelectronics, 159*, 112214.

Chen, J., Yao, B., Li, C., & Shi, G. (2013). An improved Hummers method for eco-friendly synthesis of graphene oxide. *Carbon, 64*, 225-229.

Cho, I.-H., Kim, D. H., & Park, S. (2020). Electrochemical biosensors: Perspective on functional nanomaterials for on-site analysis. *Biomaterials Research, 24*(1), 1-12.

Çiplak, Z., Yildiz, N., & Çalimli, A. (2015). Investigation of graphene/Ag nanocomposites synthesis parameters for two different synthesis methods. *Fullerenes, Nanotubes and Carbon Nanostructures, 23*(4), 361-370.

Dreyer, D. R., Park, S., Bielawski, C. W., & Ruoff, R. S. (2010). The chemistry of graphene oxide. *Chemical society reviews, 39*(1), 228-240.

Eggins, B. R. (2013). *Biosensors: an introduction*: Springer-Verlag.

Elahi, N., Kamali, M., & Baghersad, M. H. (2018). Recent biomedical applications of gold nanoparticles: A review. *Talanta, 184*, 537-556. doi:https://doi.org/10.1016/j.talanta.2018.02.088

Guan, J., He, K., & Gunasekaran, S. (2022). Self-assembled tetrahedral DNA nanostructures-based ultrasensitive label-free detection of ampicillin. *Talanta, 243*, 123292. doi:https://doi.org/10.1016/j.talanta.2022.123292

Haiss, W., Thanh, N. T. K., Aveyard, J., & Fernig, D. G. (2007). Determination of Size and Concentration of Gold Nanoparticles from UV−Vis Spectra. *Analytical Chemistry, 79*(11), 4215-4221. doi:10.1021/ac0702084

Hamza, S., Ignaszak, A., & Kiani, A. (2017). Synthesis of Electrical Conductive Silica Nanofiber/Gold Nanoparticle Composite by Laser Pulses and Sputtering Technique. *Nanoscale research letters, 12*(1), 432-432. doi:10.1186/s11671-017-2200-z

Hidayah, N., Liu, W.-W., Lai, C.-W., Noriman, N., Khe, C.-S., Hashim, U., & Lee, H. C. (2017). *Comparison on graphite, graphene oxide and reduced graphene oxide: Synthesis and characterization.* Paper presented at the AIP Conference Proceedings.

Johra, F. T., Lee, J.-W., & Jung, W.-G. (2014). Facile and safe graphene preparation on solution based platform. *Journal of Industrial and Engineering Chemistry, 20*(5), 2883-2887.

Krishnamurthy, S., Esterle, A., Sharma, N. C., & Sahi, S. V. (2014). Yucca-derived synthesis of gold nanomaterial and their catalytic potential. *Nanoscale research letters, 9*(1), 1-9.

Maduraiveeran, G., Sasidharan, M., & Ganesan, V. (2018). Electrochemical sensor and biosensor platforms based on advanced nanomaterials for biological and biomedical applications. *Biosensors and Bioelectronics, 103*, 113-129.

Robinson, J. T., Perkins, F. K., Snow, E. S., Wei, Z., & Sheehan, P. E. (2008). Reduced graphene oxide molecular sensors. *Nano letters, 8*(10), 3137-3140.

Sadak, O., Prathap, M. U. A., & Gunasekaran, S. (2019). Facile fabrication of highly ordered polyaniline–exfoliated graphite composite for enhanced charge storage. *Carbon, 144*, 756-763. doi:https://doi.org/10.1016/j.carbon.2018.12.062

Sadak, O., Sundramoorthy, A. K., & Gunasekaran, S. (2018). Facile and green synthesis of highly conducting graphene paper. *Carbon, 138*, 108-117. doi:https://doi.org/10.1016/j.carbon.2018.05.076

Sadak, O., Wang, W., Guan, J., Sundramoorthy, A. K., & Gunasekaran, S. (2019). MnO2 Nanoflowers Deposited on Graphene Paper as Electrode Materials for Supercapacitors. *ACS Applied Nano Materials, 2*(7), 4386-4394. doi:10.1021/acsanm.9b00797

Saha, K., Agasti, S. S., Kim, C., Li, X., & Rotello, V. M. (2012). Gold Nanoparticles in Chemical and Biological Sensing. *Chemical Reviews, 112*(5), 2739-2779. doi:10.1021/cr2001178

Singh, P., Pandit, S., Mokkapati, V. R. S. S., Garg, A., Ravikumar, V., & Mijakovic, I. (2018). Gold Nanoparticles in Diagnostics and Therapeutics for Human Cancer. *International journal of molecular sciences, 19*(7). doi:10.3390/ijms19071979

Song, Y., Luo, Y., Zhu, C., Li, H., Du, D., & Lin, Y. (2016). Recent advances in electrochemical biosensors based on graphene two-dimensional nanomaterials. *Biosensors and Bioelectronics, 76*, 195-212.

Strankowski, M., Włodarczyk, D., Piszczyk, Ł., & Strankowska, J. (2016). Polyurethane nanocomposites containing reduced graphene oxide, FTIR, Raman, and XRD studies. *Journal of Spectroscopy, 2016*.

Tarcan, R., Todor-Boer, O., Petrovai, I., Leordean, C., Astilean, S., & Botiz, I. (2020). Reduced graphene oxide today. *Journal of Materials Chemistry C, 8*(4), 1198-1224.

Turkevich, J., Stevenson, P. C., & Hillier, J. (1951). A study of the nucleation and growth processes in the synthesis of colloidal gold. *Discussions of the Faraday Society, 11*, 55-75.

Wang, W., Sadak, O., Guan, J., & Gunasekaran, S. (2020). Facile synthesis of graphene paper/polypyrrole nanocomposite as electrode for flexible solid-state supercapacitor. *Journal of Energy Storage, 30*, 101533. doi:https://doi.org/10.1016/j.est.2020.101533

Chapter 4. Self-assembled Tetrahedral DNA Nanostructures-Based Ultrasensitive Detection of Ampicillin[2]

Abstract

Residual ampicillin (AMP) in the milk product can potentially cause foodborne diseases in humans and develop antibiotic resistance through the food chain, leading to serious public health issues. The aptamer-based biosensor has been introduced as a novel antibiotic monitoring approach and attracted major attention due to the unique sensing properties of aptamers. Although a variety of aptamer-based electrochemical sensors was proposed for ampicillin detection, target-binding ability of aptamer was often interrupted by the poor management of orientation and conformation. In this chapter, a tetrahedral DNA nanostructure (TDN) was designed to precisely control the self-orientation of the aptasensing probe by offering a rigid immobilization base, and to maintain the functional structure of aptamer by keeping nanospacing from neighbor sequences. The electrical responses exhibited a remarkable improvement in target accessibility and detecting sensitivity with the assistance of DNA nanostructures. The designed aptasensor could identify and quantify a broad concentration range of residual ampicillin (10 pM to 1000 nM) and obtained an ultralow low LOD (1 pM) within 30 min. Additionally, the real sample test was successfully performed in the spiked milk with 96.6% to 103.95% recovery rate. Reproducibility and stability of the designed aptasensor were validated to reveal the application potential of on-site antibiotic analysis.

---

[2]This chapter was published: Guan, J., He, K., & Gunasekaran, S. (2022). Self-assembled tetrahedral DNA nanostructures-based ultrasensitive label-free detection of ampicillin. *Talanta, 243*, 123292

4.1 Introduction

Ampicillin is a β-Lactam antibiotic which is extensively used as veterinary medicine to prevent and treat various animal infections, such as respiratory tract infections, gastrointestinal infections, urinary tract infections, meningitis, salmonellosis, and endocarditis (W. Luo, Ang, & Thompson Jr, 1997). However, the overuse of antibiotics can lead to food contamination with residue antibiotics and their metabolites and threaten public health (Manyi-Loh, Mamphweli, Meyer, & Okoh, 2018). Therefore, an effective monitoring and quantification method for the residue antibiotics are required for the food safety concern (Mobarki, Almerabi, & Hattan, 2019). The conventional determinations of antibiotic levels are relied on the antimicrobial assay ("United States Department of Agriculture. Food Safety and Inspection Service, Office of Public Health Science. Bioassay for the Detection, Identification and Quantitation of Antimicrobial Residues in Meat and Poultry Tissue," 2010) or chromatography-based methods such as high-performance liquid chromatography (HPLC) (Briscoe, McWhinney, Lipman, Roberts, & Ungerer, 2012), gas chromatography-mass spectrometry (GC-MS) (Yang et al., 2015), and liquid chromatography-tandem mass spectrometry (LC-MS/MS) (Berendsen, Wegh, Memelink, Zuidema, & Stolker, 2015). Although these conventional methods are effective and widely used, the mandatory requirements, such as strict sample pre-treatment, sophisticated instruments, and highly qualified personnel, prohibit them from economical applications, and high-throughput on-site analysis (Sharma et al., 2016).

The aptamer-based electrochemical biosensor has the potential to provide a simple, rapid, and cost-effective quantification method for ultrasensitive residue antibiotics detection (Kim, Raston, & Gu, 2016; S. Song, Wang, Li, Fan, & Zhao, 2008). Aptamer offers great specificity and sensitivity as a biological recognition probe as well as structural flexibility, chemical and thermal

stability, and excellent reproducibility compared to its conventional rivals, antibodies and enzymes (R. E. Wang, Wu, Niu, & Cai, 2011). The first ampicillin aptamer was reported by Song et al., and was later used for various studies to build ampicillin biosensors (K.-M. Song, Jeong, Jeon, Cho, & Ban, 2012). This aptamer sequence showed good binding affinity to the target of interest, which was verified by several research (Daprà, Lauridsen, Nielsen, & Rozlosnik, 2013; Z. Luo et al., 2017; Rosati, Daprà, Cherré, & Rozlosnik, 2014; J. Wang, Ma, Yin, Zhou, & Ai, 2017).

However, the binding activity of aptamer is often limited by uncontrolled orientation of aptamer, self-induced perturbation, and intermolecular interaction from adjacent aptamer probes (Ghorbani, Abbaszadeh, Dolatabadi, Aghebati-Maleki, & Yousefi, 2019). Additionally, the irregular surface morphology of the designed biosensor and locally crowded immobilization environment further reduce the target accessibility (Wen et al., 2011; Wong, Chow, & Gooding, 2005). These unsolved issues disrupt the aptamer-target binding efficiency and jeopardize the reproducibility and reusability of biosensors. Herein, we mitigated these adverse effects by employing the TDN. TDN is a three-dimensional tetrahedron structure with nanoscale size, excellent programmability, high surface accessibility and biocompatibility (Xie et al., 2017). TDN can be self-assembled *via* a simple temperature-controlled approach by four single-stranded DNA sequences (ssDNA) (Gao et al., 2021). TDN with a rigid structure, where aptamer can be appended onto the top vertex, can keep aptamer from sensor surface or neighbor probe and precisely control the orientation of aptamer to create an in-solution like environment for aptamer-target binding (X. Chen et al., 2014; Lin et al., 2014). Additionally, TDN help passivate the working surface from unnecessary nonspecific adsorptions of irrelevant molecules (Huang, He, & Li, 2018).

In this chapter, we propose a label-free electrochemical aptasensor functionalized by nanomaterials and DNA nanostructures. The designed aptasensor was interrogated by

electrochemical methods, and surface morphology and functionality were evaluated by microscopy and spectroscopy. The ampicillin concentration determinations were performed in both buffer systems and real milk samples.

4.2 Experimental Section

4.2.1 Materials and Reagents

SPE (TE100) was ordered from CH Instruments, Inc. (Bee Cave, TX, USA). Phosphate buffered saline (PBS) 10X, potassium ferrocyanide trihydrate ($K_4[Fe(CN)_6]\cdot 3H_2O$), potassium ferricyanide ($K_3[Fe(CN)_6]$), potassium chloride, sodium phosphate monobasic (NaH_2PO_4), and sodium phosphate dibasic (Na_2HPO_4) were purchased from Thermo Fisher Scientific (Rockford, IL, USA). All DNA oligonucleotides (**Table 4.1**) were ordered from Sangon Biotech (Shanghai, China). All antibiotics including ampicillin were purchased from Thermo Fisher Scientific (Rockford, IL, USA). Tris-(2- carboxyethyl) phosphine hydrochloride (TCEP) was purchased from Thermo Fisher Scientific (Rockford, IL, USA). The milk samples were purchased at a local grocery store.

All chemical products were used as originally received without any purification. All solutions were prepared using deionized water with resistivity ≥18.2 MΩ·cm (Ultrapure water system, Millipore, Billerica, MA, USA) for all experiments.

4.2.2 Solution preparations

PBS buffer was made as 1X solution at pH of 7.4 unless mentioned otherwise. Tris-EDTA (TE) buffer was prepared in the concentration of 10 mM Tris and 1mM EDTA at pH of 7.4. Immobilization buffer was mixed with the TE buffer with 100 mM NaCl, 5 mM KCl, 1 mM $CaCl_2$

and 1 mM $MgCl_2$ at pH 7.4. The electrolyte of the electrochemical system was prepared in 0.5 mM K_4 [$Fe(CN)_6$] and 0.5 mM K_3[$Fe(CN)_6$ with 0.1 M KCl as supporting electrolyte at pH of 7.4.

Ampicillin powder was dissolved in TE buffer at 100 mg/mL and then diluted with deionized water to the designed concentrations for the biosensing purpose.

4.2.3 Nanostructure preparation

Table 4.1 displays the oligonucleotide sequences (Oligo-A, B, C, D) used in the TDN self-assembly procedure. All sequences were first prepared in TE buffer (pH 7.4) separately in the concentration of 100 µM and kept in a freezer for long-term storage.

Table 4.1. Oligonucleotide sequences used to build TDN

Name	Sequence (5' to 3')
Oligo A	ACATTCCTAAGTCTGAAACATTACAGCTTGCTACACGAGAAGAGCCGC CATAGTA-TTTTTTTTTT-GCGGGCGGTTGTATAGCGG
Oligo B	HS-C6-TATCACCAGGCAGTTGACAGTGTAGCAAGCTGTAAT AGATGCGAGGGTCCAATAC
Oligo C	HS-C6-TCAACTGCCTGGTGATAAAACGACACTACGTGGGAA TCTACTATGGCGGCTCTTC
Oligo D	HS-C6-TTCAGACTTAGGAATGTGCTTCCCACGTAGTGTCGT TTGTATTGGACCCTCGCAT

To initialize the TDN self-assembly, 10 µL of each strand with equal moles was mixed in the immobilization buffer (pH 7.4) with 5 mM TCEP in the final volume of 100 µL. The reduction

reaction was performed at room temperature for one hour to remove all the disulfide bonds. The resulted mixture was heated to 95 °C for 10 min to denature all the hairpin and secondary structures and then cooled to 60 °C for 10 min to perform the self-assembly. The stepwise cooling process was utilized to finish the self-assembly and minimize the side products (Gao et al., 2021). Then the solution was cooled to 4 °C for 10 min to terminate the reaction. During the controlled temperature procedure, denatured oligo strands effectively hybridized with the other partially complementary ssDNA sequences, and the reserved space at each vertex with two nucleotides offered enough degrees of freedom to bend into the triangle shape on each face (**Figure 4.1**). Therefore, four designed single-stranded oligonucleotides with open conformation could automatically assemble into the nanostructures. The assembled TDN was stored at 4 °C before further application.

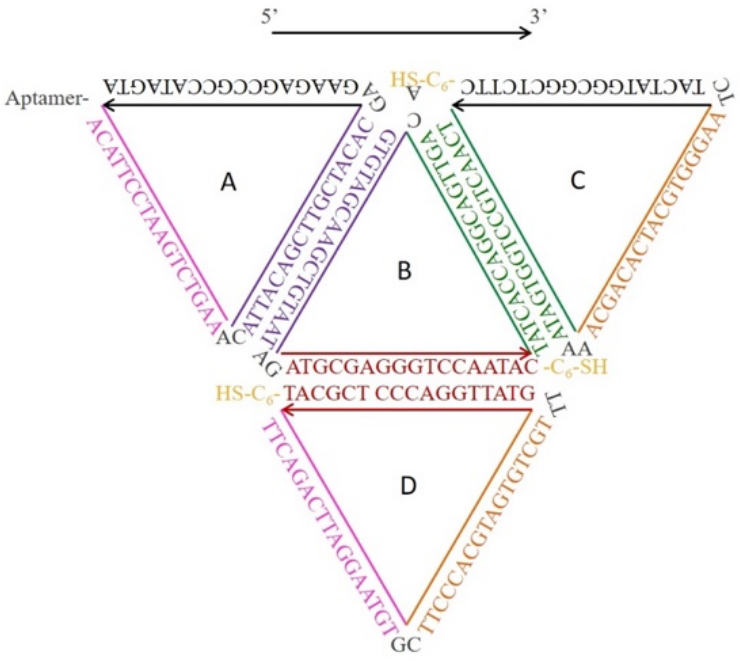

Figure 4.1. Self-assembly scheme of Oligo A, B, C, and D based on DNA hybridization of partial complementary sequences

To investigate the temperature route of the TDN self-assembly procedure, a snap-cooled procedure was introduced for optimization. After the TCEP pretreatment, the mixture was denatured at 95 °C and directly cooled to 4 °C for 30 s (Lin et al., 2016). The formed structures were analyzed using agarose gel electrophoresis (3%) at a constant 5 mA current.

4.2.4 Aptasensor surface fabrication

Figure 4.2 illustrates the fabrication scheme and detection method of the aptasensor. The SPE was first cleaned with deionized water for the complete removal of any impurities. The rGO layer was formed by drop-coating 4 mg/mL GO solution on the SPE and then chemically reduced using cyclic voltammetry (CV) as described in detail in Chapter 3. The coated SPE was rinsed with deionized water and dried at room temperature. Then, the rGO-SPE was drop-coated with 1 nM AuNPs solution as previously stated.

After the nanomaterial modifications, the SPE was incubated with the TDN solution for four hours at 25 °C to covalently anchor the nanostructures by forming the Au-S bonds. In this study, the aptasensing probe (-GCGGGCGGTTGTATAGCGG-) was appended to the Oligo A sequence. Thus, along with the assembling procedure of TDN, the aptamer was automatically aligned on the top vertex of the tetrahedron and immobilized on the SPE surface. The remained non-occupied binding sites on SPE were blocked by 6-mercaptohexanol in a 0.1% aqueous solution. The aptasensor was washed with PBS solution to remove any unbound biomolecules and stored in 1X PBS buffer at 4 °C for later analysis.

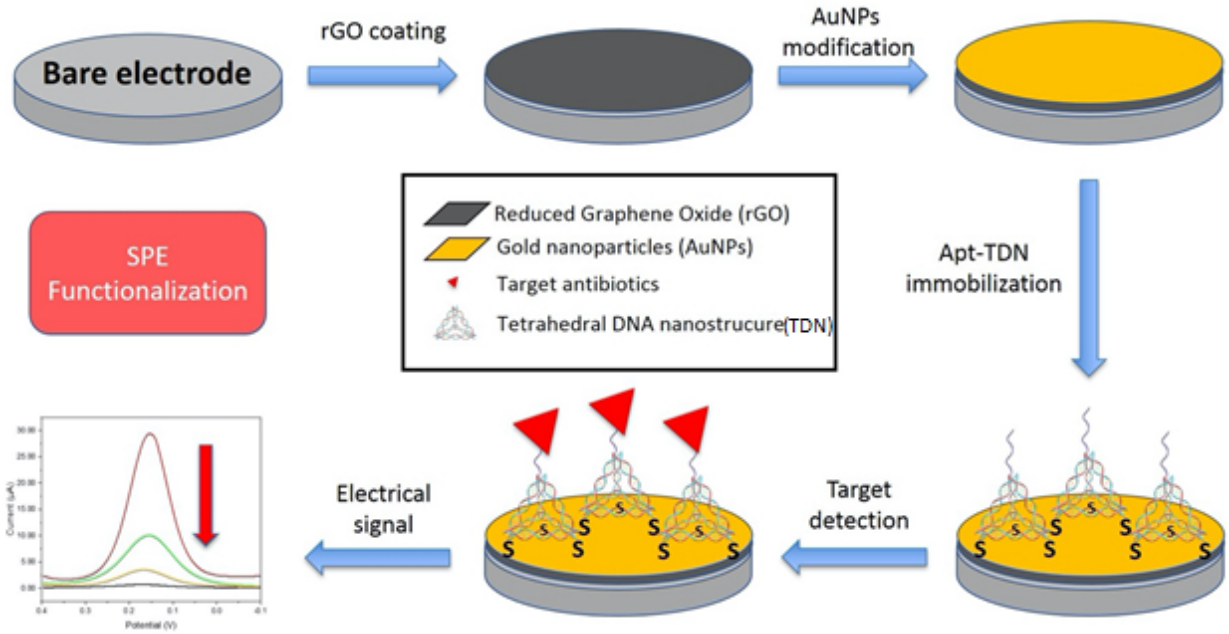

Figure 4.2. Fabrication scheme of the aptasensor with nanomaterials and aptamer appended TDN

4.2.5 Milk sample pretreatment

The milk products from a local grocery store were selected for the real sample examinations. An acid-based method was used for milk sample pretreatment to remove additional proteins and fats and reduce false-positive signals. Specifically, 1 mL of milk sample was mixed with 10 mg trichloroacetic acid under vibrate oscillation. The additional proteins and fats were denatured, precipitated, and then removed by centrifugation. The supernatant was collected and then neutralized using 1 M NaOH to about pH 7. The pretreated milk samples were spiked with ampicillin to a wide range of concentrations at 0.5, 5, 50, and 500 nM, respectively. The spiked milk samples were stored at 4 °C before the ampicillin detection.

4.2.6 Nanomaterial and electrode characterization

Scanning electron microscopy (SEM Zeiss/LEO 1530, Zeiss) and atomic force microscopy (AFM, MultiMode 8-HR, Burker) were used to monitor the surface morphological changes of the fabricated SPE. Agarose gel electrophoresis was utilized to analyze the assembly efficiency of TDN using different temperature protocols. Cyclic voltammetry (CV), differential pulse voltammetry (DPV), and electrochemical Impedance Spectroscopy (EIS) of redox couple $[Fe(CN)_6]^{3-}$/ $[Fe(CN)_6]^{4-}$ containing KCl as supporting electrolyte was employed to explore the electrical behaviors of SPE with each modification step. The CHI-660D electrochemical workstation (CHI Instruments, Inc. USA) was employed to operate all electrochemical characterizations and detections.

4.3 Results and discussions

4.3.1 The detection principle

CV, DPV, and EIS techniques were used to interrogate the aptasensor surface (TDN/AuNPs/rGO-SPE) after being exposed to ampicillin-spiked buffer or milk for 30 min. The specific biorecognition between the aptamer and ampicillin formed a target-aptamer complex on the vertex of TDN and created an organic layer on the SPE surface. As a result, a significant current signal deduction was sensed because of the impediment of electrons transmission between the working surface and the redox pair $[Fe\ (CN)_6]^{3-/4-}$. The decreased electrical signal was realized to be correlated to the ampicillin concentration in the sample solution. Therefore, a quantitative determination of the target ampicillin amount in the buffer system or milk ample solution was achieved based on the change of the measured DPV current.

4.3.2 Optimization of the nanostructure assembly procedure

To optimize the TDN assembly efficiency of two temperature protocols, 3% agarose gel electrophoresis was utilized, and the two electrophoresis bands were compared to the standard DNA ladder (lane 1) to identify the final products and the side products (**Figure 4.3**). Lane 2 was the single-stranded sequence (Oligo B) used to build the TDN, which was used for size comparison. The multiple bands with an increased number of high molecular weight and decreased intensities in lane 3 represent various side products assembled along with the ideal TDN *via* the snap-cooled procedure. We inferred that the side products were generated by the cross-structure hybridizations, which explained the increased molecular weight of these nanostructures. The reduced band intensity ratio between TDN and the side products reveals a relatively low assembly efficiency of the snap-cooled protocol.

On the other hand, a ten-minute annealing step at 60 °C reaction temperature was added in the stepwise-cooled protocol to reduce the effect of the cross-structure hybridizations. a noticeable higher intensity of the major DNA band in lane 4 confirms the major product that was kinetically favored by the stepwise-cooled procedure over other side products was the TDN with an ideal tetrahedron 3D structure. Additionally, the higher band ratio compared to lane 3 illustrates that the stepwise-cooled protocol achieved a higher assembly efficiency and obtained high purity of the desired TDNs.

4.3.3 Optimization of aptasensor fabrications

Since the purpose of AuNPs modification was to provide the aptamer-TDN immobilization site as well as to improve the surface sensitivity, both parameters were evaluated as current changes were measured on aptamer-TDN/SPE (**Figure 4.4A**). The SPE was coated with 4 mg/mL of rGO

and various concentrations of AuNPs, and then functionalized with 5 μM of aptamer-TDN. Current difference (ΔI) values were measured in 1 μM of ampicillin sample and plotted against the AuNPs concentrations in **Figure S4B**. The AuNPs modification clearly improved the sensitivity of the aptasensoras the response signal increased with more AuNPs was coated. However, as the AuNPs concentration was raised to 0.5 nM, the signal reached the maximum and slightly declined after, suggesting the surface was saturated with aptamers. Besides, the AuNPs started to aggregate in the drying process at higher concentrations, and the bigger size of AuNPs could have space for non-specific binding, which further disturbed the aptamer-specific binding with ampicillin. So, 0.5 nM was selected for AuNPs modification.

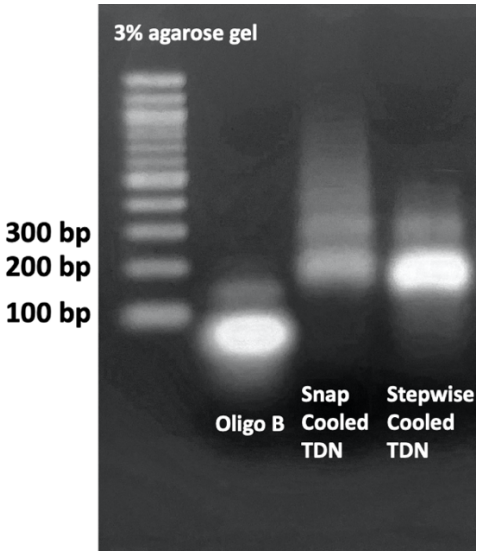

Figure 4.3. Electrophoretogram of Oligo B (lane 2) and self-assembly TDNs via snap-cooled procedure (lane 3) and stepwise-cooled procedure (lane 4) using 3% agarose gel

The optimization of the aptamer-TDN amount was accomplished by incubating various concentrations (0.1 to 10 μM) of the thiolated aptamer-TDN on the rGO-AuNPs modified SPE surface overnight and then testing with the same concentration of ampicillin sample at 1 μM. The DPV currents were measured and used to plot a scatter diagram in **Figure 4.4B**. The response

signal increased as the concentration of aptamer-TDN raised, suggesting more target antibiotics were captured by the aptamer probes. The maximum signal was detected at 5 μM, which demonstrates the immobilization sites provided by AuNPs were fully occupied with aptamer-TDN. Thus, aptamer-TDN concentration was chosen as 5 μM to functionalize the SPE surface.

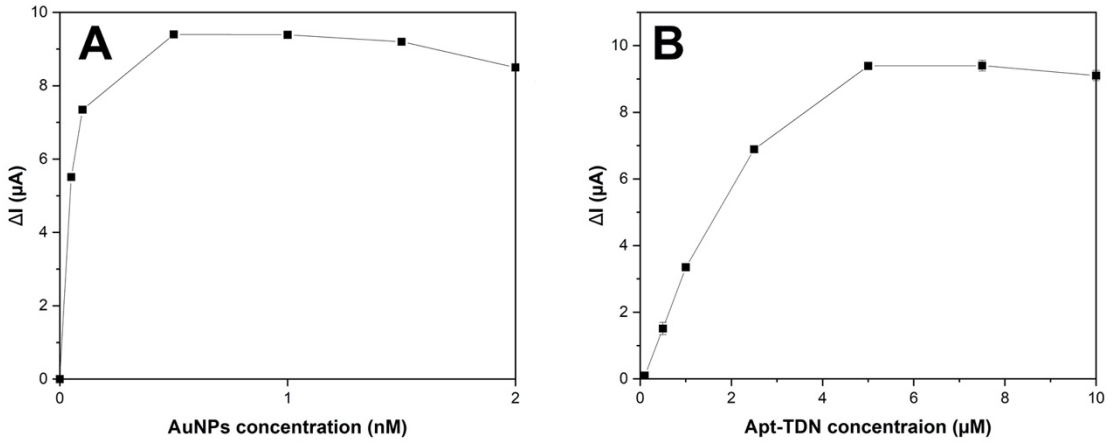

Figure 4.4. Optimization of SPE modifications (A) AuNPs coating at 0.1, 0.2, 0.5, 1, 1.5, 2 nM. (B) Apt-TDN concentrations at 0.1, 0.5, 1, 2.5, 5, 7.5, 10 μM

4.3.4 AFM validation of TDN immobilization

To verify the immobilizations of the aptamer appended TDN, AFM images were taken for both bare SPE and TDN-modified SPE for comparison (**Figure 4.5**). The bright dots (**Figure 4.5B**) on the SPE surface represent the coated AuNPs and immobilized TDN compared to the dark surface of bare SPE. The AFM image shows that the surface distribution of TDN/AuNPs is fairly even as expected. The size of each dot is measured with a relatively uniform diameter (5 ± 2 nm), which is almost identical to the predicted size of the TDN (5.78 nm). Thus, the AFM confirms the successful TDN immobilization and size and shape of the desired nanostructures.

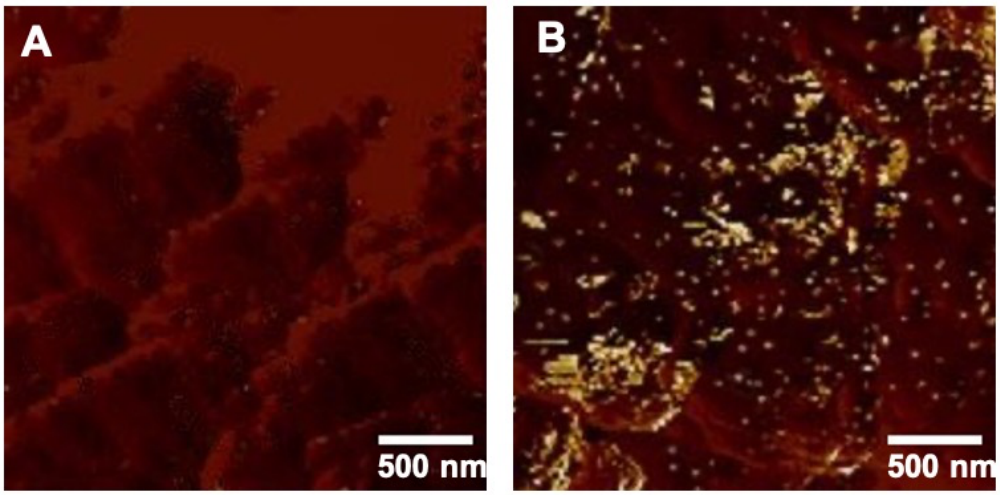

Figure 4.5. AFM image of SPE working surface (A) without aptamer/TDN modification and (B) with aptamer/TDN modification

4.3.5 Optimization of detection parameters

To fully explore the aptasensing efficiency, the detecting environment was evaluated regarding various detection parameters including pH of sample solutions and incubation time for the aptamer-antibiotic conjugates. The aptasensor was incubated with 1 μM of ampicillin solution at various pH, ranging from 5.5 to 8.5, for 60 min to test the performance of the designed aptasensor. **Figure 4.6A** shows noticeably stable DPV current at the pH range from 6.5 to 7.4, indicating that aptamers maintained the binding function in this pH range with the assistance of TDN. The functional conformation of aptamer was most effective at pH 7.4 with the maximum response current, which means the best target binding efficiency was achieved. An obvious decline of currents was observed under pH 6.5, suggesting the target bindings were suppressed in the acidic environment. The peak value of response currents is reached at pH 7.4, so pH 7.4 was selected as the optimal environment pH for later study of the calibration curve in the buffer system. The

aptasensor shows potential for milk sample detection (pH 6.7 to 6.9) as the result shows no significant difference (less than 5%) in the pH range of 6.5 to 7.4.

The incubation time of ampicillin detection was also optimized by monitoring the current change of aptasensor in the presence of 1 μM ampicillin solution (**Figure 4.6B**). The response current changed significantly for the initial 20 min, which indicates a high binding rate. Then the curve reached the maximum value at the 30 min mark, suggesting the ampicillin binding reached equilibrium. Hence, 30 min was chosen as the optimal incubation time.

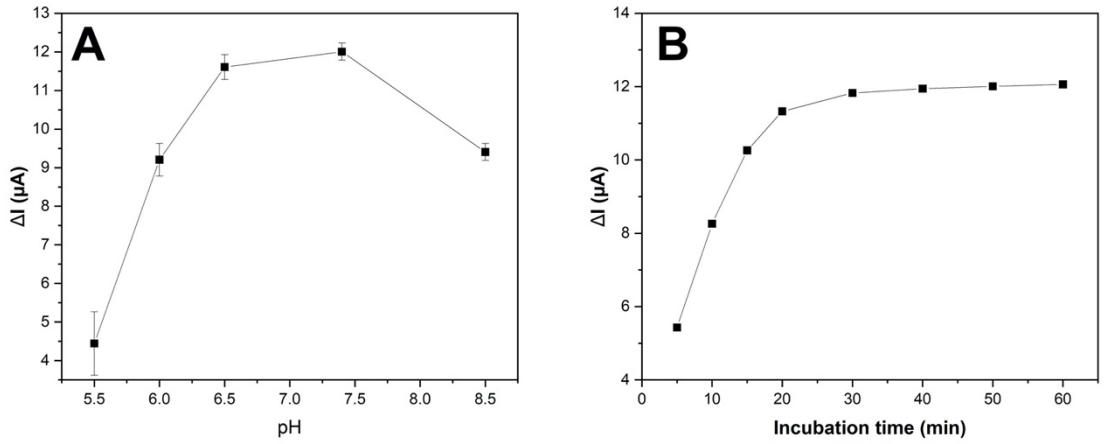

Figure 4.6. Optimization test of detection parameters (A) pH of sample solution, and (C) incubation time of ampicillin binding

4.3.6 Examination of TDN

To validate the binding efficiency improved by TDN, a control aptasensor was designed with immobilized aptamers (aptamer/AuNPs/rGO/SPE) for comparison. The aptamer/AuNPs/ rGO/SPE exhibited sensing ability towards ampicillin but with a low electrical response (**Figure 4.7**). Since the steric hindrance effect significantly reduces the target accessibility, the ultralow detection was prohibited by the low binding efficiency of the bare aptamers. The TDN-modified

SPE, in contrast, provides improved sensitivity and wider linearity with the controlled nanospacing between neighboring probes and vertical orientation of the fixed aptamers. In addition, the low standard deviation of multiple detections reveals a more precise detection result from the TDN-modified SPE. Thus, the aptamer assisted by TDN gains maximum degrees of freedom in a superior binding environment and maintains the functional conformation for the target identification so that the aptamer-ampicillin binding is more effective and similar to free aptamers in an aqueous solution.

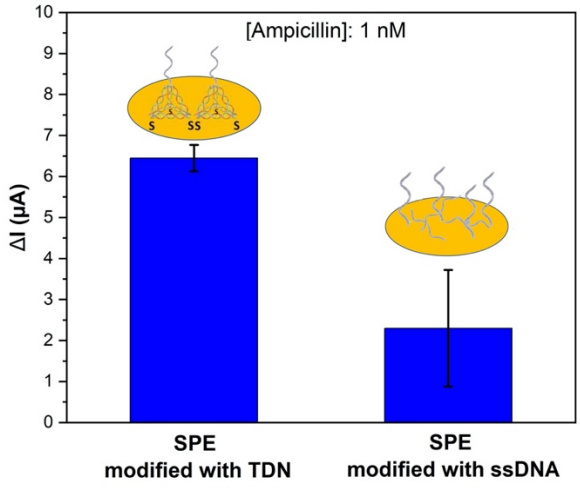

Figure 4.7. The binding effectiveness test of TDN-assisted SPE versus ssDNA modified SPE

4.3.7 Quantitative analysis of ampicillin

To explore the detecting range of the aptasensor, the DPV responses of the designed aptasensor were monitored over a wide concentration range of target ampicillin in the presence of 1 mM $[Fe(CN)_6]^{3-/4-}$ redox pair in the buffer system. It is clear that an electrical current deduction was obtained due to the selective binding between the aptamers and ampicillin on the surface of SPE (**Figure 4.8**). The organic layer of aptamer-ampicillin complex blocked the electron transfer

and caused the reduced redox reaction rate of $[Fe(CN)_6]^{3-/4-}$, which proves that the detection mechanism is feasible. The magnitude of current differences was correlated well with the ampicillin concentration. Thus, the calibration curve was built as the DPV peak current difference (ΔI) vs. the logarithmic function of ampicillin concentrations (**Figure 4.8B**). The excellent linearity ($R^2 = 0.9931$) is obtained for a wide range of ampicillin concentrations (10 pM to 1 mM). Due to the robustness of the TDN, aptamers maintain the functional conformation and remain stable upon the target binding. Hence, even very few interactions of low ampicillin concentration elicited electrical responses from the TDN-modified SPE, yielding an ultralow LOD as 1 pM, while the LOD of the control test was 100 times higher. The LOD of the system was determined as three times the standard deviation of the control solution (Signal-to-noise ratio equals to 3:1). Compared to the previously reported ampicillin aptasensors from literature (**Table 4.2**), the ampicillin sensing performance of our aptasensor has the best overall performance with ultralow LOD, wide detecting range, and fast detecting response.

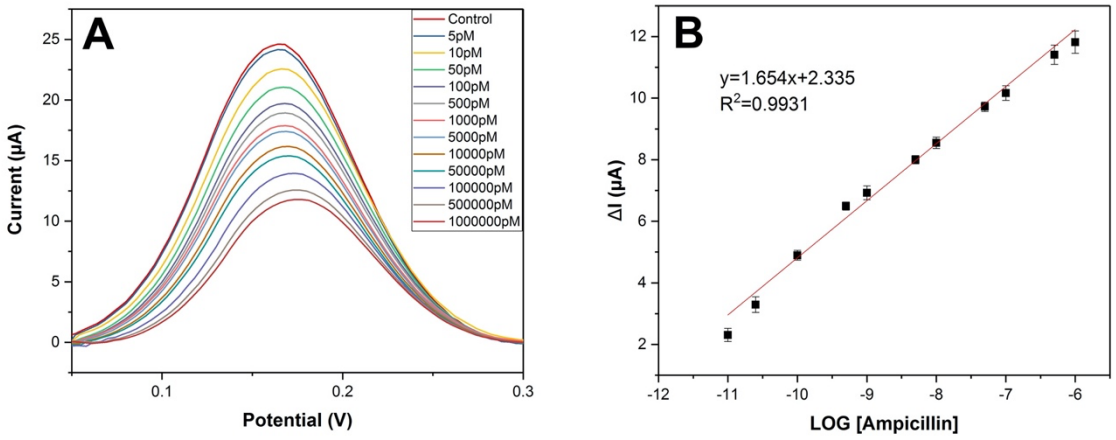

Figure 4.8. (A) DPV graph of the current response of the TDN/AuNPs/rGO/SPE at different ampicillin concentrations, and (B) the calibration curve built by plotting current change against a logarithmic function of ampicillin concentrations

Table 4.2. Recently reported aptamer-based ampicillin sensing method

Analysis method	**Linear range (nM)**	**LOD (pM)**	**Detection time (min)**	**Reference**
Aptamer based microfluidic biosensor	0.1 – 0.001	100	5	(Daprà, Lauridsen, Nielsen, & Rozlosnik, 2013)
Dual recycling amplification Aptasensor	0.02 – 40	4	90	(X. Wang, Dong, Gai, Duan, & Li, 2016)
Reagentless and reusable electrochemical aptasensor	$(5 – 5000) \times 10^6$	1×10^6	10	(Yu & Lai, 2018)
Aptamer based voltammetric determination	0.001– 5	0.38	300	(J. Wang, Ma, Yin, Zhou, & Ai, 2018)
Enzyme biofuel cell and DNA bioconjugate based aptasensor	0.010 – 100	3	30	(Gai, Gu, Hou, & Li, 2017)
Ladder shaped DNA structure based aptasensor	0.007 – 100	1	60	(Taghdisi et al., 2019)
Aptamer based colorimetric method	1.4 – 140	1400	> 60	(Song, Jeong, Jeon, Cho, & Ban, 2012)
PTCDI based fluorescent aptasensor	0.1–1	29.2	>60	(Esmaelpourfarkhani, Abnous, Taghdisi, & Chamsaz, 2020)
Aptamer based fluorescent method	0.286 – 286	200	180	(Luo et al., 2017)
rGO-SPE/AuNPs	**0.01 – 1000**	**1**	**30**	**This work**

4.3.8 Selectivity test

The selectivity test was operated by measuring DPV currents of the aptasensor when exposed to the same molarity (10 nM) of ampicillin and several other antibiotics, including amoxicillin, kanamycin, tetracycline, oxytetracycline, levofloxacin, and cloxacillin. **Figure 4.9** shows that the only significant current change was measured in the ampicillin sample. The result indicates that the aptasensor is highly selective over various antibiotics and shows high specificity to ampicillin.

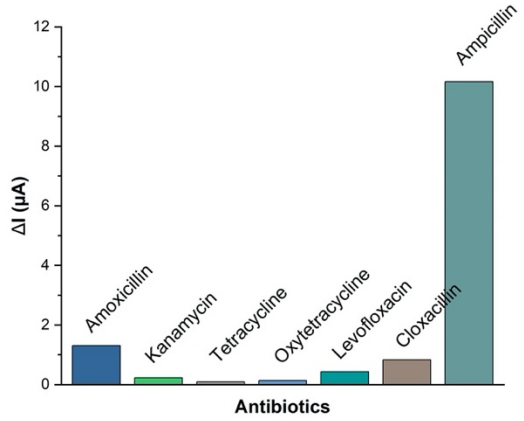

Figure 4.9. Selectivity test of aptasensor at 10 nM of various antibiotics

4.3.9 Sensor reusability and long-term stability

The designed aptasensor is considered to be reusable due to the fact that all the sensing elements are immobilized on the surface without intensive labeling. The aptasensor regeneration was accomplished by rinsing the working surface with a high concentration of Tris buffer for two minutes to remove the captured ampicillin. The regenerated SPE was verified by the blank sample test to ensure the removal of bound ampicillin and then stored in PBS at 4 ℃ for reuse. The reusability of the aptasensor was examined by comparing the regenerated DPV curves between

measurements with the control curve. **Figure 4.10A** displays the slight changes of less than 2% between each regenerated DPV curve over the five successive measurements, indicating an excellent regeneration ability and a significant cost-saving advantage over other disposable sensors.

The long-term stability was tested by monitoring the DPV peak currents of the stored aptasensors in PBS buffer at 4 ℃ over two weeks. The DPV current diagram was built in **Figure 4.10B** to show a stable electrical response in 15 days, illustrating good long-term storage stability. The obtained standard deviation was less than 8%, showing excellent reproducibility. Therefore, the good reusability, reproducibility, and long-term storage stability bode well for the wider use of the fabricated sensor.

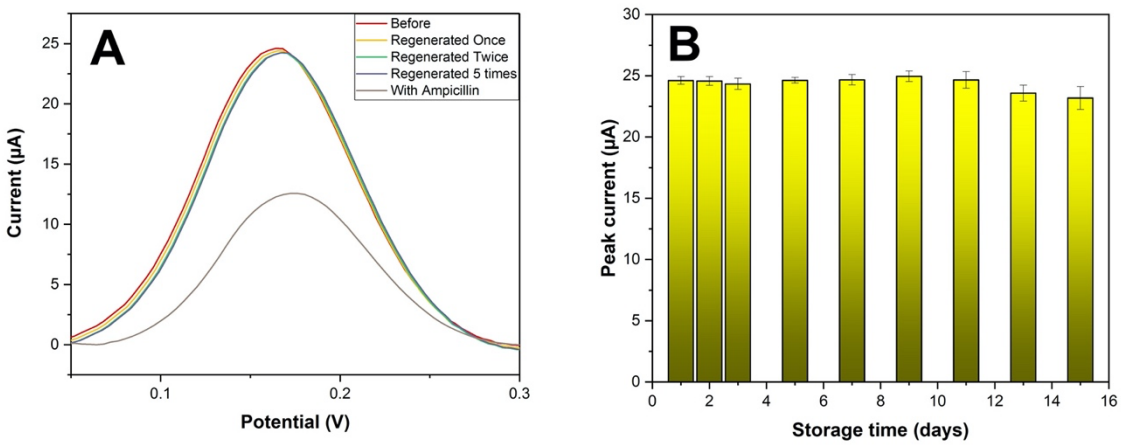

Figure 4.10. (A) The DPV graph of the regeneration curves of the aptasensor after exposed to 10 nM ampicillin, (B) The long-term stability diagram of the measured DPV peaks from three aptasensors when stored at 4 ℃ over 15 days (standard deviation shown as the error bars)

4.3.10 Milk sample detection

The real sample test was performed to verify the sensing ability of the designed aptasensor by measuring the spiked ampicillin concentrations in milk samples. Four ampicillin concentrations

were prepared in pretreated milk samples which was purchased from local grocery store (**Table 4.3**). Each sample was measured five times to calculate the mean of recovered concentration. The electrical responses of the aptasensor were collected to compare with the standard tests in PBS buffer, and the recovery rate was determined from 96.6% to 103.95%. The electrical measurements highly match the trend of the calibration curve established previously. Moreover, the relative standard deviation (RSD) of all measurements is relatively small, revealing a great degree of preciseness in ampicillin detections. The results demonstrate that the designed aptasensor is practical in real sample detection and has great potential in the quantitative analysis of residual ampicillin in milk.

Table 4.3. Milk sample detection with spiked ampicillin

Spiked concentration (nM)	**Recovered concentration (nM, mean)**	**Recovery rate (%)**	**Relative standard deviation (%)**
0.5	0.483	96.6	5.63
5	5.021	100.42	2.72
50	50.796	101.59	1.37
500	519.750	103.95	1.02

4.4 Conclusions

The proposed electrochemical aptasensor was capable of performing simple, rapid, and sensitive quantifications for target ampicillin. The TDNs were utilized to maintain the surface nanospacing and precisely control the vertical orientation of aptamers. Two temperature protocols

were compared to select the best TDN self-assembly procedure. Stepwise cooled protocol displayed a better synthesizing efficiency with a lower yield of by-products. The effectiveness of TDN modification was evaluated with a control aptasensor to show a significant improvement in the target binding efficiency and the LOD. The signal amplification with the assistance of TDN was measured to be almost 100 times. Additionally, the specificity of TDN-assisted aptamers was excellent over various interferences. The TDN-modified SPE exhibited a great ampicillin sensing ability to qualify and quantify a broad range of ampicillin concentrations from 10 pM to 1000 nM and achieve a low LOD at 1 pM within 30 min. The real sample test was performed in milk samples, the aptasensor successfully recognized the ampicillin residue in the milk with a recovery rate from 96.6% to 103.95%. Also, the sensor reproducibility and long-term storage stability were validated, showing the potential of on-site analysis application. Due to the simple testing route, the aptasensor is believed that can be tailored to detect other targets with suitable adaptions.

References

Berendsen, B. J. A., Wegh, R. S., Memelink, J., Zuidema, T., & Stolker, L. A. M. (2015). The analysis of animal faeces as a tool to monitor antibiotic usage. *Talanta, 132*, 258-268. doi:https://doi.org/10.1016/j.talanta.2014.09.022

Briscoe, S. E., McWhinney, B. C., Lipman, J., Roberts, J. A., & Ungerer, J. P. J. (2012). A method for determining the free (unbound) concentration of ten beta-lactam antibiotics in human plasma using high performance liquid chromatography with ultraviolet detection. *Journal of Chromatography B, 907*, 178-184. doi:https://doi.org/10.1016/j.jchromb.2012.09.016

Chen, X., Zhou, G., Song, P., Wang, J., Gao, J., Lu, J., . . . Zuo, X. (2014). Ultrasensitive Electrochemical Detection of Prostate-Specific Antigen by Using Antibodies Anchored on a DNA Nanostructural Scaffold. *Analytical Chemistry, 86*(15), 7337-7342. doi:10.1021/ac500054x

Daprà, J., Lauridsen, L. H., Nielsen, A. T., & Rozlosnik, N. (2013). Comparative study on aptamers as recognition elements for antibiotics in a label-free all-polymer biosensor. *Biosensors and Bioelectronics, 43*, 315-320. doi:https://doi.org/10.1016/j.bios.2012.12.058

Esmaelpourfarkhani, M., Abnous, K., Taghdisi, S. M., & Chamsaz, M. (2020). A novel turn-off fluorescent aptasensor for ampicillin detection based on perylenetetracarboxylic acid diimide and gold nanoparticles. *Biosensors and Bioelectronics, 164*, 112329. doi:https://doi.org/10.1016/j.bios.2020.112329

Gai, P., Gu, C., Hou, T., & Li, F. (2017). Ultrasensitive Self-Powered Aptasensor Based on Enzyme Biofuel Cell and DNA Bioconjugate: A Facile and Powerful Tool for Antibiotic Residue Detection. *Analytical Chemistry, 89*(3), 2163-2169. doi:10.1021/acs.analchem.6b05109

Gao, L., Liu, L., Tian, Y., Yang, Q., Wu, P., Fan, C., . . . Li, F. (2021). Probing the Formation Kinetics and Thermodynamics with Rationally Designed Analytical Tools Enables One-Pot Synthesis and Purification of a Tetrahedral DNA Nanostructure. *Analytical Chemistry, 93*(18), 7045-7053. doi:10.1021/acs.analchem.1c00363

Ghorbani, F., Abbaszadeh, H., Dolatabadi, J. E. N., Aghebati-Maleki, L., & Yousefi, M. (2019). Application of various optical and electrochemical aptasensors for detection of human prostate specific antigen: A review. *Biosensors and Bioelectronics, 142*, 111484. doi:https://doi.org/10.1016/j.bios.2019.111484

Haiss, W., Thanh, N. T. K., Aveyard, J., & Fernig, D. G. (2007). Determination of Size and Concentration of Gold Nanoparticles from UV−Vis Spectra. *Analytical Chemistry, 79*(11), 4215-4221. doi:10.1021/ac0702084

Huang, R., He, N., & Li, Z. (2018). Recent progresses in DNA nanostructure-based biosensors for detection of tumor markers. *Biosensors and Bioelectronics, 109*, 27-34. doi:https://doi.org/10.1016/j.bios.2018.02.053

Kim, Y. S., Raston, N. H. A., & Gu, M. B. (2016). Aptamer-based nanobiosensors. *Biosensors and Bioelectronics, 76*, 2-19.

Lin, M., Song, P., Zhou, G., Zuo, X., Aldalbahi, A., Lou, X., . . . Fan, C. (2016). Electrochemical detection of nucleic acids, proteins, small molecules and cells using a DNA-nanostructure-based universal biosensing platform. *Nature Protocols, 11*(7), 1244-1263. doi:10.1038/nprot.2016.071

Lin, M., Wen, Y., Li, L., Pei, H., Liu, G., Song, H., . . . Huang, Q. (2014). Target-Responsive, DNA Nanostructure-Based E-DNA Sensor for microRNA Analysis. *Analytical Chemistry, 86*(5), 2285-2288. doi:10.1021/ac500251t

Luo, W., Ang, C. Y. W., & Thompson Jr, H. C. (1997). Rapid method for the determination of ampicillin residues in animal muscle tissues by high-performance liquid chromatography with fluorescence detection. *Journal of Chromatography B: Biomedical Sciences and Applications, 694*(2), 401-407. doi:https://doi.org/10.1016/S0378-4347(97)00171-0

Luo, Z., Wang, Y., Lu, X., Chen, J., Wei, F., Huang, Z., . . . Duan, Y. (2017). Fluorescent aptasensor for antibiotic detection using magnetic bead composites coated with gold nanoparticles and a nicking enzyme. *Analytica chimica acta, 984*, 177-184. doi:https://doi.org/10.1016/j.aca.2017.06.037

Manyi-Loh, C., Mamphweli, S., Meyer, E., & Okoh, A. (2018). Antibiotic use in agriculture and its consequential resistance in environmental sources: potential public health implications. *Molecules, 23*(4), 795.

Mobarki, N., Almerabi, B., & Hattan, A. (2019). Antibiotic resistance crisis. *Int J Med Dev Ctries, 40*(4), 561-564.

Rosati, G., Daprà, J., Cherré, S., & Rozlosnik, N. (2014). Performance Improvement by Layout Designs of Conductive Polymer Microelectrode Based Impedimetric Biosensors. *Electroanalysis, 26*(6), 1400-1408. doi:https://doi.org/10.1002/elan.201400062

Sharma, A., Catanante, G., Hayat, A., Istamboulie, G., Ben Rejeb, I., Bhand, S., & Marty, J. L. (2016). Development of structure switching aptamer assay for detection of aflatoxin M1 in milk sample. *Talanta, 158*, 35-41. doi:10.1016/j.talanta.2016.05.043

Song, K.-M., Jeong, E., Jeon, W., Cho, M., & Ban, C. (2012). Aptasensor for ampicillin using gold nanoparticle based dual fluorescence–colorimetric methods. *Analytical and bioanalytical chemistry, 402*(6), 2153-2161.

Song, S., Wang, L., Li, J., Fan, C., & Zhao, J. (2008). Aptamer-based biosensors. *TrAC Trends in Analytical Chemistry, 27*(2), 108-117.

Taghdisi, S. M., Danesh, N. M., Nameghi, M. A., Ramezani, M., Alibolandi, M., & Abnous, K. (2019). An electrochemical sensing platform based on ladder-shaped DNA structure and label-free aptamer for ultrasensitive detection of ampicillin. *Biosensors and Bioelectronics, 133*, 230-235.

United States Department of Agriculture. Food Safety and Inspection Service, Office of Public Health Science. Bioassay for the Detection, Identification and Quantitation of Antimicrobial Residues in Meat and Poultry Tissue. (2010).

Wang, J., Ma, K., Yin, H., Zhou, Y., & Ai, S. (2017). Aptamer based voltammetric determination of ampicillin using a single-stranded DNA binding protein and DNA functionalized gold nanoparticles. *Microchimica Acta, 185*(1), 68. doi:10.1007/s00604-017-2566-8

Wang, J., Ma, K., Yin, H., Zhou, Y., & Ai, S. (2018). Aptamer based voltammetric determination of ampicillin using a single-stranded DNA binding protein and DNA functionalized gold nanoparticles. *Microchimica Acta, 185*(1), 1-7.

Wang, R. E., Wu, H., Niu, Y., & Cai, J. (2011). Improving the Stability of Aptamers by Chemical Modification. *Current Medicinal Chemistry, 18*(27), 4126-4138. doi:http://dx.doi.org/10.2174/092986711797189565

Wang, X., Dong, S., Gai, P., Duan, R., & Li, F. (2016). Highly sensitive homogeneous electrochemical aptasensor for antibiotic residues detection based on dual recycling

amplification strategy. *Biosensors and Bioelectronics, 82*, 49-54. doi:https://doi.org/10.1016/j.bios.2016.03.055

Wen, Y., Pei, H., Wan, Y., Su, Y., Huang, Q., Song, S., & Fan, C. (2011). DNA Nanostructure-Decorated Surfaces for Enhanced Aptamer-Target Binding and Electrochemical Cocaine Sensors. *Analytical Chemistry, 83*(19), 7418-7423. doi:10.1021/ac201491p

Wong, E. L. S., Chow, E., & Gooding, J. J. (2005). DNA Recognition Interfaces: The Influence of Interfacial Design on the Efficiency and Kinetics of Hybridization. *Langmuir, 21*(15), 6957-6965. doi:10.1021/la050725m

Xie, N., Liu, S., Yang, X., He, X., Huang, J., & Wang, K. (2017). DNA tetrahedron nanostructures for biological applications: biosensors and drug delivery. *Analyst, 142*(18), 3322-3332.

Yang, S., Zhu, X., Wang, J., Jin, X., Liu, Y., Qian, F., . . . Chen, J. (2015). Combustion of hazardous biological waste derived from the fermentation of antibiotics using TG–FTIR and Py–GC/MS techniques. *Bioresource Technology, 193*, 156-163. doi:https://doi.org/10.1016/j.biortech.2015.06.083

Yu, Z.-g., & Lai, R. Y. (2018). A reagentless and reusable electrochemical aptamer-based sensor for rapid detection of ampicillin in complex samples. *Talanta, 176*, 619-624.

Chapter 5. Selection of ssDNA Aptamers for Penicillin G using GO-SELEX

Abstract

Aptamer selections of antibiotics have always been a great challenge due to the difficulty of the aptamer partitioning step attributed to the shortage of immobilization sites and the ultralight molecular weights. Therefore, the development of antibiotic aptasensing applications has been restricted by the limited number of reported aptamer sequences, especially for β-Lactam derivatives. To fill the vacancy of high-affinity aptamers to penicillin G (PenG), an immobilization-free SELEX with the assistance of graphene oxide (GO-SELEX) was designed to select functional ssDNA sequences. The aptamer screening procedure was realized by the unspecific GO adsorption to separate the unbounded sequences from the target-aptamer complex with folded ssDNA conformations. The dissociation constants (K_d) of the selected aptamer candidates were determined by the electrochemical method based on Langmuir binding isotherm as 105.15 ± 1.94 nM, 212.8 ± 4.06 nM, and 501.4 ± 15.3 nM, respectively. A selectivity test was performed to verify the specificity of functional aptamer structures to PenG over other antibiotics and interferences. The aptamer sequences showed a higher binding affinity with excellent selectivity, compared to the previously reported aptamers.

5.1 Introduction

Aptamers as biorecognition elements have attracted tremendous attention in various research fields over decades, especially in the biosensing area, due to their unique physicochemical properties to offer high affinity and specificity to a wide range of targets (Luan, Wang, Li, Guo, & Lu, 2020). This outstanding sensing tool is usually produced *via* an *in vitro* process called Systematic Evolution of Ligands by Exponential enrichment (SELEX), which is an iterative process to screen a large ssDNA library with enough complexity until the particular ssDNA sequences with functional structures are enriched (McKeague & DeRosa, 2012; Tuerk & Gold, 1990). Because of the structural diversity of the ssDNA library with 10^{13}-10^{16} different sequences, the SELEX procedure with appropriate modifications can be utilized to generate functional sequences with high binding affinity to any desired target (Regina Stoltenburg, Reinemann, & Strehlitz, 2007). A variety of SELEX procedures with diverse adaptions has been proposed to develop aptamer sequences with specific functions in various research areas, including chemical biology, analytical chemistry, disease diagnostics and therapeutics (Darmostuk, Rimpelova, Gbelcova, & Ruml, 2015).

However, small molecules as important analytes in many areas have always been a major challenge in terms of aptamer selection. The light molecular weight of small molecules causes inconvenient separation of unbound sequences from bound complex (J. Yang & Bowser, 2013). Unlike the large compounds such as proteins or cells, small molecules (i.e., antibiotics) lack immobilization sites to be fixed onto a solid support matrix, which makes many aptamer partitioning approaches unavailable, for example, magnetic beads, acrylic beads, agarose/Sepharose (Gopinath, 2007; Huang, Lin, Shiesh, & Lee, 2010; Miyachi, Shimizu, Ogino, Fukuda, & Kondo, 2009; Song et al., 2011; R Stoltenburg, Reinemann, & Strehlitz, 2005; M. Wang

et al., 2020). Besides, the chemical immobilizations on the solid matrix may cause steric hindrance on targets and block the potential binding sites for aptamers so that the effectiveness of selected sequences would be compromised (Boussebayle, Groher, & Suess, 2019). Therefore, biosensing applications based on aptamers were limited and only a few aptamer sequences for β-lactam antibiotics were reported, especially for penicillin G (Asol Mehlhorn, Parvaneh Rahimi, & Yvonne Joseph, 2018).

An immobilization-free SELEX method by using GO as a solid support matrix has been introduced to generate aptamers for small molecules like antibiotics (Chen et al., 2014; Nguyen, Kwon, Kim, & Gu, 2014; Shi et al., 2021; WooáKim & BockáGu, 2012; Xing, Zhang, & Yang, 2019). This method solves the immobilization difficulty by using hydrophobic and π–π stacking interactions between GO and ssDNA. The unspecific adsorption is broken by the conformational change of folded ssDNA when exposed to target antibiotics. More importantly, none of the interaction moieties on the ssDNA structures are occupied by GO so the efficiency of SELEX is guaranteed. The aptamer partitioning is achieved by a simple centrifugation step based on the weight difference of unbound sequences-GO particles and the target-aptamer complex.

In this chapter, an immobilization-free aptamer screening procedure based on GO adsorption was proposed to select functional ssDNA structures with a high binding affinity towards target penicillin G antibiotics. The experimental parameters of GO-SELEX were optimized to achieve the best aptamer selection efficiency, including incubation time, the mass ratio of GO and ssDNA, and buffer concentration. The selected aptamer candidates were sequenced and then analyzed based on the free energy of formation (ΔG) and the estimated secondary structures. The electrochemical sensing platform was employed to determine the K_d of each aptamer candidate with the assistance of tetrahedral DNA nanostructures (TDN).

5.2 Experimental Section

5.2.1 Materials and Reagents

DNA library, primers, and TDN oligo sequences were synthesized and purified by Sangon Biotech Co. Ltd (Shanghai, China). Lambda exonuclease was purchased from New England Biolabs (Ipswich, MA, USA). GO was synthesized by the modified Hummer's method, and gold nanoparticles (AuNPs) were prepared by Turkevich's method (Marcano et al., 2010; Turkevich, Stevenson, & Hillier, 1951; Y. C. Wang, Cokeliler, & Gunasekaran, 2015). The details of the nanomaterial synthesis are explained in Chapter 3.

All antibiotics including penicillin G were purchased from Thermo Fisher Scientific (Rockford, IL, USA). Phosphate buffered saline (PBS) 10X, potassium ferrocyanide trihydrate ($K_4[Fe(CN)_6]\cdot 3H_2O$), potassium ferricyanide ($K_3[Fe(CN)_6]$), potassium chloride, sodium phosphate monobasic (NaH_2PO_4), and sodium phosphate dibasic (Na_2HPO_4) were purchased from Thermo Fisher Scientific (Rockford, IL, USA). SPEs were purchased from CH Instruments, Inc. (TE100, Bee Cave, TX, USA).

All chemical products were used as received without any purification. All solutions were prepared using deionized water with resistivity ≥18.2 MΩ·cm (Ultrapure water system, Millipore, Billerica, MA, USA) for all experiments.

5.2.2 Solution preparations

PBS buffer was made as 1X solution at pH of 7.4 unless mentioned otherwise. Tris HCl buffer was prepared in the concentration of 20 mM Tris at pH of 7.4. SELEX binding buffer was mixed with the Tris HCl buffer with 100 mM NaCl, 5 mM KCl, 1 mM $CaCl_2$ and 2 mM $MgCl_2$ at

pH 7.4. The 25 µL of PCR reaction mixture consisted of 2 µL of 2.5 mM dNTP, 1 µL of 10 µM forward primer, 1 µL of 10 µM biotinylated reverse primer, 0.1 µL of 2.5 U/µL Taq DNA polymerase, 1 µL of 0.1 µM template ssDNA, and 2.5 µL PCR buffer. The electrolyte of the electrochemical system was prepared in 0.5 mM K_4 $[Fe(CN)_6]$ and 0.5 mM $K_3[Fe(CN)_6$ with 0.1 M KCl as supporting electrolyte at pH of 7.4.

5.2.3 ssDNA library preparations

The DNA library was designed to contain 10^{15} different sequences to offer enough complexity for aptamer selection. The 66 bases ssDNA sequence consisted of a randomized 30 nucleotide region, which was flanked by two 18 nucleotide priming regions for amplification purposes (**Table 5.1**). Two primers were prepared for PCR amplification and cloning, in which the reverse primer was modified with a phosphate group at 5' end for Lambda exonuclease digestion. The DNA library was prepared in 20 mM Tris HCl buffer (pH 7.4) and placed in a freezer for long-term storage.

Table 5.1. Oligonucleotide sequences used in GO-SELEX

Name	**Sequence (5' to 3')**
ssDNA library	CACCAGTCAGACAGCACG - N30 -GAGTGACGTCGGTACCTG N30: 30nt random sequence
Forward primer	CACCAGTCAGACAGCACG
Reverse primer	P - CAGGTACCGACGTCACTC Reverse 5' modified with phosphate group

To initialize the SELEX process, the ssDNA library was denatured at 95 °C for 10 min and cooled on ice for 5 min to obtain the best conformation. In each SELEX round, the amplification step of recovered ssDNA was performed by PCR. The PCR procedure was set as initial denaturation at 95 °C for 10 min, followed by 30 cycles of 95 °C denaturation for 30 s, 56 °C annealing for 30 s, and 72 °C extensions for 30 s. The procedure was terminated after the final extension at 72 °C for 10 min.

5.2.4 GO-SELEX

The GO-SELEX procedure of positive and negative rounds is illustrated in **Figure 5.1**. In the first positive round, 800 pmol of denatured ssDNA library was incubated with 800 pmol Penicillin G in the binding buffer at room temperature with constant oscillation. During the two-hour incubation, ssDNA sequences with functional structures would bind to target antibiotics, while the others remained in the binding solution. After the complete aptamer-antibiotic interaction, 4 mg/mL GO was added to the mixture and incubated for another 30 min. Upon the GO addition, ssDNA sequences with low affinity are adsorbed on the surface of GO *via* π–π stacking. Subsequently, a separation step was carried out by centrifuging the mixture at 10,000 relative centrifugal force (RCF) for 15 min, where the precipitate GO with unwanted sequences was discarded. The mass ratio between ssDNA and GO was optimized to increase the efficiency of the separation steps. The 800 µL supernatant, which contained ssDNA-PenG complex, was collected and purified by ethanol precipitation. The ethanol precipitation was achieved by mixing the ssDNA with 80 µL of 3 M sodium acetate and 2 mL of 95% ethanol and letting it sit in the freezer for 2 hours. After centrifugation at 10,000 RCF at 4 °C for 15 min, wash the precipitated ssDNA with 75% ethanol three times. The recovered ssDNA was dispersed in sterile water and quantified by Nanodrop 8000 spectrophotometer, and the recovery ratio of each round was calculated to monitor

the progress of aptamer screening. The incubation condition of the next round was adjusted according to the recovery rate. The harvested ssDNA pool was amplified by PCR, and then separated and purified by Lambda exonuclease digestion to remove the phosphorylated complementary strands (Avci-Adali, Paul, Wilhelm, Ziemer, & Wendel, 2010). The PCR products were digested by the Lambda exonuclease at 37 °C for 30 min, and the resulted ssDNA sequences were validated by 3% agarose gel electrophoresis. The obtained ssDNA pool was used for the subsequent rounds.

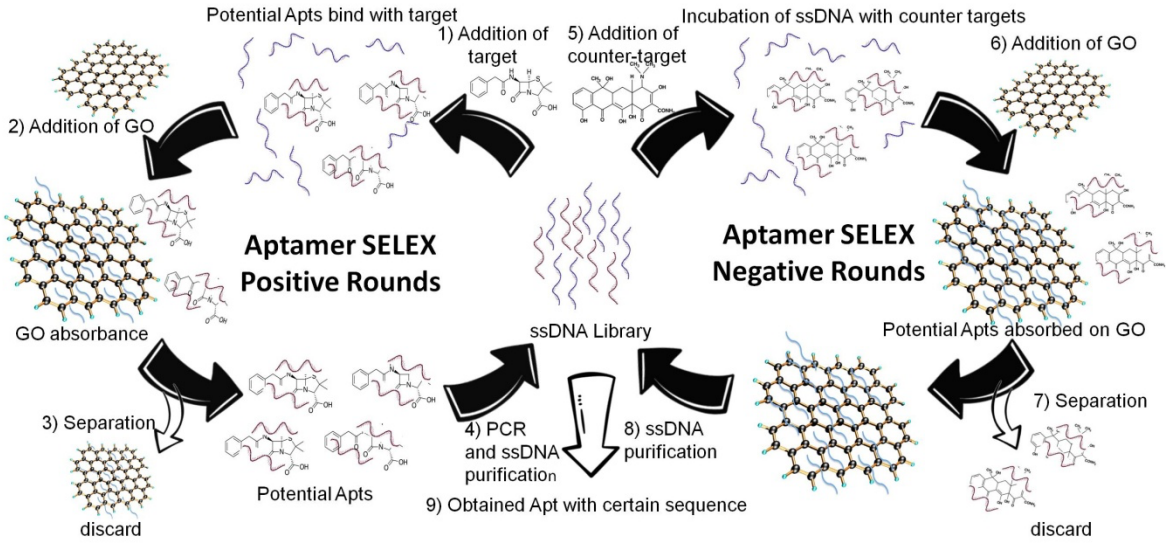

Figure 5.1. An immobilization-free GO-based strategy for the selection of antibiotic-specific DNA aptamers

5.2.5 Negative rounds

Negative SELEX rounds were designed to eliminate a portion of functional ssDNA structures which were not able to selectively bind to penicillin G. In the negative SELEX rounds, the prepared ssDNA library was incubated with counter targets (tetracycline, kanamycin, etc.) for 60 min at 1:1 mole ratio, followed by the same GO incubation step as positive rounds. The

unwanted ssDNA sequences with low specificity would bind to the interferences and were later removed by centrifugation, while the desired ssDNA with centrifuged GO was collected. The precipitate was washed thrice with binding buffer to remove ssDNA from the surface of GO, and the recovered ssDNA was re-dispersed in Tris buffer. The negative SELEX rounds ensured the selectivity of aptamer candidates and reduced the false-positive binding against molecules with similar structures so that real sample test would be available.

5.2.6 Aptamer sequencing and analysis

The recovery rate of each SELEX round was monitored by UV-vis spectrum. After the recovery rate reached saturation, the SELEX was terminated, and the final ssDNA pool was cloned and sequenced by the next-generation sequencing. The secondary structures and ΔG of obtained aptamer sequences were analyzed using the online UNAFold and OligoAnalyzer tool by IDT (Integrated DNA Technologies, Coralville, IA, USA). The aptamers with the lowest ΔG were selected and used for electrochemical analysis.

Table 5.2. Oligonucleotide sequences used in TDN assembly

Name	**Sequence (5' to 3')**
Oligo A	ACATTCCTAAGTCTGAAACATTACAGCTTGCTACACGAGAA GAGCCGCCATAGTA-TTTTTTTTTT- Aptamer sequence
Oligo B	HS-C6-TATCACCAGGCAGTTGACAGTGTAGCAAGC TGTAATAGATGCGAGGGTCCAATAC
Oligo C	HS-C6-TCAACTGCCTGGTGATAAAACGACACTACG TGGGAATCTACTATGGCGGCTCTTC
Oligo D	HS-C6-TTCAGACTTAGGAATGTGCTTCCCACGTAGT GTCGTTTGTATTGGACCCTCGCAT

The selected aptamer candidates were synthesized at the 3' end of Oligo A to build TDNs for the electrochemical K_d determination (**Table 5.2**). The self-assembly protocol was optimized in Chapter 4. The K_d value of each aptamer candidate was determined using the electrochemical sensing platform which was described in Chapter 4.

5.2.7 Electrode fabrications and measurements

The electrochemical sensing platform was detailly described in Chapter 4. The SPE was used as an electrode with electrochemically reduced GO and AuNPs fabrications. The modified AuNPs-rGO-SPE was further immobilized with aptamer-appended TDN for the best aptamer conformation and target binding efficiency. Differential pulse voltammetry (DPV) was employed for the target binding measurements and the K_d determination. The current values of response signal peaks at various PenG concentrations were measured using the fabricated aptasensor in 1 mM $[Fe(CN)_6]^{3-/4-}$ and 0.1 M KCl with an applied potential range from -0.2 V to +0.6 V and a 50 mV/s scan rate. The calculated aptamer fractional saturation values were plotted as the function of PenG concentrations to build the Langmuir isotherm plot, and then the K_d values of aptamer candidates were calculated using the binding equation. The CHI-660D electrochemical workstation (CHI Instruments, Inc. USA) was operated for all electrochemical experimentation.

5.3 Results and discussions

5.3.1 Optimization of SELEX condition

The optimization of the mass ratio between ssDNA and GO was performed before the GO-SELEX to ensure the partition of functional ssDNA structures from unbounded ssDNA in the separation step. The optimization was carried out by incubating the ssDNA pool in a binding buffer

with GO at different mass ratios without the presence of target penicillin. The UV intensity of the recovered supernatant after centrifugation was measured by Nanodrop 8000. Theoretically, unbounded ssDNA would adsorb on the surface of GO *via* π–π interaction and precipitate under centrifugation. Therefore, with enough amount of GO addition, the characteristic absorbance peak of ssDNA at 260 nm should not be measured in the recovered supernatant.

In **Figure 5.2**, absorbance peaks at 260 nm are observed with a lower mass of GO addition, meaning GO amounts are insufficient for the complete removal of ssDNA. The UV intensities are reduced as the mass of GO increases. The absorbances of unbounded ssDNA reached the minimum value with a mass ratio of 1:500 or more, which suggests complete adsorption between ssDNA and GO. Since higher GO mass would provide stronger competition against target antibiotics with functional ssDNA structures, the amount of GO addition was adjusted according to the progress of SELEX rounds to offer better aptamer screening ability. In the first round of SELEX, the mass ratio of 1:500 was chosen to initialize aptamer screening.

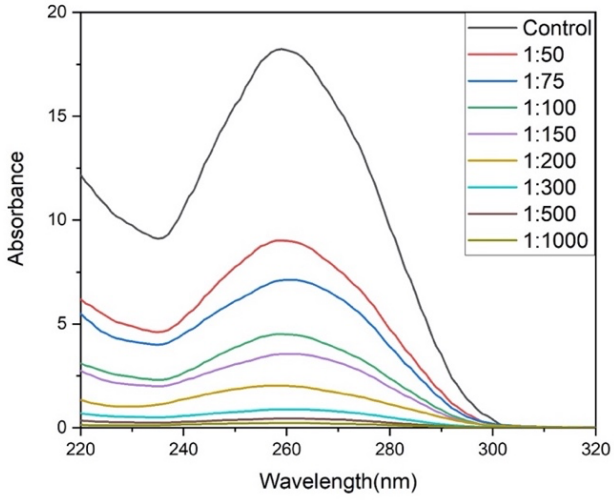

Figure 5.2. Optimization of mass ratio of ssDNA:GO used in ssDNA screening

Besides the mass ratio of ssDNA and GO, various other parameters were tuned to accomplish the most efficient aptamer selection procedure, including ssDNA quantity to launch each SELEX round, binding buffer concentration, penicillin G concentration, and incubation time. The reduced ssDNA and PenG amount were utilized to create a stronger competition along with grown mass ratio to eliminate the functional structures with low affinity. Increased concentration of binding buffer concentration provides a harsher aptamer screening environment. Reduced incubation time sequentially from 120 min to 30 min was used to select and train the aptamer candidates with better sensitivity and faster binding response. All the incubation conditions are listed in **Table 5.3**.

Table 5.3. The incubation conditions for aptamers selection

Selection round	**ssDNA (pmol)**	**Binding buffer**	**Penicillin G (pmol)**	**Mass ratio of ssDNA vs GO**	**Incubation time (min)**
1	800	10 mM Tris	800	500:1	120
2	800	20 mM Tris	800	500:1	90
3	800	20 mM Tris	800	500:1	90
4-5	400	40 mM Tris	400	1000:1	60
6-7	400	40 mM Tris	400	1000:1	30
8	800	20 mM Tris	N.A.	2000:1	120
9	800	20 mM Tris	N.A.	2000:1	120

5.3.2 GO-SELEX evaluation

In each SELEX round, the ssDNA pool was first denatured to obtain the best conformational structures and mixed with target PenG and GO in the binding buffer solution with the maximum degrees of freedom to ensure high screening efficiency. The initial concentration of the ssDNA pool and the final concentration of eluted target-binding ssDNA were quantified using the UV/Vis spectrum at the wavelength of 260 nm. The recovery rate of each round was measured and analyzed to evaluate the aptamer selection progress. **Figure 5.3** displays an increasing trend of recovery rate at each SELEX round, especially the first two rounds, which demonstrates that the GO addition effectively partitions the functional ssDNA structures from unwanted sequences. The recovery rate increased from 6% at the 1st round to 53% at the 7th round under even harsher conditions, suggesting the functional structures in the ssDNA pool gained enhanced binding affinity as the selection proceeded. Additionally, the increased ratio indicates that the binding interactions between the target antibiotics and the eluted aptamers barely rely on electrostatic adsorption. The conformational change of ssDNA structures is the major reason that causes effective aptamer screening and enrichment of sequence-specific folded secondary structures. The growth of the recovery rate started to decelerate starting in the 4th round, and the rate reached the peak value in the 7th round, indicating that the binding affinity of the ssDNA pool reached the maximum. The gel electrophoresis image (**Figure 5.3B**) confirms that the aptamer pool from the 7th round has a relatively higher abundance of sequences than the 3rd pool and the 5th pool, which proves that the 7th pool contains a higher amount of recovered ssDNA.

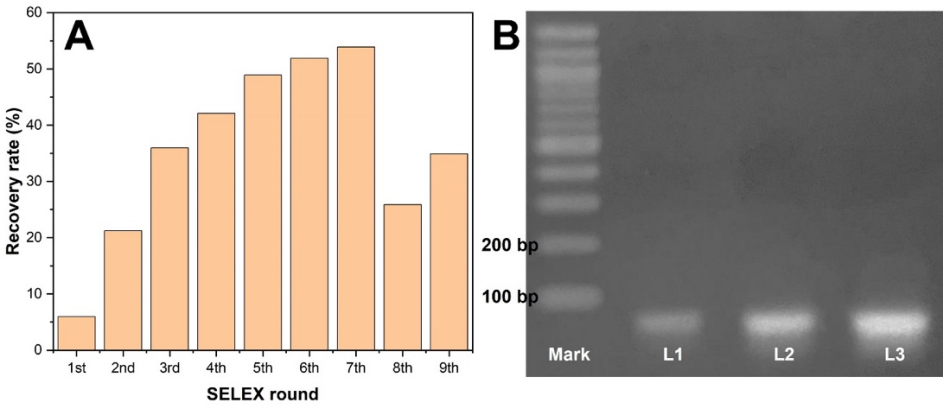

Figure 5.3. (A) The recovery rate of eluted ssDNA from the initial ssDNA library in each SELEX round, (B) Agarose gel analysis of SELEX pools from each round, L1: 3rd pool, L2: 5th pool, L3: 7th pool

After that, two negative rounds were introduced to reduce the unspecific binding affinity. The quantity of recovery ssDNA plummeted in the following round due to the binding elution from other antibiotics and interferences. The sequences with an unwanted affinity towards the molecules with similar structures as penicillin G or other interferences were discarded. Since most of the unwanted sequences were eliminated at the 8th round, the recovery rate of the 9th round exhibited a higher value, meaning the subsequent pool owned higher specificity to the desired target antibiotic. The final ssDNA pool was purified and then cloned and sequenced by the next-generation sequencing. Upon the elution of unwanted structures, the negative SELEX procedure improved the selectivity of aptamer candidates in the resulted pool. The online tool UNAFold and OligoAnalyzer were employed to analyze the ΔG and estimate the secondary structures of sequenced aptamer candidates. Three aptamers with the lowest free energy (listed in **Table 5.4**) were chosen and further tested for their binding affinity using the electrochemical aptasensor.

Table 5.4. Chosen aptamers sequences and the measured K_d values

Name	Sequence (5' to 3')	ΔG (Kcal/mol)	K_d
PenG-1	CACCAGTCAGACAGCACGGTGACTGGAGT GACGTCGGTACCTGAGATCGAGTGACGTC GGTACCTG	-10.85	105.15 ± 1.94 nM
PenG-2	CACCAGTCAGACAGCACGTGGAGTGGTGA CGTCTGAGATCGACGTCACGAGTGACGTC GGTACCTG	-14.49	212.8 ± 4.06 nM
PenG-3	CACCAGTCAGACAGCACGGTGCGCGGTG CCTCTTCTTGAGCGGGGTCTGAGTGACGTC GGTACCTG	-6.75	501.4 ± 15.3 nM

5.3.3 Dissociation constant determination

Recent research has revealed the limitation of binding efficiency caused by the surface morphological deficiency of aptasensors due to the reduced target accessibility induced by self-perturbation of the fixed aptamers with irregular orientation (Wong, Chow, & Gooding, 2005). Since most of the research designed the aptasensing surface by immobilizing thiolated aptamers *via* a single-point attachment on the sensing surface, heterogeneous distribution of aptamers on the locally crowded surfaces provokes the steric hindrance effect and aggravates the binding rates, which increases the difficulty of electrochemical determination of association constants (K_a) and K_d.

Herein, the TDN was utilized in this research to control the orientation of aptamers to limit self-induced perturbation and afford nanospacing from the neighbor aptamers to reduce cross-interactions. Since the aptamer appended TDN obtained a fixed vertical orientation that was pointed away from the surface of SPE, aptamers were granted more degrees of freedom to maintain the functional conformations for target binding. Thus, the TDNs-modified sensing surface provided a superior environment for aptamer recognition and effective antibiotic captures similar to free aptamer binding in the solution. To validate the binding affinity of the aptamer candidates, the K_d value of each aptamer was determined using an electrochemical method with the assistance of TDNs (X. Li et al., 2008; Souada et al., 2015). We assume a 1:1 stoichiometry of the aptamer-target binding behavior, so the equilibrium can be described by the K_d:

$$K_d = \frac{[Aptamer][Penicillin\ G]}{[Complex]} \tag{1}$$

To calculate K_d, each aptamer interacted with an increasing concentration of PenG, and the change of response current on the electrode was measured. The formed aptamer-PenG complex caused a proportional reduction in the current signal since it hinders the electron transfer between the electrode surface and the redox pairs. Therefore, the fraction of bound aptamers (f_a) was determined as:

$$f_a = \frac{I_{blank} - I_{test}}{I_{blank} - I_{saturated}} \tag{2}$$

To build a pseudo-first-order scenario, a relatively low amount (5 µL of 5 µM) of aptamers-TDNs was used for the surface immobilization so that the concentration of free PenG in the test solution remained relatively constant throughout the binding process. Thus, K_d can be expressed as:

$$f_a = \frac{[Penicillin\ G]}{K_d + [Penicillin\ G]} \quad (3)$$

Thus, K_d was determined by plotting f_a against PenG concentration (**Figure 5.4**). The plot was fitted by nonlinear regression, and K_d was estimated using the Langmuir isotherm equation (eq. 3).

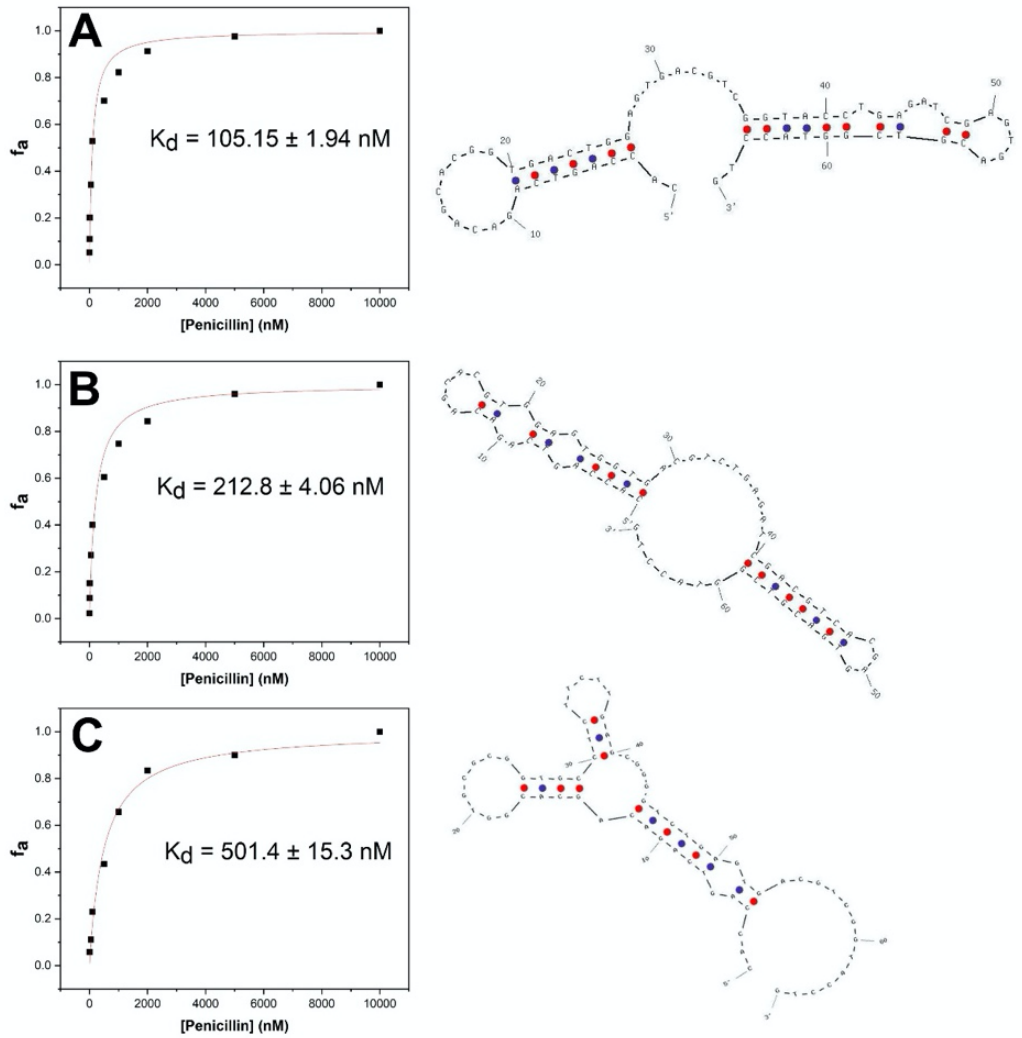

Figure 5.4. Langmuir isotherm plot of the aptamer candidates at various penicillin G concentrations and estimated secondary structures (A) PenG-1, (B) PenG-2, and (C) PenG-3

Figure 5.4 illustrates the target binding behavior of the aptamer candidates with a typical Langmuir isotherm plot. The binding fraction reached saturation around 4 μM, which was correlated to the increasing PenG concentration. The nonlinear regression was fitted closely to the general trend of the Langmuir isotherm plot. The K_d values were determined as 105.15 ± 1.94 nM, 212.8 ± 4.06 nM, and 501.4 ± 15.3 nM for PenG-1, PenG-2, and PenG-3, respectively. The sequence with the lower K_d value represents a more stable bound complex, and the nanomolar scaled K_d values indicate a high affinity between PenG and the aptamers. The lowest K_d value was achieved by PenG 1, indicating this aptamer sequence exhibited the highest binding affinity. This sequence has the lowest K_d value among all reported penicillin aptamers (**Table 5.5**).

Table 5.5. Reported penicillin G aptamers

Sequence (5' to 3')	**Analysis method**	**LOD (nM)**	**Kd (nM)**	**Reference**
GGGAGGACGAAGCGGAACGAGATG TAGATGAGGCTCGATCCGAATGCG TGACGTCTATCGGAATACTCGTTTT TACGCCTCATAAGACACGCCCGACA	Impedimetric sensor	0.5	N/A	(Paniel et al., 2017)
GGGTCTGAGGAGTGCGCGGTGCCA GTGAGT	Fluorescence sensor	9.2	383.4	(Lee et al., 2017)
CTGAATTGGATCTCTCTTCTTGAGC GATCTCCACA	Nanocomposite electrochemical sensor	0.17	N/A	(Zhao, Guo, Pei, & Ding, 2016)
This work	Voltametric	0.05	105.15	

5.4 Conclusions

The GO-SELEX successfully selected a ssDNA pool with binding affinity to penicillin G under optimized conditions, and the efficiency of GO-SELEX was evaluated by UV spectrum. The amount of recovered ssDNA was increased over the positive SELEX rounds, suggesting the binding affinity of the ssDNA pool evolved iteratively. With the introduction of two negative rounds, the unspecific sequences were eliminated, and the rest of the ssDNA pool was sequenced. Three aptamer candidates were chosen based on the low ΔG and their estimated secondary structures. The TDN-assisted electrochemical platform was employed to build the Langmuir isotherm plot and determine the K_d value of each aptamer candidate as 105.15 ± 1.94 nM, 212.8 ± 4.06 nM, and 501.4 ± 15.3 nM for PenG-1, PenG-2, and PenG-3, respectively. Compared to the previously reported penicillin G-specific aptamer sequences, these aptamers show the highest binding affinity with the lowest K_d values, indicating a successful aptamer selection practice. Therefore, the GO-SELEX is expected to use in various applications of aptamer development for other small molecules.

References

Avci-Adali, M., Paul, A., Wilhelm, N., Ziemer, G., & Wendel, H. P. (2010). Upgrading SELEX technology by using lambda exonuclease digestion for single-stranded DNA generation. *Molecules, 15*(1), 1-11.

Boussebayle, A., Groher, F., & Suess, B. (2019). RNA-based Capture-SELEX for the selection of small molecule-binding aptamers. *Methods, 161*, 10-15. doi:https://doi.org/10.1016/j.ymeth.2019.04.004

Chen, X., Huang, Y., Duan, N., Wu, S., Xia, Y., Ma, X., . . . Wang, Z. (2014). Screening and identification of DNA aptamers against T-2 toxin assisted by graphene oxide. *Journal of agricultural and food chemistry, 62*(42), 10368-10374.

Darmostuk, M., Rimpelova, S., Gbelcova, H., & Ruml, T. (2015). Current approaches in SELEX: An update to aptamer selection technology. *Biotechnology advances, 33*(6), 1141-1161.

Gopinath, S. C. B. (2007). Methods developed for SELEX. *Analytical and bioanalytical chemistry, 387*(1), 171-182.

Huang, C.-J., Lin, H.-I., Shiesh, S.-C., & Lee, G.-B. (2010). Integrated microfluidic system for rapid screening of CRP aptamers utilizing systematic evolution of ligands by exponential enrichment (SELEX). *Biosensors and Bioelectronics, 25*(7), 1761-1766.

Lee, A. Y., Ha, N.-R., Jung, I.-P., Kim, S.-H., Kim, A. R., & Yoon, M.-Y. (2017). Development of a ssDNA aptamer for detection of residual benzylpenicillin. *Analytical biochemistry, 531*, 1-7. doi:https://doi.org/10.1016/j.ab.2017.05.013

Li, X., Shen, L., Zhang, D., Qi, H., Gao, Q., Ma, F., & Zhang, C. (2008). Electrochemical impedance spectroscopy for study of aptamer–thrombin interfacial interactions. *Biosensors and Bioelectronics, 23*(11), 1624-1630. doi:https://doi.org/10.1016/j.bios.2008.01.029

Luan, Y., Wang, N., Li, C., Guo, X., & Lu, A. (2020). Advances in the Application of Aptamer Biosensors to the Detection of Aminoglycoside Antibiotics. *Antibiotics, 9*(11), 787. Retrieved from https://www.mdpi.com/2079-6382/9/11/787

Marcano, D. C., Kosynkin, D. V., Berlin, J. M., Sinitskii, A., Sun, Z., Slesarev, A., . . . Tour, J. M. (2010). Improved Synthesis of Graphene Oxide. *ACS Nano, 4*(8), 4806-4814. doi:10.1021/nn1006368

McKeague, M., & DeRosa, M. C. (2012). Challenges and opportunities for small molecule aptamer development. *Journal of nucleic acids, 2012*.

Mehlhorn, A., Rahimi, P., & Joseph, Y. (2018). Aptamer-based biosensors for antibiotic detection: A review. *Biosensors, 8*(2), 54.

Miyachi, Y., Shimizu, N., Ogino, C., Fukuda, H., & Kondo, A. (2009). Selection of a DNA aptamer that binds 8-OHdG using GMP-agarose. *Bioorganic & medicinal chemistry letters, 19*(13), 3619-3622.

Nguyen, V. T., Kwon, Y. S., Kim, J. H., & Gu, M. B. (2014). Multiple GO-SELEX for efficient screening of flexible aptamers. *Chem Commun (Camb), 50*(72), 10513-10516. doi:10.1039/c4cc03953j

Paniel, N., Istamboulié, G., Triki, A., Lozano, C., Barthelmebs, L., & Noguer, T. (2017). Selection of DNA aptamers against penicillin G using Capture-SELEX for the development of an impedimetric sensor. *Talanta, 162*, 232-240. doi:https://doi.org/10.1016/j.talanta.2016.09.058

Shi, H., Kou, Q., Wu, P., Sun, Q., Wu, J., & Le, T. (2021). Selection and Application of DNA Aptamers Against Sulfaquinoxaline Assisted by Graphene Oxide–Based SELEX. *Food Analytical Methods, 14*(2), 250-259.

Song, K.-M., Cho, M., Jo, H., Min, K., Jeon, S. H., Kim, T., . . . Ban, C. (2011). Gold nanoparticle-based colorimetric detection of kanamycin using a DNA aptamer. *Analytical biochemistry, 415*(2), 175-181.

Souada, M., Piro, B., Reisberg, S., Anquetin, G., Noël, V., & Pham, M. C. (2015). Label-free electrochemical detection of prostate-specific antigen based on nucleic acid aptamer. *Biosensors and Bioelectronics, 68*, 49-54. doi:https://doi.org/10.1016/j.bios.2014.12.033

Stoltenburg, R., Reinemann, C., & Strehlitz, B. (2005). FluMag-SELEX as an advantageous method for DNA aptamer selection. *Analytical and bioanalytical chemistry, 383*(1), 83-91.

Stoltenburg, R., Reinemann, C., & Strehlitz, B. (2007). SELEX—a (r) evolutionary method to generate high-affinity nucleic acid ligands. *Biomolecular engineering, 24*(4), 381-403.

Tuerk, C., & Gold, L. (1990). Systematic Evolution of Ligands by Exponential Enrichment - Rna Ligands to Bacteriophage-T4 DNA-Polymerase. *Science, 249*(4968), 505-510. doi:DOI 10.1126/science.2200121

Turkevich, J., Stevenson, P. C., & Hillier, J. (1951). A study of the nucleation and growth processes in the synthesis of colloidal gold. *Discussions of the Faraday Society, 11*, 55-75.

Wang, M., Wang, Q., Li, X., Lu, L., Du, S., & Zhang, H. (2020). Selection and identification of diethylstilbestrol-specific aptamers based on magnetic-bead SELEX. *Microchemical Journal, 159*, 105354.

Wang, Y. C., Cokeliler, D., & Gunasekaran, S. (2015). Reduced graphene oxide/carbon nanotube/gold nanoparticles nanocomposite functionalized screen-printed electrode for sensitive electrochemical detection of endocrine disruptor bisphenol A. *Electroanalysis, 27*(11), 2527-2536.

Wong, E. L. S., Chow, E., & Gooding, J. J. (2005). DNA Recognition Interfaces: The Influence of Interfacial Design on the Efficiency and Kinetics of Hybridization. *Langmuir, 21*(15), 6957-6965. doi:10.1021/la050725m

WooáKim, D., & BockáGu, M. (2012). Immobilization-free screening of aptamers assisted by graphene oxide. *Chemical Communications, 48*(15), 2071-2073.

Xing, L., Zhang, Y., & Yang, J. (2019). Graphene oxide-assisted non-immobilized SELEX of chiral drug ephedrine aptamers and the analytical binding mechanism. *Biochemical and biophysical research communications, 514*(1), 134-139.

Yang, J., & Bowser, M. T. (2013). Capillary Electrophoresis–SELEX Selection of Catalytic DNA Aptamers for a Small-Molecule Porphyrin Target. *Analytical Chemistry, 85*(3), 1525-1530. doi:10.1021/ac302721j

Zhao, J., Guo, W., Pei, M., & Ding, F. (2016). GR–Fe 3 O 4 NPs and PEDOT–AuNPs composite based electrochemical aptasensor for the sensitive detection of penicillin. *Analytical Methods, 8*(22), 4391-4397.

Chapter 6. Ultralow Penicillin G Detection Based on Nanomaterial modified Electrochemical Aptasensing platform

Abstract

Penicillin is among the most used antibiotic for the prevention and treatment of intramammary infections in dairy farms. However, the overuse of penicillin in dairy cows can lead to a public health crisis. Herein, we proposed an electrochemical aptasensor for penicillin G (PenG) based on nanomaterial modification and DNA nanostructure assistance to explore the possibility of building a universal aptasensing platform. The electrochemical aptasensor was constructed based on nanomaterial deposition and aptamer appended TDN functionalization. The aptasensor was rigorously optimized and exanimated for the best electrical performance. The designed electrochemical aptasensor was able to selectively and sensitively detect PenG, and the mathematic model of electrochemical responses to PenG concentrations was built in a broad concentration range from 0.2 nM to 1 mM with an ultralow limit of detection (LOD) at 0.05 nM. Additionally, the aptasensor was exanimated by a real sample test with PenG-spiked milk to achieve recovery rates in the range of 98.0 to 108.9% with the RSD less than 3.9%. This aptasensing platform exhibited great potential for practical application in on-site residual antibiotic monitoring in milk.

6.1 Introduction

Penicillin G (PenG) or benzylpenicillin is the most commonly used antibiotic for the prevention and treatment of infections such as mastitis in lactating cows (Gustavsson, Bjurling, & Sternesjö, 2002). Research shows that penicillin can potentially be released from the cattle body into milk, and pasteurization only reduces the residual penicillin by approximately 10 to 20 % (Payne, Craigmill, Riviere, & Webb, 2006). Although penicillin poses a low risk of toxicity compared to other biologically active substances, the consumption of contaminated food products with penicillin residues can cause an allergic immune response or induce several human diseases (Founou, Founou, & Essack, 2016). To avoid public health risks, the United States Food and Drug Administration (FDA) has established a tolerance/safe level of PenG residues in milk samples at 5 ppb ("U.S. Food and Drug Administration. Center for Veterinary Medicine. Milk drug residue sampling survey," 2015). To date, penicillin residues are detected and quantified by conventional antimicrobial assays ("United States Department of Agriculture. Food Safety and Inspection Service, Office of Public Health Science. Bioassay for the Detection, Identification and Quantitation of Antimicrobial Residues in Meat and Poultry Tissue," 2010). Even though these conventional methods are reliable, they are time-consuming and expensive to perform. Alternatively, several novel screening techniques are being employed to detect antibiotics such as capillary electrophoresis (Santos, Henriques, Duarte, & Esteves, 2007) or chromatography-based methods including high-performance liquid chromatography (HPLC)(Briscoe, McWhinney, Lipman, Roberts, & Ungerer, 2012), gas chromatography-mass spectrometry (GC-MS)(S. Yang et al., 2015), liquid chromatography-tandem mass spectrometry (LC-MS/MS)(Berendsen, Wegh, Memelink, Zuidema, & Stolker, 2015), and liquid chromatography-electrospray ionization mass spectrometry (LC-ESI/MS)(D. Li et al., 2008). These conventional methods often request

complicated procedures, tedious sample pre-treatment, sophisticated instruments with highly trained personnel to operate; and more importantly, as-mentioned methods are not readily amenable to on-site application and high-throughput analyses (Sharma et al., 2016). Therefore, a simple and fast method with low cost for residual penicillin detection is in urgent need to alleviate the safety issues of dairy products (A. Mehlhorn, P. Rahimi, & Y. Joseph, 2018).

In this chapter, a biosensing surface with reduced graphene oxide (rGO) and gold nanoparticles (AuNPs) modification was prepared and evaluated. The selected aptamer sequence in Chapter 5 (PenG-1) was utilized to build an aptasensing platform with the assistance of tetrahedral DNA nanostructures (TDN). The sensitivity and selectivity tests were operated to validate the biorecognition performance of the functionalized aptasensor. The mathematic model of electrochemical responses to target penicillin G concentrations was built for the identification and quantification of PenG in both a buffer system and milk samples.

6.2 Experimental Section

6.2.1 Materials and Reagents

Aptamers and TDN oligo sequences were synthesized and HPLC purified by Sangon Biotech Co. Ltd (Shanghai, China). GO was synthesized by the modified Hummer's method, and AuNPs were prepared by the Turkevich's method (Marcano et al., 2010; Turkevich et al., 1951; Y. C. Wang et al., 2015). The details of the synthesis methods are described in Chapter 3.

All antibiotics including Penicillin G were purchased from Thermo Fisher Scientific (Rockford, IL, USA). Tris-(2- carboxyethyl) phosphine hydrochloride (TCEP), phosphate buffered saline (PBS) 10X, sulfuric acid (96%), hydrogen peroxide (50%), hydrochloric acid (37%), potassium ferrocyanide trihydrate ($K_4[Fe(CN)_6]\cdot 3H_2O$), potassium ferricyanide

($K_3[Fe(CN)_6]$), potassium chloride, sodium phosphate monobasic (NaH_2PO_4), and sodium phosphate dibasic (Na_2HPO_4) were purchased from Thermo Fisher Scientific (Rockford, IL, USA). SPE (TE100) was supplied by CH Instruments, Inc. (Bee Cave, TX, USA).

All chemical products were used as received without any purification. All solutions were prepared using deionized water with resistivity ≥18.2 MΩ·cm (Ultrapure water system, Millipore, Billerica, MA, USA) for all experiments.

6.2.2 Solution preparation

PBS buffer was made as 1X solution at pH of 7.4 unless mentioned otherwise. Tris HCl buffer was prepared in the concentration of 20 mM Tris at pH of 7.4. Immobilization buffer was prepared by the Tris-EDTA (TE) buffer with 100 mM NaCl, 5 mM KCl, 1 mM $CaCl_2$, and 2 mM $MgCl_2$ at pH 7.4. The electrolyte of the electrochemical system was prepared in 0.5 mM $K_4[Fe(CN)_6]$ and 0.5 mM $K_3[Fe(CN)_6$ with 0.1 M KCl as supporting electrolyte at pH of 7.4. Oligonucleotides were prepared in TE buffer at the concentration of 100 μM and kept in a freezer for long-term storage. Penicillin G powder was dissolved in TE buffer at a concentration of 100 mg/mL as stock solution. The stock solution was diluted with sterile water to the designed concentrations for the biosensing purpose.

The milk products were purchased at a local grocery store for the real sample tests. The milk samples were pretreated with trichloroacetic acid to denature additional proteins and fats. After centrifugation, the precipitates were discarded, and the supernatant was collected and neutralized by sodium hydroxide. The pretreated milk samples were then spiked with penicillin G solution to the desired concentrations at 0.5, 5, 50, and 500 nM, respectively. The spiked milk samples were stored at 4 °C before the real sample examinations.

6.2.3 Self-assembly of aptamer appended TDN

Oligo-A, B, C, D listed in **Table 6.1** were dissolved in 20 mM Tris HCl buffer (pH 7.4) and later used to build TDN-assisted aptasensing probes. The self-assembly procedure was initialized by mixing 10 μL of each oligonucleotide solution with equal moles and 5 mM TCEP reducing agent in a total 100 μL immobilization buffer to reduce disulfide bonds. Then, the mixture was treated by a precisely controlled temperature scheme (described in Chapter 4) to assemble the aptamer appended TDNs (Lin et al., 2016). The formed TDNs were stored at 4 °C for further use.

Table 6.1. Oligonucleotide sequences used in Apt-TDN assembly

Name	**Sequence (5' to 3')**
Oligo A	ACATTCCTAAGTCTGAAACATTACAGCTTGCTACACGAGAAGAGCCGC CATAGTA-TTTTTTTTTT-CACCAGTCAGACAGCACGGTGACTGGAGTG ACGTCGGTACCTGAGATCGAGTGACGTCGGTACCTG
Oligo B	HS-C6-TATCACCAGGCAGTTGACAGTGTAGCAAGCTGTAATAGATGCG AGGGTCCAATAC
Oligo C	HS-C6-TCAACTGCCTGGTGATAAAACGACACTACGTGGGAATCTACTA TGGCGGCTCTTC
Oligo D	HS-C6-TTCAGACTTAGGAATGTGCTTCCCACGTAGTGTCGTTTGTATTG GACCCTCGCAT

6.2.4 Electrode fabrication

The fabrication scheme is illustrated in **Figure 6.1**. The working surface of the SPE was fabricated with GO and further reduced to remove oxidative functional groups by electrochemical reduction using cyclic voltammetry (CV) with linearly swept potential from 0 to -1.4 V in nitrogen-purged PBS. Then, AuNPs were synthesized *in situ* by electrochemically reducing gold precursor

on the SPE. The SPE was immersed in 2 mM $HAuCl_4$ solution containing 0.5 M H_2SO_4 with constant applied potential at -0.25 V for 360 s.

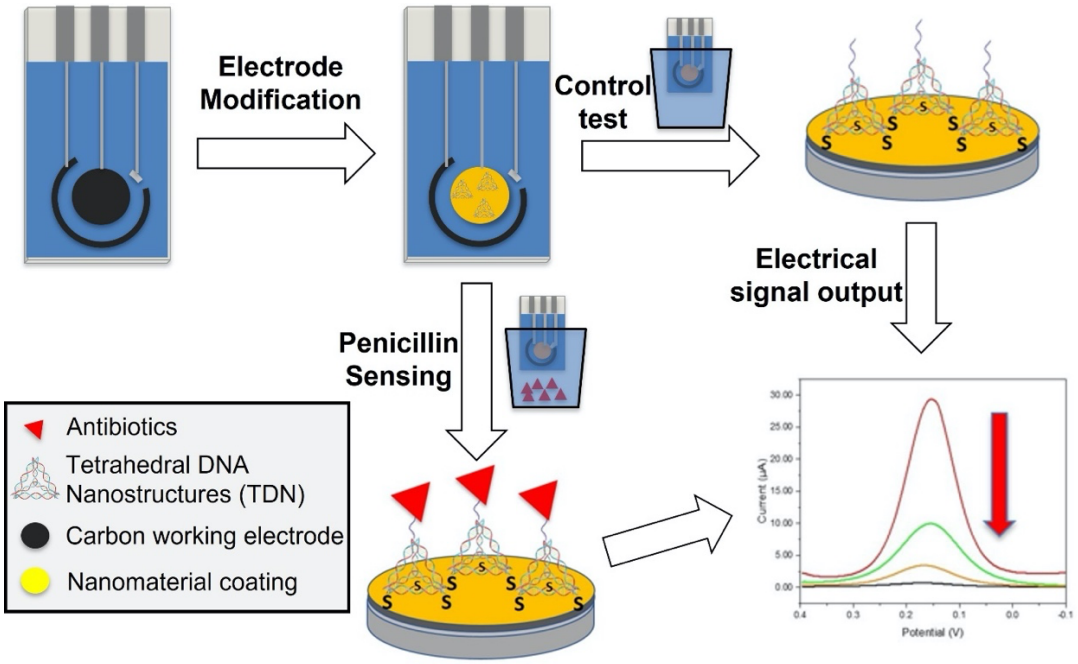

Figure 6.1. Nanomaterials and TDN based aptasensing platform design

The nanocomposite fabricated SPE was rinsed with deionized water to remove impurities before TDN modification. 10 µL as-prepared Apt-TDN solution was incubated on the working surface for four hours at 25 °C to covalently form gold-thiol bond between the thiolated nanostructures with AuNPs. The aptamer (-CACCAGTCAGACAGCACGGTGACTGGAGTG ACGTCGGTACCTGAGATCGAGTGACGTCGGTACCTG-) was fixed on the SPE along with TDN. The remained non-occupied binding sites on SPE were blocked by 6-mercaptohexanol in a 0.1% aqueous solution. The aptasensor was washed with PBS solution to remove any unbound biomolecules and stored in 1X PBS buffer at 4 °C for later analysis.

6.2.5 Electrochemical characterization and measurements

Scanning electron microscopy (SEM Zeiss/LEO 1530, Zeiss) and X-ray photoelectron spectroscopy (XPS, K-Alpha, ThermoFisher) were utilized to monitor the surface morphology changes of the fabricated SPE. Cyclic voltammetry (CV), differential pulse voltammetry (DPV), and electrochemical Impedance Spectroscopy (EIS) were employed to explore the electrical behaviors of SPE and perform penicillin detections. The CHI-660D electrochemical workstation (CHI Instruments, Inc. USA) was employed to operate all electrochemical experiments.

6.3 Results and discussions

6.3.1 SPE surface characterization and detection principle verification

A graphite-based screen-printed electrode (SPE) was used for its practical applicability and cost-effectiveness. The electrical performance and detecting principle were validated by CV in **Figure 6.2**. Referring to bare SPE (curve d in **Figure 6.2A**), a low electrical response and a large separation between oxidation and reduction peaks were observed in the CV, representing a unsatisfied conductivity. Upon the nanomaterial modifications, the coated AuNPs/rGO/SPE (curve a) displayed a remarkable response current boost compared to the bare SPE from 18 μA to 81 μA along with a narrower peak separation, suggesting the electron transmission efficiency was improved by the nanocomposite depositions and changes of the working surface morphology. This speculation was verified by SEM images. The surface morphology adaptions were confirmed as expected by the thin and uniform paper-like rGO structure (**Figure 6.2B**) and an abundance of evenly distributed AuNPs on the electrode surface (**Figure 6.2C**), which help improve electron exchange rate and electrical conductivity. Additionally, the fairly uniform distributed AuNPs provided immobilization sites for the aptamer appended TDNs *via* Au-S bond. The aptamer/TDN

formed a biomolecule layer on the electron exchange interface and resulted in a current deduction (curve d).

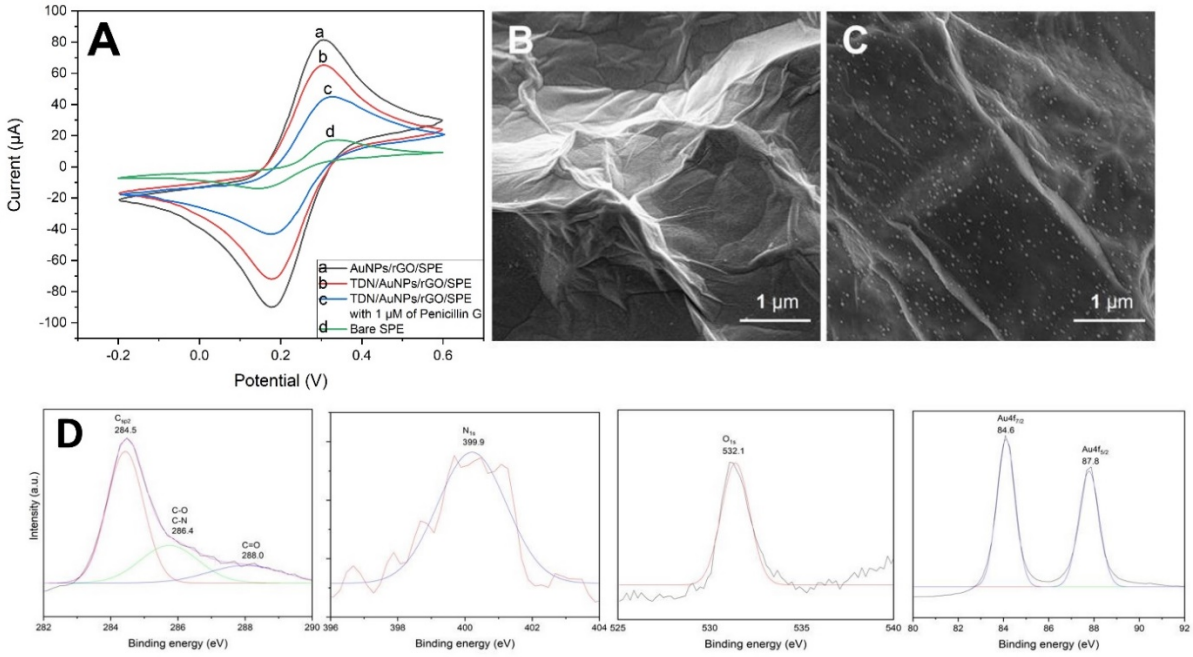

Figure 6.2. (A) CVs of SPE with different surface modifications. Surface morphology of (B) rGO/SPE and (C) AuNPs/rGO/SPE. (D) XPS spectrum of C1s, N1s, O1s, and Au4f characteristic peaks of TDN/AuNPs/rGO/SPE

The successful immobilization was evidenced by the XPS spectrum (**Figure 6.2D**) with the C_{1s}, N_{1s}, and O_{1s} characteristic peaks. The aptamer/TDN functionalized SPE was able to recognize target penicillin G (PenG) and form a complex with a conformational change of aptamers. The aptamer-PenG complex generated an organic layer, which would hinder electron transfer from electrolytes to the working surface. The negatively charged phosphate backbone of aptamer shielded the negatively charged electrons to aggravate the electron transmission prohibition. Thus, a detectable current reduction change was measured by the electrochemical biosensing system to complete the identification of target penicillin G (curve c). The concentration

of the PenG in the sample was expected to be correlated to the change of electrical signals according to the aptamer-target binding equilibrium. So, the quantification of target PenG was realized by building the mathematical model between current values and concentrations.

6.3.2 Penicillin G quantification

The penicillin quantification was performed by incubating the functionalized SPE in the penicillin G spiked TE buffer solution for 30 min and testing the electrical response of aptasensor surface in electrolyte using DPV. 1 mM $[Fe(CN)_6]^{3-/4-}$ was utilized as the redox pair to generate electrical signals, and the current response of the redox reaction was monitored. The specific binding between the aptamer functional structure and target PenG formed an organic layer which caused a blockage to hinder the redox electrons exchange from buffer solution to detecting surface. A response current deduction was caused by the decline of the redox reaction rate, which further proved the electrochemical detecting mechanism was feasible (**Figure 6.3A**).

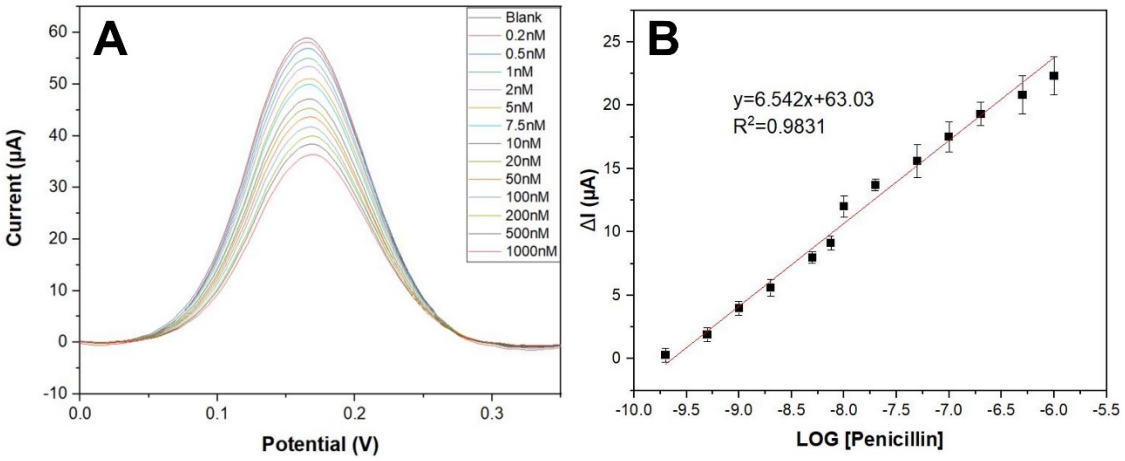

Figure 6.3. (A) DPV response of the aptasensor in the PenG solution with various concentrations from 0 to 1000 nM and (B) Mathematic model of DPV peak current as a logarithm function of PenG concentrations

To test the detecting range of the aptasensor, a wide range of PenG concentrations from very high contamination (1000 nM) to a very low amount (0.2 nM) was prepared and incubated with the aptasensor. The measured DPV peak current difference (ΔI) and the logarithmic function of PenG concentrations were plotted to explore the correlation. The highly linear relationship (R^2=0.9831) is illustrated as a calibration curve (**Figure 6.3B**) for a wide range of PenG concentration (0.2 nM to 1000 nM), yielding an ultralow limit of LOD of 0.05 nM. The LOD of the system was defined as three times of standard deviation of the control solution (Signal-to-noise ratio equals to 3:1). Compared to the previously reported aptamer-based penicillin sensors (**Table 6.2**), our sensor has the lowest LOD and a large detection range.

Table 6.2. A list of electrochemical biosensors for penicillin G detections

Sensor Description	Linear range	LOD	Reference
Amperometric immunosensor based on avidin-peroxidase and anti-penicillin G antibody	0.03 to 300000 nM	0.01 nM	(Merola, Martini, Tomassetti, & Campanella, 2015)
Penicillinase-based multisegmented nanowire/nanoparticle hybrid arrays as electrochemical immunosensor	20 to 310 μM	10.5 μM	(Li, Liu, Sarpong, & Gu, 2019)
Single graphene nanosheet / hematein / ionic liquids / penicillinase based amperometric immunosensor	1.25 pM to 7.5 mM	1 pM	(Gonçalves, Callera, Sotomayor, & Bueno, 2014; Wu et al., 2014)
PtE functionalized by a single layer GLA-BSA-penicillinase based potentiometric immunosensor	3 to 283 μM	3 μM	(Ismail & Adeloju, 2015)
Tobacco Mosaic Virus Nanotubes modified field-effect penicillin biosensor	0.1 to 10 mM	50 μM	(Jablonski et al., 2017; Qin, Yin, Yu, Guo, & Pei, 2016)
GR–Fe_3O_4NPs / PEDOT–AuNPs nanocomposite modified impedimetric electrochemical sensor	0.3 – 600 nM	0.17 nM	(Zhao, Guo, Pei, & Ding, 2016)
FAM-labeled fluorescence sensor	0 – 50 nM	9.2 nM	(Lee et al., 2017)

4-nitrobenzenediazonium modified impedimetric electrochemical sensor	0.4 to 1000 µg/L	0.17 µg/L	(Paniel et al., 2017)
Tobacco mosaic virus / nanorods / penicillinase based colorimetric sensor		100 µM	(Poghossian et al., 2018)
This work	0.2 to 1000 nM	50 pM	

6.3.3 Selectivity test

The selectivity test of the designed aptasensor was performed by measuring various common antibiotics (kanamycin, tetracycline, oxytetracycline, cloxacillin, amoxicillin, ampicillin) over PenG at the same molarity (**Figure 6.4**). Cloxacillin, amoxicillin, and ampicillin belonging to the β-lactam antibiotic group share a similar structure as penicillin derivatives, while kanamycin, tetracycline, and oxytetracycline have a significant structural difference. The results suggest that the aptamer has a high affinity only towards PenG with substantially lower binding probability with other antibiotics. The remarkable differences in electrical signals *ΔI* show a great selectivity of the chosen aptamers from target PenG to other interferences. Therefore, the designed aptasensor can be used for electrochemical detection and quantification for PenG.

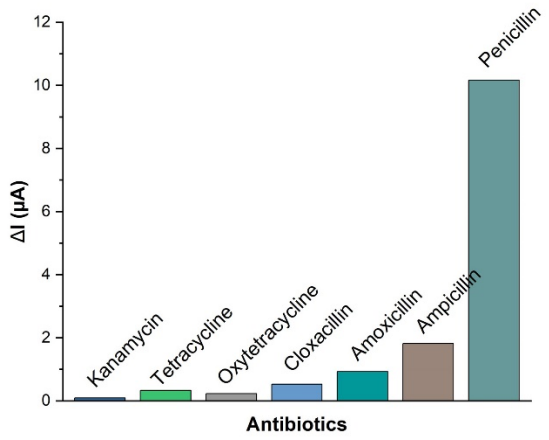

Figure 6.4. Selectivity test of the designed aptasensor with various antibiotics at same molarity (10 nM)

6.3.4 Milk samples examination

The milk samples from local grocery stores were spiked with penicillin G, and then used to validate the sensing ability of the aptasensor. The milk samples were pretreated to reduce false-positive signals with the removal of additional proteins and fats. The proteins and fats were denatured by mixing with trichloroacetic acid under vibrate oscillation and then was removed by centrifugation. pH value was neutralized using 1 M NaOH for further analysis. To ensure the veracity, the milk samples were spiked in four different PenG concentrations (**Table 6.3**). Each spiked milk sample was tested five times through the standard procedure, and the results were compared to the previous detection performed in the buffer system. The penicillin concentrations determined in milk samples matched the trend of the calibration curve with the recovery rate in the range of 98.0 to 108.9%. In addition, the result shows a good reproducibility with a RSD value less than 3.9%. The results reveal excellent practicability of the fabricated aptasensor with great potential in the quantitative analysis of PenG in milk.

Table 6.3. PenG detection in real milk samples

PenG concentration in milk (nM)	**Electrochemical determination (nM, Mean)**	**Recovery rate (%)**	**Relative Standard Deviation (%)**
1	1.09	108.9	3.15
5	5.28	105.6	3.88
50	51.22	102.4	1.35
500	489.8	98.0	1.05

6.4 Conclusions

The aptamer sequence with high affinity to PenG selected by GO-SELEX in Chapter 5 was utilized to construct an ultrasensitive electrochemical aptasensor. A selectivity test was performed to validate the selectivity of the aptamer to other antibiotics. The selected aptamer was able to specifically identify penicillin G over various antibiotics which has similar structures. The electrochemical aptasensor was modified by rGO and AuNPs to obtain the ideal electrical behaviors and then functionalized by aptamer appended TDNs to achieve the best binding environment. Upon the rGO and AuNPs modifications, the sensor surface offered a great electron transferring capability and excellent biocompatibility. The TDN precisely controlled the orientation of aptamers and the nano-spacing between adjacent aptamer probes to limit self-perturbation and cross-interaction so that individual aptamer probes could maintain their secondary structure and access the target PenG efficiently. The fabricated aptasensor could determine the concentration of penicillin in a wide range of 0.2 nM to 1000 nM, yielding an ultralow LOD of 0.05 nM. Additionally, the aptasensor was proved to be practical in a real milk sample test with a great recovery rate from 97.96 to 108.87% with limited sample pretreatment. The results demonstrate that the designed aptasensor is capable of specifically recognizing target PenG, forming a complex with high affinity and performing a simple, fast, and sensitive penicillin G detection in real milk samples.

References

Berendsen, B. J. A., Wegh, R. S., Memelink, J., Zuidema, T., & Stolker, L. A. M. (2015). The analysis of animal faeces as a tool to monitor antibiotic usage. *Talanta, 132*, 258-268. doi:https://doi.org/10.1016/j.talanta.2014.09.022

Briscoe, S. E., McWhinney, B. C., Lipman, J., Roberts, J. A., & Ungerer, J. P. J. (2012). A method for determining the free (unbound) concentration of ten beta-lactam antibiotics in human plasma using high performance liquid chromatography with ultraviolet detection. *Journal of Chromatography B, 907*, 178-184. doi:https://doi.org/10.1016/j.jchromb.2012.09.016

Founou, L. L., Founou, R. C., & Essack, S. Y. (2016). Antibiotic Resistance in the Food Chain: A Developing Country-Perspective. *Frontiers in microbiology, 7*, 1881-1881. doi:10.3389/fmicb.2016.01881

Gonçalves, L. M., Callera, W. F. A., Sotomayor, M. D. P. T., & Bueno, P. R. (2014). Penicillinase-based amperometric biosensor for penicillin G. *Electrochemistry Communications, 38*, 131-133. doi:https://doi.org/10.1016/j.elecom.2013.11.022

Gustavsson, E., Bjurling, P., & Sternesjö, Å. (2002). Biosensor analysis of penicillin G in milk based on the inhibition of carboxypeptidase activity. *Analytica chimica acta, 468*(1), 153-159. doi:https://doi.org/10.1016/S0003-2670(02)00599-8

Hong, F., Chen, X., Cao, Y., Dong, Y., Wu, D., Hu, F., & Gan, N. (2018). Enzyme- and label-free electrochemical aptasensor for kanamycin detection based on double stir bar-assisted toehold-mediated strand displacement reaction for dual-signal amplification. *Biosensors and Bioelectronics, 112*, 202-208. doi:https://doi.org/10.1016/j.bios.2018.04.017

Kim, D.-M., Rahman, M. A., Do, M. H., Ban, C., & Shim, Y.-B. (2010). An amperometric chloramphenicol immunosensor based on cadmium sulfide nanoparticles modified-dendrimer bonded conducting polymer. *Biosensors and Bioelectronics, 25*(7), 1781-1788. doi:https://doi.org/10.1016/j.bios.2009.12.024

Li, D., Yang, M., Hu, J., Zhang, Y., Chang, H., & Jin, F. (2008). Determination of penicillin G and its degradation products in a penicillin production wastewater treatment plant and the receiving river. *Water Res, 42*(1-2), 307-317. doi:10.1016/j.watres.2007.07.016

Lin, M., Song, P., Zhou, G., Zuo, X., Aldalbahi, A., Lou, X., . . . Fan, C. (2016). Electrochemical detection of nucleic acids, proteins, small molecules and cells using a DNA-nanostructure-based universal biosensing platform. *Nature Protocols, 11*(7), 1244-1263. doi:10.1038/nprot.2016.071

Liu, X., Zheng, S., Hu, Y., Li, Z., Luo, F., & He, Z. (2016). Electrochemical Immunosensor Based on the Chitosan-Magnetic Nanoparticles for Detection of Tetracycline. *Food Analytical Methods, 9*(10), 2972-2978. doi:10.1007/s12161-016-0480-z

Liu, Y., Yan, K., Okoth, O. K., & Zhang, J. (2015). A label-free photoelectrochemical aptasensor based on nitrogen-doped graphene quantum dots for chloramphenicol determination. *Biosensors and Bioelectronics, 74*, 1016-1021. doi:https://doi.org/10.1016/j.bios.2015.07.067

Marcano, D. C., Kosynkin, D. V., Berlin, J. M., Sinitskii, A., Sun, Z., Slesarev, A., . . . Tour, J. M. (2010). Improved Synthesis of Graphene Oxide. *ACS Nano, 4*(8), 4806-4814. doi:10.1021/nn1006368

Mehlhorn, A., Rahimi, P., & Joseph, Y. (2018). Aptamer-Based Biosensors for Antibiotic Detection: A Review. *Biosensors (Basel), 8*(2). doi:10.3390/bios8020054

Payne, M. A., Craigmill, A., Riviere, J. E., & Webb, A. I. (2006). Extralabel use of penicillin in food animals. *J Am Vet Med Assoc, 229*(9), 1401-1403. doi:10.2460/javma.229.9.1401

Poghossian, A., Jablonski, M., Koch, C., Bronder, T. S., Rolka, D., Wege, C., & Schöning, M. J. (2018). Field-effect biosensor using virus particles as scaffolds for enzyme immobilization. *Biosensors and Bioelectronics, 110*, 168-174. doi:https://doi.org/10.1016/j.bios.2018.03.036

Qin, X., Yin, Y., Yu, H., Guo, W., & Pei, M. (2016). A novel signal amplification strategy of an electrochemical aptasensor for kanamycin, based on thionine functionalized graphene and hierarchical nanoporous PtCu. *Biosensors and Bioelectronics, 77*, 752-758. doi:https://doi.org/10.1016/j.bios.2015.10.050

Rosati, G., Ravarotto, M., Scaramuzza, M., De Toni, A., & Paccagnella, A. (2019). Silver nanoparticles inkjet-printed flexible biosensor for rapid label-free antibiotic detection in milk. *Sensors and Actuators B: Chemical, 280*, 280-289. doi:https://doi.org/10.1016/j.snb.2018.09.084

Santos, S. M., Henriques, M., Duarte, A. C., & Esteves, V. I. (2007). Development and application of a capillary electrophoresis based method for the simultaneous screening of six antibiotics in spiked milk samples. *Talanta, 71*(2), 731-737. doi:10.1016/j.talanta.2006.05.049

Sharma, A., Catanante, G., Hayat, A., Istamboulie, G., Ben Rejeb, I., Bhand, S., & Marty, J. L. (2016). Development of structure switching aptamer assay for detection of aflatoxin M1 in milk sample. *Talanta, 158*, 35-41. doi:10.1016/j.talanta.2016.05.043

Sui, C., Zhou, Y., Wang, M., Yin, H., Wang, P., & Ai, S. (2018). Aptamer-based photoelectrochemical biosensor for antibiotic detection using ferrocene modified DNA as both aptamer and electron donor. *Sensors and Actuators B: Chemical, 266*, 514-521. doi:https://doi.org/10.1016/j.snb.2018.03.171

Turkevich, J., Stevenson, P. C., & Hillier, J. (1951). A study of the nucleation and growth processes in the synthesis of colloidal gold. *Discussions of the Faraday Society, 11*, 55-75.

U.S. Food and Drug Administration. Center for Veterinary Medicine. Milk drug residue sampling survey. (2015).

United States Department of Agriculture. Food Safety and Inspection Service, Office of Public Health Science. Bioassay for the Detection, Identification and Quantitation of Antimicrobial Residues in Meat and Poultry Tissue. (2010).

Wang, Y. C., Cokeliler, D., & Gunasekaran, S. (2015). Reduced graphene oxide/carbon nanotube/gold nanoparticles nanocomposite functionalized screen-printed electrode for sensitive electrochemical detection of endocrine disruptor bisphenol A. *Electroanalysis, 27*(11), 2527-2536.

Wei, Q., Zhao, Y., Du, B., Wu, D., Li, H., & Yang, M. (2012). Ultrasensitive detection of kanamycin in animal derived foods by label-free electrochemical immunosensor. *Food Chemistry, 134*(3), 1601-1606. doi:https://doi.org/10.1016/j.foodchem.2012.02.126

Yan, K., Liu, Y., Yang, Y., & Zhang, J. (2015). A Cathodic "Signal-off" Photoelectrochemical Aptasensor for Ultrasensitive and Selective Detection of Oxytetracycline. *Analytical Chemistry, 87*(24), 12215-12220. doi:10.1021/acs.analchem.5b03139

Yang, S., Zhu, X., Wang, J., Jin, X., Liu, Y., Qian, F., . . . Chen, J. (2015). Combustion of hazardous biological waste derived from the fermentation of antibiotics using TG–FTIR and Py–GC/MS techniques. *Bioresource Technology, 193*, 156-163. doi:https://doi.org/10.1016/j.biortech.2015.06.083

Yin, J., Guo, W., Qin, X., Zhao, J., Pei, M., & Ding, F. (2017). A sensitive electrochemical aptasensor for highly specific detection of streptomycin based on the porous carbon nanorods and multifunctional graphene nanocomposites for signal amplification. *Sensors and Actuators B: Chemical, 241*, 151-159. doi:https://doi.org/10.1016/j.snb.2016.10.062

Yuan, Y., Zhang, F., Wang, H., Gao, L., & Wang, Z. (2018). A sensor based on Au nanoparticles/carbon nitride/graphene composites for the detection of chloramphenicol and ciprofloxacin. *ECS Journal of Solid State Science and Technology, 7*(12), M201.

Zhao, J., Guo, W., Pei, M., & Ding, F. (2016). GR–Fe 3 O 4 NPs and PEDOT–AuNPs composite based electrochemical aptasensor for the sensitive detection of penicillin. *Analytical Methods, 8*(22), 4391-4397.

Zhou, L., Li, D.-J., Gai, L., Wang, J.-P., & Li, Y.-B. (2012). Electrochemical aptasensor for the detection of tetracycline with multi-walled carbon nanotubes amplification. *Sensors and Actuators B: Chemical, 162*(1), 201-208. doi:https://doi.org/10.1016/j.snb.2011.12.067

Zhou, Y., Li, F., Wu, H., Chen, Y., Yin, H., Ai, S., & Wang, J. (2019). Electrochemical aptasensing strategy for kanamycin detection based on target-triggered single-strand DNA adsorption on MoS2 nanosheets and enzymatic signal amplification. *Sensors and Actuators B: Chemical, 296*, 126664. doi:https://doi.org/10.1016/j.snb.2019.126664

Zhu, Y., Chandra, P., Song, K.-M., Ban, C., & Shim, Y.-B. (2012). Label-free detection of kanamycin based on the aptamer-functionalized conducting polymer/gold nanocomposite. *Biosensors and Bioelectronics, 36*(1), 29-34. doi:https://doi.org/10.1016/j.bios.2012.03.034

Chapter 7. Conclusions and Future work

7.1 Conclusions

In this dissertation, we elaborated on the food safety requirements for effectively monitoring the levels of residual antibiotics in milk and the urgent need for designing a fast, simple, and cost-effective sensing approach to replace the conventional antibiotic quantification methods. To best construct the research plan, we investigated the recent developments of aptamer-based electrochemical biosensors and realized the main issues which limited the advancement of ultrasensitive antibiotic detection. Therefore, the nanomaterial modifications were introduced to ameliorate the electrical behaviors of the biosensing surface and offer great biocompatibility to afford immobilization sites for biorecognition elements. Additionally, the DNA nanostructures were employed to thoroughly release the binding affinity of biosensing probes to acquire the best sensitivity. Moreover, an immobilization-free aptamer selection procedure was proposed to fill the vacancy of high-affinity aptamers to antibiotics with light molecular weight. The ultimate goal of this research is to build a universal electrochemical aptasensing platform for antibiotic detection.

In Chapter 3, reduced graphene oxide and gold nanoparticles were synthesized *via* environmentally friendly methods and then used to modify the surface morphology of the electrode surface to obtain the enhanced electron transmission rate and improved surface conductivity. The nanocomposite modified electrode exhibited a significantly better electrical performance compared to the bare electrode. DNA oligonucleotide probe was utilized to perform the *E. coli* genomic DNA detection based on the DNA hybridization scheme, which verified the biosensing ability of modified electrode. However, we discovered that the poor controllability of ssDNA orientation restrained the sensitivity and reproducibility of the designed biosensor.

In Chapter 4, we introduced the tetrahedral DNA nanostructures (TDNs) as the aptamer immobilization pedestals to maintain the vertical orientations and preserve the functional conformations of aptamer sequences. Furthermore, the cross-interactions from neighbor aptamers were prohibited by the precisely controlled nanospacing attributed to the tailored size of DNA nanostructures. The self-assembled procedure of the TDN nanostructures was optimized in terms of a controlled temperature route to reduce by-products. Because of the improved target accessibility, quantification of the residual ampicillin in a wide range of concentration from 10 pM to 1000 nM was performed in both buffer solution and milk sample, and an ultrasensitive label-free detection was achieved at 1 pM in less than 30 min.

In the review of antibiotic aptasensors, we discovered the vacancy of high-affinity aptamer sequences to small molecules, such as penicillin G, due to the challenge of aptamer screening on account of the ultralight molecular weights and shortage of immobilization sites. In Chapter 5, a GO-SELEX procedure based on the unspecific GO adsorption to separate the unbounded sequences from the target-aptamer complex was designed and optimized to select aptamer sequences specific to penicillin G. The secondary structures and the dissociation constants (K_d) of three aptamer candidates were analyzed to prove the high binding affinity. A selectivity test was performed to confirm the specificity of selected aptamers to penicillin G over other antibiotics.

To continue the work in Chapter 6, a label-free electrochemical aptasensor for penicillin G was designed and optimized using the selected aptamers with the assistance of nanomaterial modifications and DNA nanostructure functionalization. The designed aptasensor was able to quantify residual penicillin G concentration in the range of 0.2 nM to 1000 nM, yielding an ultralow LOD of 0.05 nM. Moreover, the aptasensor was proved to be practical in the milk sample with the recovery rates from 97.96% to 108.87% and RSD less than 3.88%. The reproducibility

and stability of the designed aptasensor were exanimated to show the potential of on-site antibiotic analysis.

In summary, the results of this research demonstrate the potential of electrochemical biosensors with specific aptamer sequences, nanocomposite coating, and DNA nanostructures. With suitable optimization, this universal aptasensing platform can be adapted to the fast, simple, and cost-effective detection of various analytes with high sensitivity and selectivity.

7.2 Future perspective of the research

According to the conclusions of this dissertation, the suggested future plan is listed below:

(1) The relationship between the size of TDN and different aptamer sequences needs to be investigated to control the nanospacing and conformational change more precisely to further improve the binding performance of the fixed aptamer probes.

(2) In this dissertation, two commonly used antibiotics were tested by the designed aptasensor to show an excellent result in both buffer and milk samples. There are other antibiotics in the food industry that lack reported effective aptamers and are in need of sensitive detection, such as cephalosporin and amoxicillin. The GO-SELEX can be adapted for these small molecule targets and identify high-affinity aptamers. The TDN needs to be tailored in size and shape to cooperate with different aptamer sequences and antibiotics.

(3) An aptasensing array should be designed to meet the commercial requirements of multiple target determination for antibiotics and other analytes. A possible solution is to screen-print an aptasensing platform with a multi-electrode pattern to simultaneously

detect multiple analytes and generate separate electrical signals for individual analyte quantification.

(4) To commercialize the sensor platform for the on-site application, the incorporation of microfluidic devices and a computer programing system will be important to minimize human errors and generate an automated equipment for the food industry. This automated equipment can be incorporated with a smartphone-based application to operate on-site and in real-time to generate an instant readout.